TECHNIQUES IN DISPLAY HOLOGRAPHY

KAVEH BAZARGAN MSc, DIC, ARCS

April 1986

A Thesis submitted for the degree of Doctor of Philosophy of the University of London.

Optics Section
Blackett Laboratory
Imperial College of Science and Technology
London SW7 2BZ

Copyright ©KAVEH BAZARGAN, 1986. No part of this thesis may be reproduced, stored in a retrieval system, or transmitted in any form or by any means, electronic, mechanical, holographic, photocopying or otherwise, without the prior written permission of the author.

To My Parents

ABSTRACT

A survey of display holography is presented. Formulæ are derived for the position and the aberrations of a holographic point image as a function of the recording and the reconstruction parameters, and the viewing position. The effect of changes in the thickness and refractive index of volume reccording materials is considered, and formulæ for the correct reconstruction parameters are derived. Colour rendition in multicolour holograms is discussed, independently of the recording technique.

Laser transmission holography is examined, including factors affecting the choice of the mode of polarisation of the recording beams. Experimental results in multicolour laser transmission holography are presented.

White light transmission holography is divided into image-plane, rainbow, and dispersion compensation techniques, and each is separately discussed, with particular emphasis on dispersion compensation. A new technique—multicolour dispersion-compensated holography—is presented.

Reflection holography is described, including details of recording in dichromated gelatin. Experimental results in multicolour reflection holography are presented.

PREFACE

Display holography is a unique interdisciplinary subject, involving science and technology, art and craft. I believe that the potential of the subject is still underestimated, and that the present rapid growth in its appliation will continue. With this belief in mind, I have tried to address some of the important technical issues such as multicolour holography and methods of display.

Although most of this work was completed by 1982, I have not, for various reasons, been able to complete the thesis until now. At this point I should thank all those friends and colleagues whose perseverance and encouragement helped me complete the document!

A few word about the production of the thesis—I typeset the text on an Autologic APS μ–5 phototypesetter, using Donald Knuth's brilliant computer typesetting system, TEX (using limited implementation of TEX V 1.0.0 available at the Imperial College Computer Centre.) I am indebted to Mr. Malcolm Clark for his advice on TEX and on its implementation at Imperial College. All diagrams were produced on 35mm microfilm using a vector graphics software package that I have been developing at Imperial College, and using the facilities of the Imperial College Computer Centre.

I must extend my gratitude to all members of the Optics section at Imperial College who have always been more than helpful. In particular, I would like to thank my supervisor, Dr. Robin Smith, for constant advice and encouragement, Dr. Michael Forshaw, for his expert and generous advice on volume holograms and holographic aberrations, Mr. Fred Reavel, for invaluable assistance with the design and manufacture of the holographic recording system described in §3.10, and Messrs. Min-Joong Kim and Stephen Hart for the kind loan of computer equipment during the preparation of this thesis.

Last, but not least, I am grateful to my parents for their encouragement and guidance throughout my educational career, and for their generous financial support without which this project would not have been possible.

K.B. April 1986

CONTENTS

CHAPTER 1

INTRODUCTION

1.1 DEFINITION

Display holography is an area of holography which is often not clearly defined. It is therefore useful to start by stating what we understand by the term. We define display holography as that area of holography in which the reconstructed wavefronts produce an image which is observed visually. The image is normally diffuse (as opposed to specular) and exhibits parallax.

1.2 ORIGINAL CONTRIBUTIONS

As we have chosen to incorporate our original findings into a survey of display holography, we have included this section to point out those parts of the thesis which we believe to be original contributions.

In §3.7.3 we propose a simple method for manufacturing a linearly variable beamsplitter using a vacuum deposition chamber. After examining the optical and mechanical requirements, we describe a system for producing small-format display holograms (§3.10). The system is designed for versatility and ease of use.

The question of which polarisation to use in display work is addressed in §4.3 and §4.6. Although most academic texts on holography favour *s*–polarisation, we have found that *p*–polarisation may be more suitable.

Chapter 5 deals with image-plane holography. The geometry used for recording an image-plane hologram is examined, and in §5.3.1 we define a 'virtual window' effect arising from image 'cut-off' by a window apparently behind the image. The effect can arise if an unsuitable geometry is used in the 'transfer' stage, and we have found it especially disconcerting. We define a volume (Fig. 5.9) within which an intermediate image must lie to avoid the effect. The effect can be present in any type of two-stage hologram. In §5.7 we report on an interesting visual effect arising from astigmatism introduced into an image-plane hologram during the transfer stage

Chapter 7 deals with dispersion compensation—a technique we study in detail. Although dispersion compensation is achieved in the first approximation whether the hologram is placed before or after a compensating grating, the relative merits have not been examined in previous work. In §7.3 we examine these. In §7.6 we analyse the distortions and the third order aberrations of a dispersion-compensated image. In §7.7 we report on an interesting property of a dispersion compensated system comprising a hologram, a diffraction grating, and a miniature Venetian blind structure. In §7.8 we propose a compact hologram viewing device as a solution to the lighting problem in

display holography, namely that to observe a sharp, undistorted holographic image the reconstruction parameters, such as the reconstruction angle, must be set correctly.

In §7.9 we apply dispersion compensation to volume holograms by modifying the Ewald sphere construction. The general treatment leads to results in reflection holograms and gratings. In §7.10 we report on a new method of producing multicolour holograms, using dispersion compensation and exploiting the wavelength sensitivity of thick emulsions.

In §8.6 we examine dispersion in reflection holograms, and in §8.7.1 we suggest a simple technique for producing multicolour reflection holograms.

CHAPTER 2

FUNDAMENTALS OF DISPLAY HOLOGRAPHY

2.1 INTRODUCTION

In this chapter we discuss the fundamental principles of display holography, and derive some general formulæ which will be applied to specific cases in the following chapters.

2.2 DIFFRACTION GRATING MODEL

The simplest hologram is one made by recording the interference pattern formed by two plane waves on a suitable photosensitive medium. Suppose that two plane waves A and B are incident at angles θ and ϕ at a plane recording medium (Fig. 2.1). (Using the Cartesian convention both angles are positive.) The interference planes formed in space lie parallel to the bisector of the included angle—ie. at angle $(\theta + \phi)/2$ to the normal. The fringe plane spacing Λ is given by

$$\Lambda = \frac{\lambda}{2\sin\left(\frac{\theta-\phi}{2}\right)}. \tag{2.1}$$

The surface fringe spacing d recorded on the photosensitive plate is greater by a factor $(1/\cos\delta)$, where δ is the fringe plane tilt angle $(\theta + \phi)/2$. Therefore

$$d = \frac{\lambda}{2\sin\left(\frac{\theta-\phi}{2}\right)\cos\left(\frac{\theta+\phi}{2}\right)}$$

$$= \frac{\lambda}{\sin\theta - \sin\phi}. \tag{2.2}$$

If the photosensitive plate is suitably processed, it behaves as a diffraction grating when re-illuminated. Now the general equation for diffraction by a plane diffraction grating is

$$d(\sin\alpha - \sin\beta) = n\lambda, \tag{2.3}$$

where d is the grating period, λ is the wavelength of the incident light, n is the order of diffraction, and α and β are the incident and diffracted angles. Comparing this equation with Eqn. 2.2, if $\alpha = \theta$, then $\beta = \phi$ when $n = 1$ and the wavelength of the incident light is equal to that of the original interfering beams. The plane wave B is thus 'reconstructed' by a reconstruction wave identical to A. This model can be qualitatively extended to an arbitrarily shaped object wave B' if the latter is considered as being composed, within any small region of the hologram, of many plane waves $B_1, B_2 \ldots B_n$, each being recorded and reconstructed independently.

The diffraction grating model is ideal for ray-tracing through holograms [1].

2.3 LOCATION AND THIRD ORDER ABERRATIONS OF A POINT IMAGE

2.3.1 Introduction

When the holographic image of a point object is observed using a reconstruction beam identical to the original reference beam, the image is free from aberrations, and its apparent position is independent of the position of the observer (Fig. 2.2). If, however, the reconstruction geometry is altered or a different wavelength is used, then the apparent position of the image will depend on the position of the observer and, in general, the image will be aberrated (Fig. 2.3). In this section a computational method is described whereby the position of an image and its third order aberrations can be determined in terms of the recording and reconstruction parameters, and the observer position. The aberrations are calculated on the basis of the original treatment by Champagne [2], and for completeness Champagne's study is briefly reviewed.

2.3.2 Champagne's Derivation of Holographic Aberrations

Let us consider the system in Fig. 2.4. The holographic recording plate is coincident with the x–y plane. R_q is the distance from any point Q to the centre of the recording plate (taken to be the origin of the co-ordinate system). The subscript q can be replaced by O, r, c or I to denote the object, reference source, reconstruction source, or image respectively. The complex amplitude at (x,y) on the recording plate due to a point source at Q can be written as

$$\mathcal{E}_q = \frac{A_q}{r_q} \exp i\left(\frac{2\pi}{\lambda_q}\right) r_q \tag{2.4}$$

where A_q is the source strength, r_q is the distance from the point source Q to the point (x,y), and λ_q is the wavelength of the light emanating from Q.

A hologram is recorded by simultaneously illuminating the recording plate with an object source O, and a coherent reference source r. The plate is then suitably processed such that its optical transmittance is a function of the original irradiance, and it is subsequently illuminated with a reconstruction source c. (In general, $\lambda_r \neq \lambda_c$.) After diffraction, several waves emerge, corresponding to different orders of diffraction. If we neglect the $1/r$ variations in amplitude, the wave corresponding to the primary diffracted order is of the form

$$\mathcal{E}_p = A_p \exp\left[i\left(\frac{2\pi}{\lambda_c}\right) r_c \right] \exp\left[i\left(\frac{2\pi}{\lambda_r}\right)(r_O - r_r) \right]. \tag{2.5}$$

To investigate the location and aberrations of the primary image, we assume that the complex amplitude of the primary image is of the form

$$\mathcal{E}_I = A_I \exp\left[i\left(\frac{2\pi}{\lambda_c}\right) r_I \right]. \tag{2.6}$$

Any phase mismatch between $\mathcal{E}_I$ and $\mathcal{E}_p$ can be considered to be the aberrations.

Now

$$r_q^2 = z_q^2 + (x - x_q)^2 + (y - y_q)^2$$

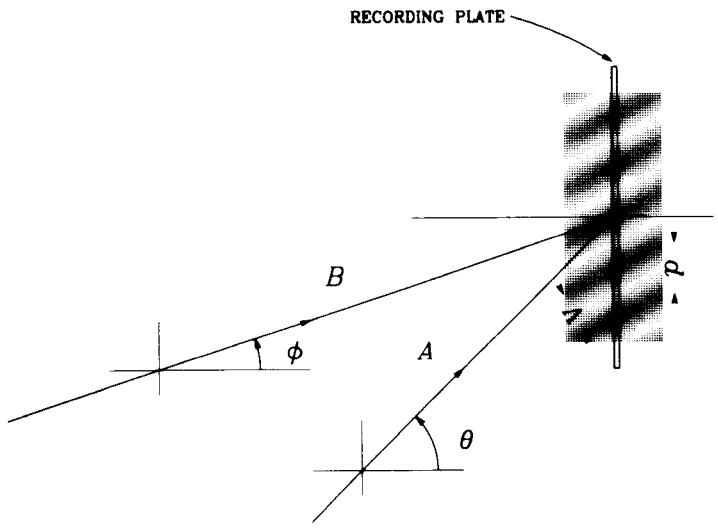

Fig. 2.1 Formation of an interference pattern by two plane waves.

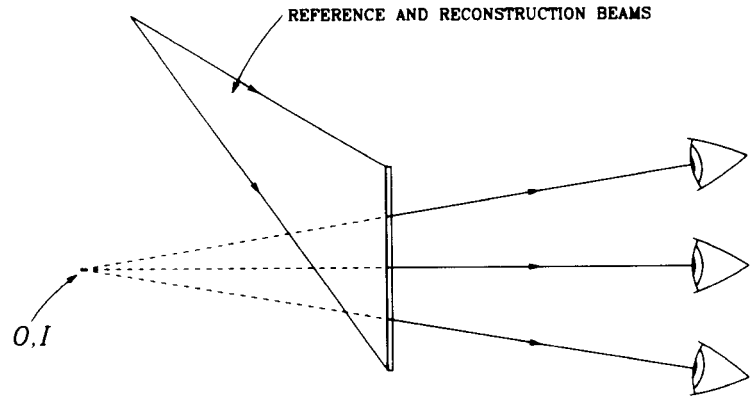

Fig. 2.2 Aberration-free reconstruction of a holographic image.

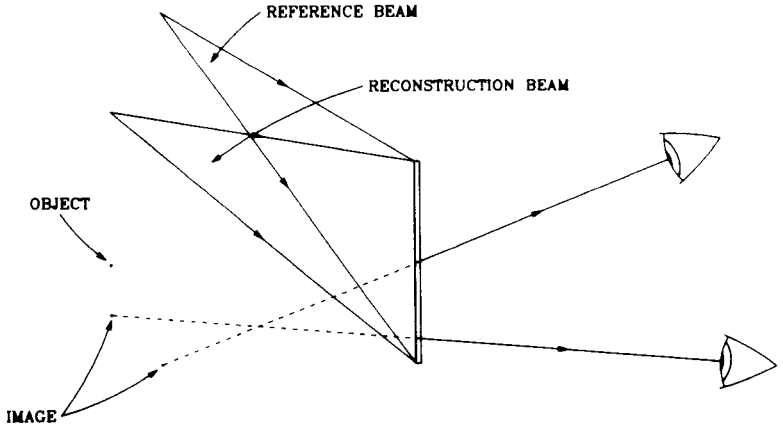

Fig. 2.3 Aberrated reconstruction of a holographic image.

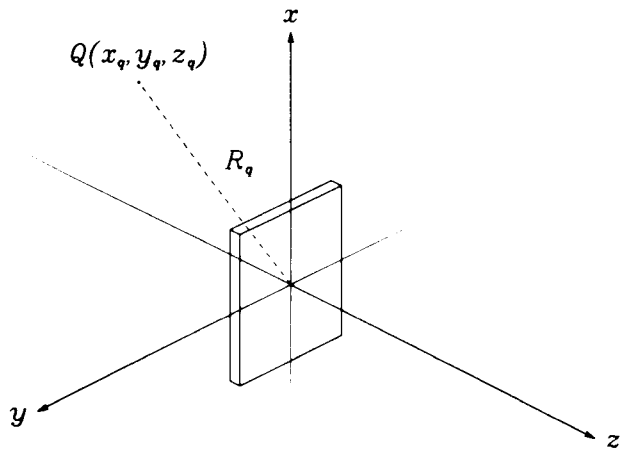

Fig. 2.4 Coordinate system for calculations in §2.3.2.

and

$$R_q^2 = z_q^2 + x_q^2 + y_q^2.$$

Therefore

$$\begin{aligned} r_q &= (x^2 + y^2 - 2xx_q - 2yy_q + R_q^2)^{\frac{1}{2}} \\ &= R_q\left(1 + \frac{x^2+y^2}{R_q^2} - \frac{2(xx_q+yy_q)}{R_q^2}\right)^{\frac{1}{2}}. \end{aligned} \tag{2.7}$$

A binomial expansion of r_q about R_q produces

$$\begin{aligned} r_q = R_q + \frac{x^2+y^2}{2R_q} - \frac{xx_q+yy_q}{R_q} \\ - \frac{(x^2+y^2)^2-4(x^2+y^2)(xx_q+yy_q)+4(xx_q+yy_q)^2}{8R_q^3} + \cdots \end{aligned} \tag{2.8}$$

Expanding r_r, r_O, r_c, and r_I according to Eqn. 2.8 and matching terms in $(x^2 + y^2)$ and in x and y, we obtain

$$\frac{1}{R_I} = \frac{1}{R_c} + \mu\left(\frac{1}{R_O} - \frac{1}{R_r}\right), \tag{2.9}$$

$$\frac{x_I}{R_I} = \frac{x_c}{R_c} + \mu\left(\frac{x_O}{R_O} - \frac{x_r}{R_r}\right) \tag{2.10}$$

and

$$\frac{y_I}{R_I} = \frac{y_c}{R_c} + \mu\left(\frac{y_O}{R_O} - \frac{y_r}{R_r}\right) \tag{2.11}$$

where $\mu = \lambda_c/\lambda_r$. Eqns. 2.9 and 2.10–2.11 respectively define the distance and the direction of the gaussian image.

The classical Seidel aberrations appear as the mismatch between the third order terms. If we let $x = \rho\cos\theta$ and $y = \rho\sin\theta$, the third order phase aberration is given by [3]:

$$\phi_3 = \frac{2\pi}{\lambda}\Big[-\frac{1}{8}\rho^4 S + \frac{1}{2}\rho^3(\cos\theta C_x + \sin\theta C_y) - \frac{1}{2}\rho^2(\cos^2\theta A_x + \sin^2\theta A_y + 2\sin\theta\cos\theta A_{xy})\Big] \tag{2.12}$$

where

$$S = \frac{1}{R_c^3} + \mu\left(\frac{1}{R_O^3} - \frac{1}{R_r^3}\right) - \frac{1}{R_I^3}, \tag{2.13}$$

$$C_x = \frac{x_c}{R_c^3} + \mu\left(\frac{x_O}{R_O^3} - \frac{x_r}{R_r^3}\right) - \frac{x_I}{R_I^3}, \tag{2.14}$$

$$C_y = \frac{y_c}{R_c^3} + \mu\left(\frac{y_O}{R_O^3} - \frac{y_r}{R_r^3}\right) - \frac{y_I}{R_I^3}, \tag{2.15}$$

$$A_x = \frac{x_c^2}{R_c^3} + \mu\left(\frac{x_O^2}{R_O^3} - \frac{x_r^2}{R_r^3}\right) - \frac{x_I^2}{R_I^3} \tag{2.16}$$

$$A_y = \frac{y_c^2}{R_c^3} + \mu\left(\frac{y_O^2}{R_O^3} - \frac{y_r^2}{R_r^3}\right) - \frac{y_I^2}{R_I^3} \tag{2.17}$$

and

$$A_{xy} = \frac{x_c y_c}{R_c^3} + \mu\left(\frac{x_O y_O}{R_O^3} - \frac{x_r y_r}{R_r^3}\right) - \frac{x_I y_I}{R_I^3}. \tag{2.18}$$

S, C and A are the coefficients for Spherical aberration, Coma and Astigmatism respectively. In most of our analyses we assume that all points of interest lie in the x–z plane, ie. $y_q = 0$ (Fig. 2.5), in which case C_y, A_y and A_{xy} vanish.

2.3.3 Effect of Viewing Position

The relationships derived by Champagne can be used to predict the location and the aberrations of a point image when the principal ray passes through the coordinate origin $x = y = z = 0$.

If the hologram is being used as an imaging system so that the image is projected onto a screen, say, these formulæ suffice. If, on the other hand, the image is viewed directly by an observer, the intersection of the principal ray with the plate is determined by the position of the observer $E(x_E, y_E, z_E)$. To calculate the location and the aberrations of the image, the position of the principal ray at the hologram plane $(x_{pr}, y_{pr}, 0)$ and the effective imaging area of the hologram around that point must be determined.

2.3.4 Position of the Principal Ray

Let us assume, for simplicity, that all points of interest lie in the x–z plane ($y_q = 0$). In the recording geometry in Fig. 2.6 a holographic image is recorded in the normal manner, and is subsequently reconstructed. If the reconstruction beam is identical to the original reference beam, the image is undistorted and $(x_I, z_I) = (x_O, z_O)$. The principal ray position $P(x_{pr}, 0)$ is then located at the intersection of the recording plate and the line joining O and E.

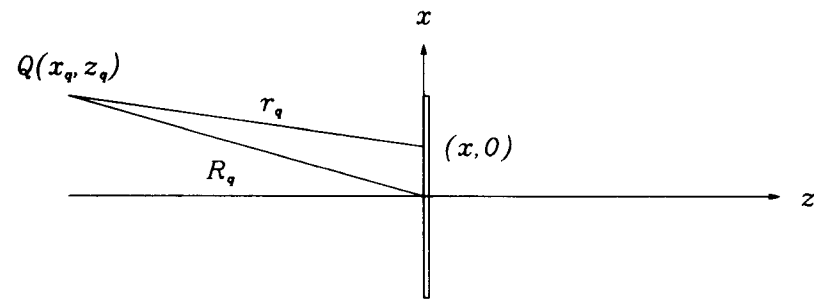

Fig. 2.5 Simplified coordinate system (all $y_q = 0$).

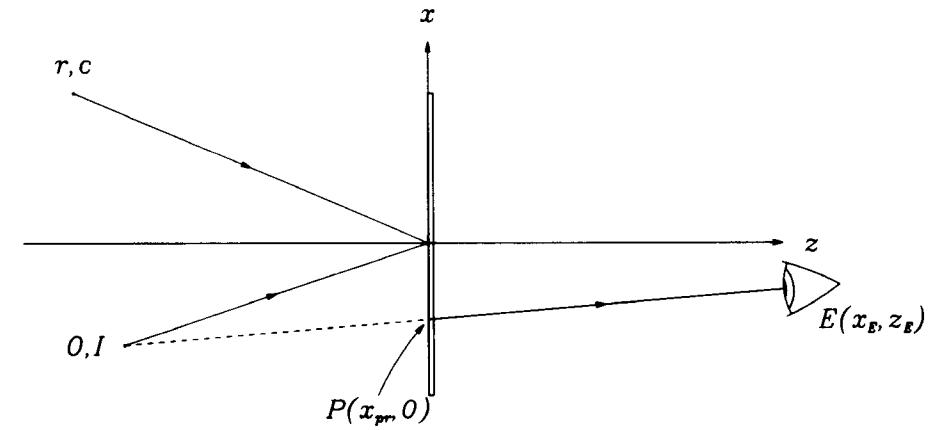

Fig. 2.6 Observation of an aberration-free holographic image.

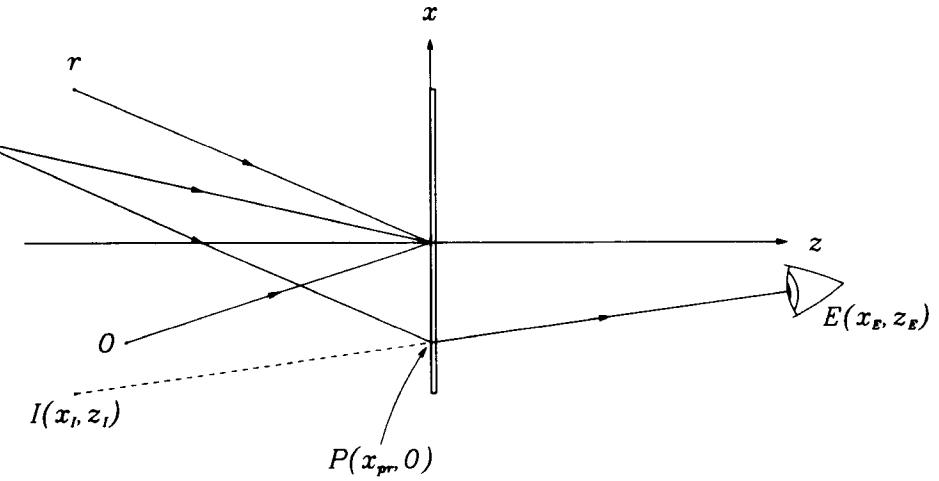

Fig. 2.7 Observation of an aberrated holographic image.

If the reconstruction geometry differs from that of recording, the position of the principal ray, P, is more difficult to ascertain. In Fig. 2.7 the observer views an aberrated point image at I, through an imaging area around $P(x_{pr}, 0)$.

Eqns. 2.9–2.18 can only be applied to the present case after transforming the origin of the coordinate system to $(x_{pr}, 0)$ so that, for example,

$$R_q' = \sqrt{(x_q - x_{pr})^2 + z_q^2}$$
$$= z_q \sqrt{1 + (x_q - x_{pr})^2 / z_q^2}. \tag{2.19}$$

(The second form retains the correct sign for R_q.) x_{pr} can be determined as follows:

As EP and PI are colinear,

$$\frac{x_E - x_{pr}}{R_E'} = \frac{x_I - x_{pr}}{R_I'}. \tag{2.20}$$

Substituting 2.20 into the transformed version of 2.10 we obtain

$$\frac{x_E - x_{pr}}{R_E'} = \frac{x_c - x_{pr}}{R_c'} + \mu\left(\frac{x_O - x_{pr}}{R_O'} - \frac{x_r - x_{pr}}{R_r'}\right) \tag{2.21}$$

which can be solved iteratively to find x_{pr}.

2.3.5 Size of the Imaging Area

To convert the aberration coefficients S, C_x and A_x to wavefront aberrations, the size of the aperture of the effective reference sphere at the hologram must be determined, and Eqn. 2.12 applied. Fig. 2.8 shows an image being observed from (x_E, z_E) in the cases where the image is (a) virtual and (b) real. In both cases the diameter of the effective wavefront is given by

$$D = \left|\frac{D_E R_I'}{R_E' - R_I'}\right| \tag{2.22}$$

Where D_E is the diameter of the pupil of the observer, and R_I and R_E are, respectively, the distances of the image and the observer from the principal ray position P. If we assume that the observer's line of sight is roughly normal to the plate, as is usually the case, then the effective area of the hologram contributing to the image is circular and has the same diameter as the effective aperture. Therefore

$$\rho = \left|\frac{D_E R_I'}{2(R_E' - R_I')}\right|. \tag{2.23}$$

We can now investigate the distortions and the aberrations of an image by substituting ρ into each term of Eqn. 2.12 and setting the cosine terms to unity, thus obtaining the maximum wavefront deviation due to any aberration. For example, the maximum wavefront deviation arising from x–astigmatism is

$$\phi_{3A_x max} = -\frac{\pi}{\lambda_c}\rho^2 A_x$$

where A_x is given by the transformed version of Eqn. 2.16.

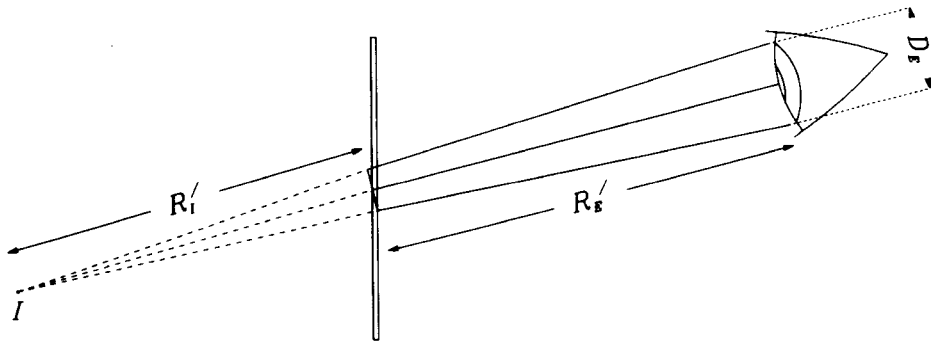

Fig. 2.8 a Calculation of the size of the reference sphere for a virtual image.

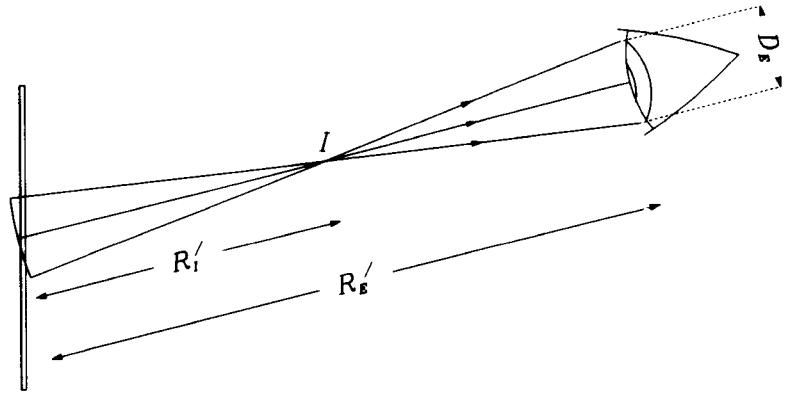

Fig. 2.8 b Calculation of the size of the reference sphere for a real image.

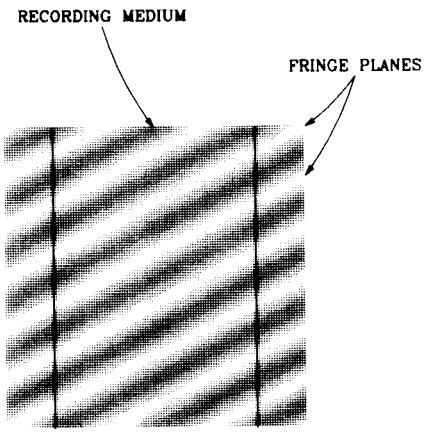

Fig. 2.9 Recording interference fringes in a volume recording medium.

2.4 THICKNESS OF RECORDING MATERIAL

2.4.1 Classification of Holograms according to Thickness of the Recording Material

Holograms can be classified according to the thickness of the material used in recording. These classes can be defined as 'thin', 'thick' and 'semi-thick', the latter exhibiting some of the properties of both the former two. Thick holograms are of particular interest and are treated in detail in §2.4.2.

A *thin* or *plane* hologram is defined as one in which the spacing of the interference fringes is much greater than the thickness of the recording material. The properties of such holograms can be investigated using conventional plane diffraction grating formulæ. In this class are surface-relief holograms made on, say, photoresist, although when very deep modulations are involved volume- or 'Bragg'-type effects are observed [4,5]. The imaging properties and the aberrations of thin holograms can be derived using Champagne's equations—see §2.3.2.

Thick or *volume* holograms are those in which the thickness of the recording material is much greater than the fringe spacing. When reconstructing images from volume holograms the reconstruction parameters, such as the reconstruction angle and wavelength of the reconstruction beam, must be identical or close to those of recording.

Semi-thick holograms are those that show both 'thin' and 'thick' properties. These holograms can be theoretically treated using either thin or thick hologram formulæ, depending on the property being examined. For example the geometric optics properties can be examined using thin hologram formulæ, while the angle and wavelength sensitivities can be predicted using thick hologram formulæ. Most display holograms made on photographic materials fall into this category.

2.4.2 Volume Holograms

2.4.2.1 Introduction

Most practical holographic recording media have thicknesses of the order of, or greater than, the fringe spacing (Fig. 2.9). The recorded hologram possesses some interesting properties which can be beneficially applied in display holography.

The reconstruction process can be treated similarly to Bragg diffraction, the fringe planes being analogous to crystal planes. Efficient image reconstruction can, in general, only be obtained if the Bragg condition is satisfied, ie. when

$$2\Lambda \sin\theta = \lambda \tag{2.24}$$

where λ is the wavelength of the reconstruction beam, and Λ and θ are defined in Fig. 2.10. Deviation from the Bragg condition leads to loss of diffraction efficiency. Volume recording media can be used to record reflection holograms, in which case the object and reference beams impinge on the recording medium from opposite sides (Fig. 2.11). Both transmission and reflection volume holograms are theoretically treated in an elegant analysis by Kogelnik [6].

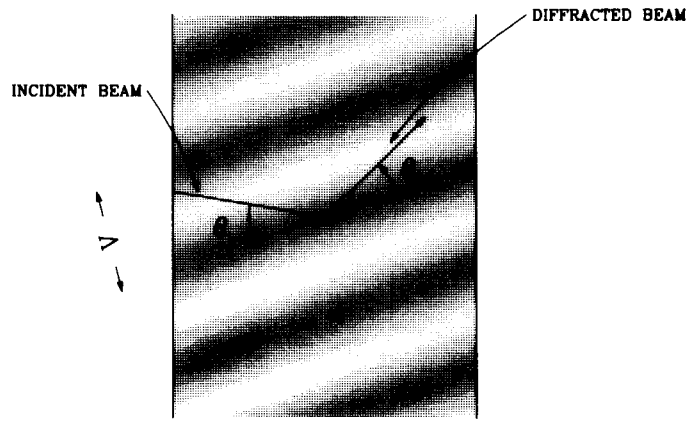

Fig. 2.10 Definition of Λ and θ for the Bragg condition (Eqn. 2.24).

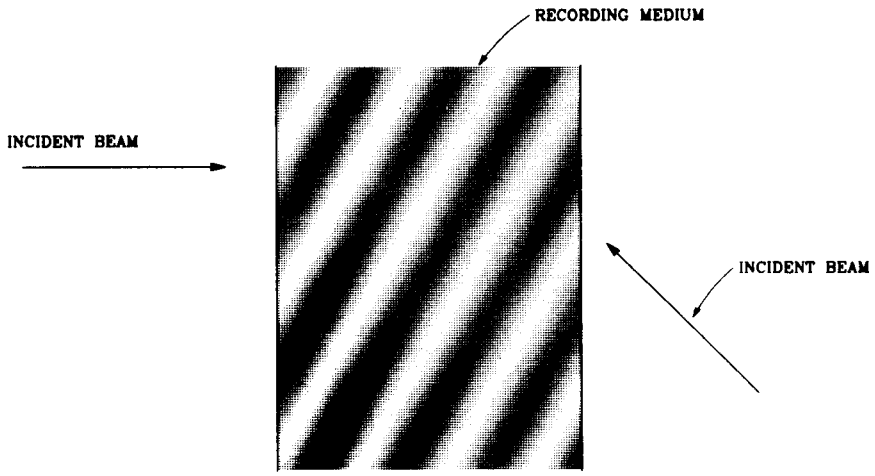

Fig. 2.11 Recording a volume hologram in the reflection mode.

2.4.2.2 Effect of Emulsion Refractive Index

In the previous sections, and in Figs. 2.9–2.11 we have assumed that the refractive index of the recording medium is equal to that of the surrounding medium (usually air), and therefore the beams entering it are not deviated—in practice this is not the case. Photographic emulsions, for example, have refractive indices of about 1.5. The beams are therefore refracted according to Snell's law. Fig. 2.12 shows the effect for the transmission case. Incident beams a and b are refracted to form a' and b' inside the recording medium. The interference fringes inside the medium are correspondingly deviated.

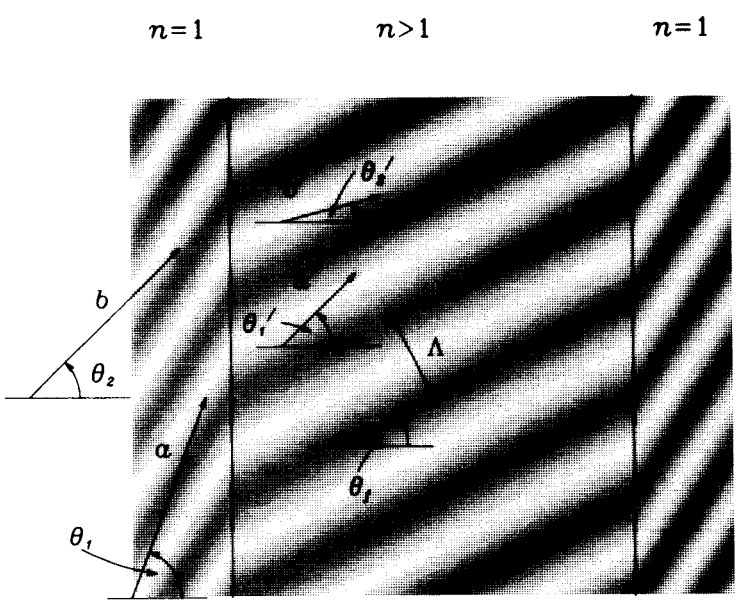

Fig. 2.12 Deviation of the incident beams, and hence the interference fringes, due to the refractive index of the recording material.

2.4.2.3 Fringe Spacing in Volume Holograms

Consider the system in Fig. 2.12. a and b are plane waves of wavelength λ, incident at θ_1 and θ_2 respectively at a recording medium of refractive index n. The corresponding angles inside the medium are θ_1' and θ_2', where

$$\theta_1' = \sin^{-1}\left(\frac{\sin\theta_1}{n}\right)$$

and

$$\theta_2' = \sin^{-1}\left(\frac{\sin\theta_2}{n}\right).$$

If the fringe plane spacing inside the emulsion is Λ, then

$$2\Lambda \sin\left(\frac{\theta_1' - \theta_2'}{2}\right) = \lambda'$$

where $\lambda' = \lambda/n$, or

$$\Lambda = \frac{\lambda'}{2\sin\left(\frac{\theta_1' - \theta_2'}{2}\right)}. \tag{2.25}$$

The orientation of the fringes with respect to the normal to the recording medium, α, is given by

$$\alpha = \frac{\theta_1' + \theta_2'}{2}$$

$$= \frac{1}{2}\left[\sin^{-1}\left(\frac{\sin\theta_1}{n}\right) + \sin^{-1}\left(\frac{\sin\theta_2}{n}\right)\right].$$

Eqn. 2.25 shows that the fringe spacing is minimum when $\sin[(\theta_1' - \theta_2')/2] = 1$, ie. when $\theta_1' = \theta_2' + 180°$, or when the two beams are travelling in directly opposing directions, in which case

$$\Lambda = \frac{\lambda'}{2} = \frac{\lambda}{2n}. \tag{2.26}$$

This case only occurs in reflection holograms.

2.4.2.4 Effective Fringe Spacing for Transmission Holograms

In transmission holography it is usually more useful to consider the effective surface fringe spacing, so that the geometrical optics properties can be investigated. The surface fringe spacing in a transmission hologram is

$$\begin{aligned} d &= \frac{\Lambda}{\cos\alpha} \\ &= \frac{\lambda'}{2\sin\left(\frac{\theta_1' - \theta_2'}{2}\right)\cos\left(\frac{\theta_1' + \theta_2'}{2}\right)} \\ &= \frac{\lambda'}{\sin\theta_1' - \sin\theta_2'} \\ &= \frac{\lambda}{\sin\theta_1 - \sin\theta_2}, \end{aligned} \tag{2.27}$$

which is independent of n, and is identical to the thin hologram formula in Eqn. 2.2. If the beams are incident symmetrically and $\theta_1 = -\theta_2$, then $d = \Lambda$.

2.4.2.5 Changes in Emulsion Thickness and Refractive Index

Often, due to chemical processing of the hologram, the emulsion thickness and its average refractive index change. These changes must be taken into account when determining reconstruction parameters.

In this section we describe a procedure for the calculation of the correct reconstruction angles for a given reconstruction wavelength. Let us consider the recording geometry in Fig. 2.13. Two plane, phase-related beams of wavelength λ are incident, at incidence angles θ_{1a} and θ_{1b} in free space, onto a volume recording medium of refractive index n_1 and thickness D_1. The corresponding angles inside the medium are θ_{1a}' and θ_{1b}'. The interference fringes are tilted at angle θ_{f1} and have spacing Λ_1. The effective surface fringe spacing is d. After processing (Fig. 2.14) D_1 and n_1 change to D_2 and n_2 respectively, and all other corresponding values are subscripted with '2' in place of '1' in the following derivation:

Using Snell's law,

$$\begin{aligned} \theta_{1a}' &= \sin^{-1}\left(\frac{\sin\theta_{1a}}{n_1}\right), \\ \theta_{1b}' &= \sin^{-1}\left(\frac{\sin\theta_{1b}}{n_1}\right). \end{aligned} \tag{2.28}$$

The fringe tilt is given by

$$\theta_{f1} = \left(\frac{\theta_{1a}' + \theta_{1b}'}{2}\right), \tag{2.29}$$

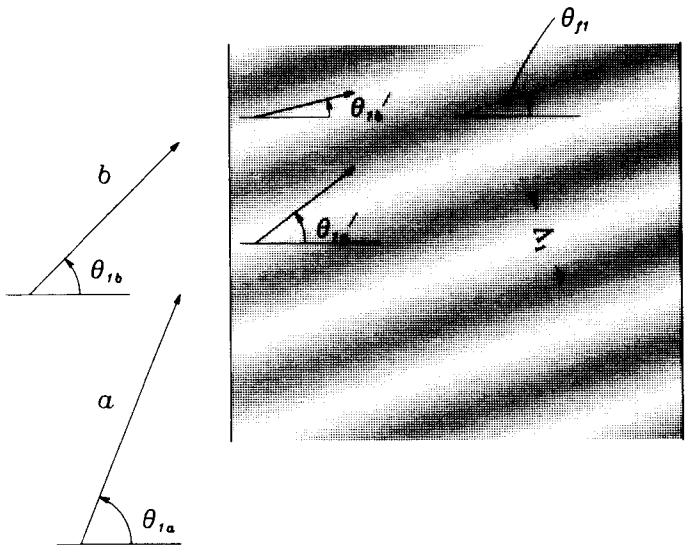

Fig. 2.13 Recording an interference pattern in a volume hologram.

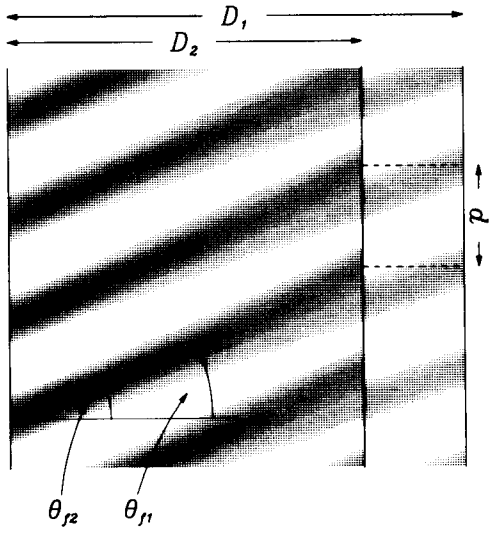

Fig. 2.14 Change of fringe angle θ_f after processing.

the Bragg angle by

$$\theta_{1\,\text{Bragg}} = \left(\frac{\theta_{1a}' - \theta_{1b}'}{2}\right), \tag{2.30}$$

and the fringe spacing by

$$\Lambda_1 = \frac{\lambda_1}{2n_1 \sin\theta_{1\,\text{Bragg}}}. \tag{2.31}$$

After processing,

$$\tan\theta_{f2} = \frac{D_1 \tan\theta_{f1}}{D_2}.$$

Now,

$$d = \frac{\Lambda_1}{\cos\theta_{f1}} = \frac{\Lambda_2}{\cos\theta_{f2}}$$

therefore

$$\Lambda_2 = \frac{\Lambda_1 \cos\theta_{f2}}{\cos\theta_{f1}}.$$

If the processed hologram is illuminated with light of wavelength λ_2, then, using the Bragg condition,

$$\theta_{2\,\text{Bragg}} = \sin^{-1}\left(\frac{\lambda_2}{2n_2\Lambda_2}\right). \tag{2.32}$$

The corresponding equations to Eqns. 2.29 and 2.30 are now

$$\theta_{f2} = \frac{\theta_{2a}' + \theta_{2b}'}{2} \tag{2.33}$$

and

$$\theta_{2\,\text{Bragg}} = \frac{\theta_{2a}' - \theta_{2b}'}{2} \tag{2.34}$$

whence

$$\theta_{2a}' = \theta_{f2} + \theta_{2\,\text{Bragg}}$$

$$\theta_{2b}' = \theta_{f2} - \theta_{2\,\text{Bragg}}.$$

Finally, using Snell's law,

$$\theta_{2a} = \sin^{-1}[n_2 \sin\theta_{2a}']$$

and

$$\theta_{2b} = \sin^{-1}[n_2 \sin\theta_{2b}'],$$

where either θ_{2a} or θ_{2b} is the correct angle to use to illuminate the processed hologram so as to reconstruct efficiently a plane wave emerging at the other angle.

2.5 COLOUR RENDITION IN MULTICOLOUR HOLOGRAPHY

2.5.1 Introduction

In their original paper, Leith and Upatnieks [7] pointed out that multicolour holographic images could be obtained by incoherently superposing two or more holographic images, each recorded in a different wavelength. In the following chapters of this dissertation different methods for recording multicolour holograms will be described in detail. The subject of colour rendition, however, can be dealt with independently of the recording method, and in terms only of the laser emission wavelengths used in the recording. (A complete literature search and historical review of colour holography has been published by the author [8]—see Appendix.)

2.5.2 Reproducible Range of Colours

The range of colours that are, in principle, obtainable in multicolour holography can be determined by inspection of a chromaticity diagram—eg. the 1931 CIE colour chromaticity diagram [9, 10]. If two wavelengths are used, then the range of colours obtainable are those that lie on the straight line joining the points representing the two wavelengths on the chromaticity diagram. If three or more wavelengths are used, then any colour within the convex polygon bounded by the lines joining the corresponding points can be produced by the appropriate mixture of those colours. In multicolour holography, if a particular colour is to be produced, it is a necessary *but not sufficient*

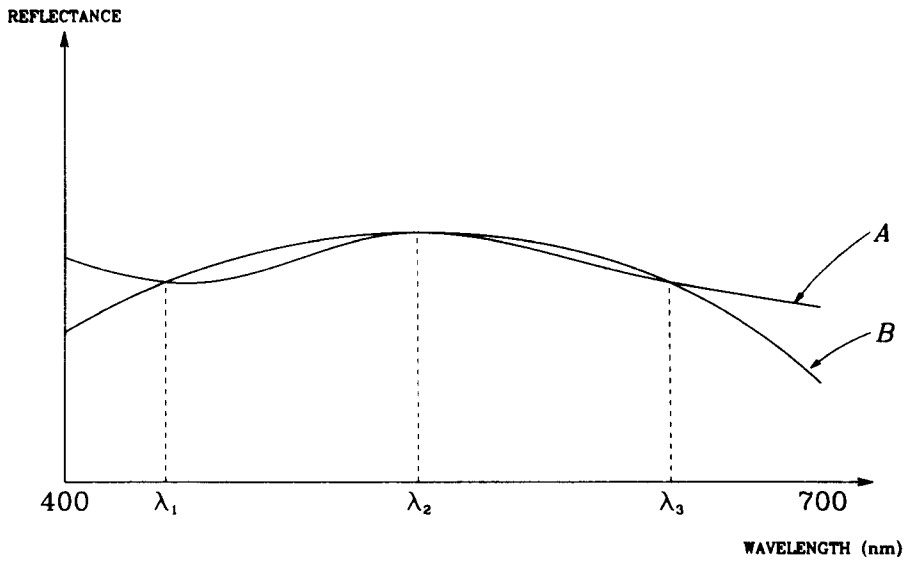

Fig. 2.15 Spectral reflectance curves for two hypothetical objects *A* and *B*, which appear identical when illuminated by light containing only wavelengths λ_1, λ_2 and λ_3.

condition that on the CIE diagram that colour lies within the polygon formed by the component spectral colours used in recording the hologram—see following section. (The fact that this condition is not sufficient is often overlooked by researchers in multicolour holography.)

2.5.3 Colour Rendition

When an object is observed in daylight or under a typical artificial white-light source, the eyes receive information about the spectral reflectance of the object over the entire visible spectrum. The perceived colour is therefore a function of the spectral reflectance of the object, the Spectral Power Distribution (SPD) of the illuminating source, and the characteristics of the eye.

When the object is illuminated by a number of discrete wavelengths, as when recording a multicolour hologram, the spectral reflectance is only significant at those discrete wavelengths. Consider the two hypothetical non-luminous objects *A* and *B* with with spectral reflectance curves as shown in Fig. 2.15. At wavelengths λ_1, λ_2 and λ_3 both objects have the same reflectance values, so they are perceived as having identical colours (ie. as metamers), although in daylight they may look quite different. In order to collect sufficient data about the spectral reflectance to determine its colour with sufficient accuracy one might expect that a large number, say ten, different wavelengths need to be used. It turns out, however, that only three or four judiciously chosen wavelengths can produce excellent colour rendition.

A measure of the colour rendering capability of an illuminating source is the colour rendering index (CRI) as defined by the 'Commission Internationale de l'Éclairage' [10]. Thornton [11] showed that an illuminating source emitting three narrow spectral bands near 450, 540 and 610 nm had a CRI of about 80. Walter [12], using nonlinear mathematical optimization techniques, suggested a set of four wavelengths with a CRI of over 90.

These results, which have been confirmed by Soviet work in colour holography [13,14], imply that multicolour holograms with excellent colour rendition can be produced using three or four laser lines. At present there are practical difficulties in obtaining these lines, although more conveniently available wavelengths near the optimum ones can be used as a compromise [13].

2.5.4 Colour Distortion

Colour distortion has been observed in multicolour holography by previous researchers [15–17] and by ourselves [8]. The most noticeable distortion has been desaturation or hue shift in yellow objects. Most researchers have assigned this distortion to the fact that the colour polygon on the CIE diagram did not cover a large enough range of colours. We believe that the distortion is usually due to the non-optimal choice of laser emission wavelengths—most object colours have CIE x–y coordinates lying well within the range of colours reproducible by the commonly used sets of laser wavelengths. Plate I shows severe colour distortion in one of our experiments.

CHAPTER 3

BASIC EQUIPMENT AND TECHNIQUES

3.1 INTRODUCTION

In the previous chapter the fundamental theoretical aspects of display holography were discussed. In this chapter we deal with the practical aspects. Most of the contents of this chapter are applicable to all types of display holograms. Techniques relating to specific types of holograms are covered in later chapters.

3.2 LASERS

3.2.1 Introduction

Lasers suitable for display holography can be broadly divided into pulsed and continuous-wave sources. Pulsed lasers can be used for recording holograms of animate subjects, and do not require the use of vibration isolation systems. We have not investigated the use of pulsed-laser sources.

Continuous-wave (cw) laser sources are at present the most popular for display holography. The three major requirements for holography are sufficient power, sufficient coherence length, and single transverse mode operation. Almost all commercially available cw lasers operate reliably in the single transverse (TEM00) mode.

3.2.2 Coherence Length

An important parameter in choosing a laser for holography is its coherence length. This is defined as the maximum optical path difference between two beams, derived from the same laser, at which some degree of interference takes place. The coherence length effectively limits the maximum size of object which can be used in display holography. As a rough guide, for the entire object to be holographically recorded, its size must not exceed half the coherence length of the laser.

3.2.3 Helium–Neon Laser

The Helium–Neon (He–Ne) laser is by far the most popular laser for display holography. It is compact, reliable and inexpensive, and does not normally require water-cooling. The output power of the He–Ne laser is, however, limited. The maximum power available from commercial He–Ne lasers is 50mW at a wavelength of 632.8nm. The coherence length of the He–Ne laser is typically 20cm. Although this can, in principle, be increased by introducing an intracavity etalon, the power reduction is significant.

3.2.4 Ion Lasers

The most popular ion lasers for holography are the Argon–Ion (Ar^+) and the Krypton–Ion (Kr^+) lasers. These generally require water-cooling.

The Ar^+ laser produces several emission wavelengths in the blue and green parts of the spectrum. The most powerful are the 514.5nm and the 488.0nm lines. Outputs of several Watts are possible in each line. The coherence length is of the order of only 8cm, but by introduction of an intracavity etalon this can be increased to several metres. The power is reduced by some 50% with the etalon present. Recently, low-power, air-cooled Ar^+ lasers have become available. These have integral sealed mirrors, and are of lower price than the water-cooled variety. It is generally not possible to incorporate intracavity etalons .

The Kr^+ laser is of similar construction to the Ar^+ laser, but emits a strong line at 647.1nm. It also has less powerful emission lines at 520.8nm and 476.2nm. The coherence length is similar to the Ar^+ laser, and can be increased by using an etalon. Krypton lasers are generally considered to be less reliable than Argon lasers, but are the best source for high-power red light.

3.2.5 Dye Lasers

Dye lasers can be wavelength tuned within a specified range of wavelengths, depending on the dye used, and are therefore of great potential interest in multicolour holography where the exact choice of wavelengths is important—see §2.5. They must, however, be pumped by another powerful laser, and a total system can be costly and cumbersome. The reliability is steadily improving, and it seems that dye lasers will have an important future rôle in multicolour holography.

An interesting variation of the dye laser is the ring dye laser which produces extremely coherent output with a coherence length of kilometres.

3.3 WORKING SURFACE

The working surface used in display holography is probably the most important mechanical component and so must be chosen carefully. The rôle of the table is to allow the use of a wide range of recording geometries and to eliminate effectively movements and vibrations due to external factors.

3.3.1 Optical Research Tables

Purpose-built optical research tables usually consist of two parts: The table-top and the isolation legs. The top is typically 10″ thick and is designed to be resistant to distortions and to resonance arising from external forces. The bulk of the top is typically of a honeycomb structure, and the two surfaces are normally covered with steel plates of some 1/8″ thickness. One surface may have a matrix of tapped holes to allow the use of threaded poles to hold optics (§3.4.1). The outer surfaces of the steel tops are usually accurately flat, allowing work involving precise registration.

The isolation legs support the table-top via a set of air-filled pistons which absorb floor vibrations.

3.3.2 Engineering Tables

Engineering tables are made of solid iron, and have either integral or separate legs. The sur-

face is normally accurately machined flat. This type of table is less expensive than the research table, and is ideal for display holography. The table must, of course, be isolated from external vibrations. We have found that using partially inflated motor-cycle tyre inner tubes is effective in vibration isolation. Thick wooden boards can be used to distribute the load from each table leg onto the tubes.

3.4 MOUNTS FOR OPTICS

The main goals in the design of optical mounts are maximum stability and maximum versatility. These two requirements are often incompatible.

3.4.1 Rod Mounting

A system which provides good three dimensional flexibility of movement is to mount the optical components onto rigid vertical rods of typically 1″ diameter and 10″ height. The optics are placed on compatible 'riders' which can be moved up and down the rod and securely clamped. The rods can be positioned on the table either by using screw threads fitting directly into the table, or by mounting them on strong switchable magnets. The former is a more permanent method of mounting and is ideal when all or parts of a set-up need not be moved for long periods. The disadvantage is that the rods can only be placed at predetermined positions where tapped holes are provided.

The material used to manufacture the rods is an important consideration, as the shape of the rods renders them especially susceptible to vibration. Steel is the most popular material for such use.

3.4.2 Reduction of Vibrations and Movements

Detrimental vibrations and movements encountered in holography can be broadly divided into (i) component drift, (ii) air drift, and (iii) periodic vibrations:

3.4.2.1 Component drift

Continuous drift of optical components during a holographic exposure can be extremely deleterious to hologram recording, and can result in the total obliteration of the holographic record. This type of motion can only be eliminated by detailed attention to all parts of the optical mounts. In general, it is best to hold optical components with just enough force to prevent drift.

The stability of each component can be checked by incorporating it in a Michelson interferometer and observing the interference fringes. Component drift will then show up as steady movement of fringes in one direction. As a guide, the fringe movement should be less than, say, 1/8 of the fringe spacing for the duration of a typical exposure.

3.4.2.2 Air Drift

Air motion in the vicinity of a holographic set-up can cause changes in local air pressure, and thus in the local refractive index, which in turn can lead to undesirable optical path changes. Air drift can be minimised by placing a 'tent' over the optical table, and by placing baffles amongst the components to break up air currents. Using shorter component mounts also reduces the detrimental effect because, analogously to water flowing in a river, air currents near the table surface are slower than higher up. In a Michelson interferometer air drift shows up as random to-and-fro mo-

tion of the fringes.

3.4.2.3 Periodic Vibrations

Periodic vibrations can be picked up either by the table-top, or by the optical mounts. In both cases the optical path changes produced are roughly proportional to the height of the optical mounts. In a Michelson interferometer vibrations show up as a regular oscillatory motion of the fringes about a fixed position.

3.5 PLATEHOLDERS

Recording plates generally need to be held in a vertical position during exposure. A golden rule regarding plateholders is to apply the minimum force necessary to hold the plate in position. A plate that is under tension is prone to slow drift during exposure. If kinematic mounting is used, then any springs or clips holding the plate in position must be placed so that the plate is not under tension.

We have found that if a slight tilt of the plate is tolerable, a reliable way of holding the plate is not to hold it at all, but to lean it against a rigid support along the vertical edge, the lower edge resting on the table. This method ensures, of course, minimum tension in the plate. Abramson [18] has devised a simple kinematic mount by extending this method. The disadvantage is that the plate is held in a slightly tilted and rotated position, whereas in most quantitative work a vertical position is desirable.

3.6 MIRRORS

Mirrors should be front-surface coated, and be of the highest reflectivity so as to conserve light. A good variety is front-surface aliminium coating with an enhanced dielectric layer which increases the reflectivity and the durability. The most convenient mounting for mirrors is one with two adjustment screws allowing fine vertical and horizontal adjustment with no backlash.

3.7 BEAMSPLITTERS

The rôle of the beamsplitter is to divide a (usually unexpanded) laser beam into two parts. The ideal beamsplitter would be completely non-absorbing, continuously variable between 0% and 100% transmittance with no wavelength dependance, and would not deviate the transmitted or reflected beam as the ratio was changed. Beamsplitting can be achieved using different devices, and we shall consider each in turn:

3.7.1 Float Glass

The simplest beamsplitter is a piece of float glass. The reflectance depends on the polarisation and the angle of incidence of the laser light. at small angles of incidence ($< 30°$) both *s*– and *p*–polarisations have some 4% of their total intensity reflected from each glass surface. The thickness of the glass must be great enough to spacially separate the two reflected beams and thus to eliminate unwanted interference fringes. We have found that a thickness of $1/4''$ usually suffices. The ratio of reflected to transmitted light is often ideal for simple transmission holograms, one of

the reflected beams being used as the reference beam.

To help separate the two reflected beams a small angle wedge prism can be used. We have found, however, that this type of beamsplitter is not convenient to use because the direction of the transmitted beam changes if the beamsplitter is rotated, calling for major realignment.

3.7.2 Metal Coating

An inexpensive beamsplitter allowing higher reflectances is a piece of float glass coated with a thin semi-transparent layer of a metal such as aluminium, which may then be overcoated with a protective layer such as silicon dioxide.

One disadvantage of metal coatings is that they absorb a proportion of the incident light. When using low-power lasers—less than 200mW, say—the light absorption is not serious and simply results in light loss, but when higher intensity lasers are used the absorption can cause significant heating of the metal coating and thus bend the substrate, analogously to a bimetallic strip. We have observed optical path changes of several wavelengths caused by this effect. Because metal-coated beamsplitters do not depend on interference effects they are, to a good degree, wavelength-independent, making them suitable for multicolour work.

3.7.3 Graduated and Variable Metal Coatings

Different parts of the glass substrate may have diferent amounts of metal coating, either in discrete steps or in a continuously variable form. Different reflectances can be chosen either by moving the beamsplitter linearly in its own plane or, if the coating variation is annular, rotated in its own plane around a fixed point. In either case the mount must be free of 'wobble' so that beam ratios can be changed after final alignment of the recording system.

We have devised a convenient way to manufacture linearly variable aluminium-coated beamsplit ters in a vacuum deposition chamber. Aluminium is normally deposited by wrapping aluminium wire around a tungsten spiral and heating it until it melts and evaporates onto the glass substrate above the spiral. Normally the coating is quite uniform. By introducing a baffle between the spiral and the substrate, thus partially obscuring the substrate, a variation in the thickness of aluminium is obtained (Fig. 3.1). The rate of variation of thickness accross the substrate can be controlled by adjusting the vertical position of the baffle.

3.7.4 Dielectric Coating

Dielectric coatings do not absorb light and therefore do not have the problems associated with metal coatings. A useful beamsplitter is one with a 50% reflection coating on one side and an antireflection coating on the other. The reflective properties of dielectric coatings are normally wavelength dependent.

3.7.5 Polarisation Beamsplitters

Beamsplitting devices whose reflectance properties depend on the polarisation of the incoming beam are among the most convenient and versatile. There are several variations based on birefrin-gent crystals [19, 20], but one of the most convenient is the polarising cube beamsplitter:

3.9 COLLIMATORS

It is often desirable to use collimated reference beams, especially on 'master' holograms—§5.3. The choice of the collimating element depends on the quality of collimation required, and on the recording geometry used. Collimating elements can be reflecting, refracting or diffracting:

3.9.1 Reflecting Collimators

The parabolic mirror is probably the most common optical element used for collimation, and has been the traditional method of obtaining high-quality collimation in optical research. For perfect collimation a parabolic mirror must be used on-axis, in which case the expanding lens at the focal point impedes the centre of the collimated beam. This can be prevented by using an off-axis element, but such elements are usually costly. In practice, if the f–number of the mirror is greater than say $f/8$, an on-axis mirror can be used off-axis and, we have found, normally causes negligible aberrations in the holographic image. At such apertures it is even possible to use a mirror with a spherical profile without appreciable image degradation.

We have found that the main disadvantage of parabolic reflectors is that a large area is occupied on the recording table, and that the extra path length required increases the risk of hologram failure due to fringe movement. In addition, recording geometries are often cumbersome and inconvenient.

An important advantage of the reflecting collimator is that it is wavelength-independent, and is therefore particularly useful in multicolour work.

3.9.2 Refracting Collimators

Refracting collimators consist of simple or compound converging lenses. As collimating elements are usually relatively large, compound lenses for such use can be prohibitively expensive, and singlets are invariably used.

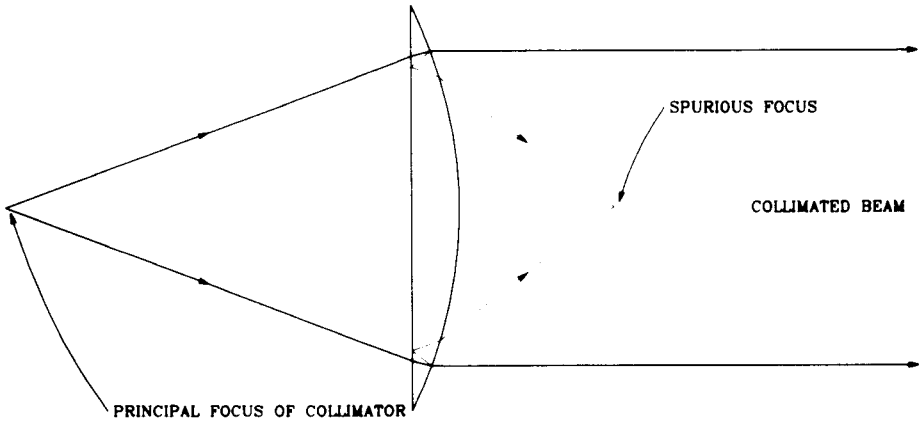

Fig. 3.2 Formation of the spurious focus from a plano-convex collimating lens.

3.9.2.1 Simple Spherical Lenses

As the lens is used on-axis, the only monochromatic aberration present is spherical aberration. The spherical aberration of a converging spherical lens used with an infinite conjugate—as in collimation—can be minimised by 'bending' [eg. 23]. The optimum shape is biconvex with one face having a much greater radius of curvature than the other. In fact a plano-convex lens is a close approximation to this 'ideal form', and the extra cost of producing the ideal form lens is rarely justified.

We have found that the plano-convex lens is an excellent collimator for display work, the transmissive nature allowing simple geometries to be used with relatively short path lengths. One pitfall to avoid is the weak spurious focus arising from unwanted reflections from both surfaces (Fig. 3.2). In our experience this is not a problem if the recording plate is placed a few inches inside or outside this focus. To eliminate the focus entirely, anti-reflection coatings can be used.

It is generally desirable to use lenses of short focal length so that the optical path lengths are minimised. As the f–number is decreased, however, spherical aberration increases. The choice of f–number is therefore a compromise. We have found that plano-convex lenses with an f–number of 3 or 4 produce good collimation for display work. Smaller f–numbers start to show unacceptable aberrations at the edges.

3.9.2.2 Aspheric Lenses

The spherical aberration present in a converging singlet can only be completely eliminated by using an aspheric surface. Although this is prohibitively costly on glass elements, plastic lenses with aspheric surfaces can be competitively priced.

3.9.3 Diffracting Collimators

A collimated beam can be holographically recorded to form a holographic optical element (HOE) which can act as a collimator. Fig. 3.3 shows possible recording and reconstruction arrangements. The HOE must have high efficiency and low scatter noise, as any noise present is recorded in the final hologram. One way to reduce the noise recorded in the final hologram is to increase the distance between the HOE and the hologram. Any grain noise reduces in intensity as the distance between the two elements is increased, the intensity of the collimated beam remaining constant.

The advantages of holographic collimators are that they are relatively light in weight, and that a broad collimated beam can be obtained on a small table. The disadvantages are that they are strongly wavelength dependent and therefore inappropriate for colour holography, and that they can increase the background noise in the final hologram.

Holographic collimators can also be manufactured using two diverging beams. By reconstructing the recorded beam using a longer reconstruction beam a collimated beam can be produced. This type of HOE always produces aberrations. Using Eqn. 2.9, if $R_I = \infty$,

$$\frac{1}{R_c} = \mu\left(\frac{1}{R_r} - \frac{1}{R_o}\right) \tag{3.1}$$

where R_c is the effective focal length of the HOE.

HOE's can add versatility to recording arrangements. Fig. 3.4 shows a possible compact arrangement which could produce large holograms with a collimated reference beam. The HOE is some 10% efficient, allowing most of the incident beam to fall on the object. Small adjustments to the beam ratio may be achieved by slightly tilting the HOE thus violating the Bragg condition.

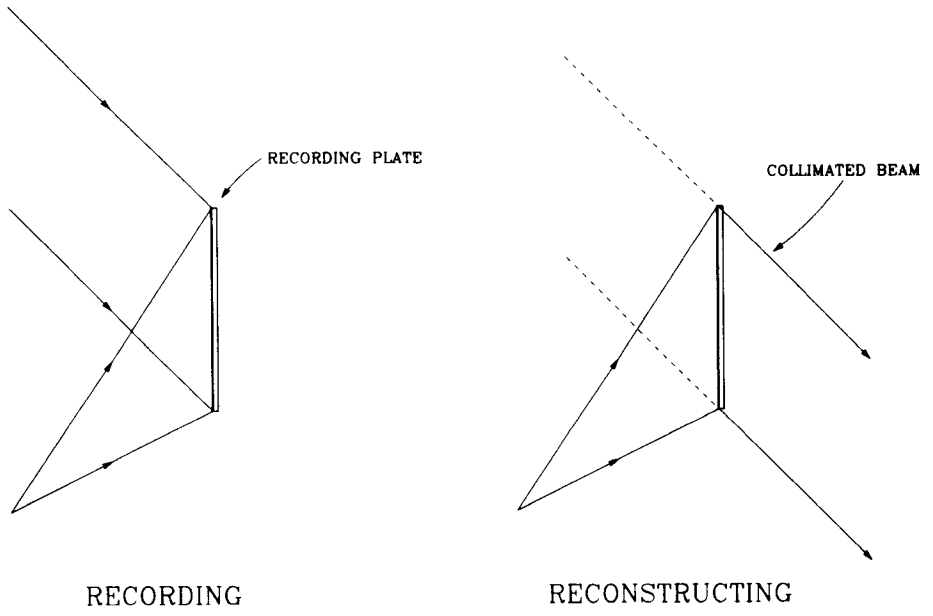

Fig. 3.3 Manufacturing a Holographic Optical Element (HOE) to act as a collimator.

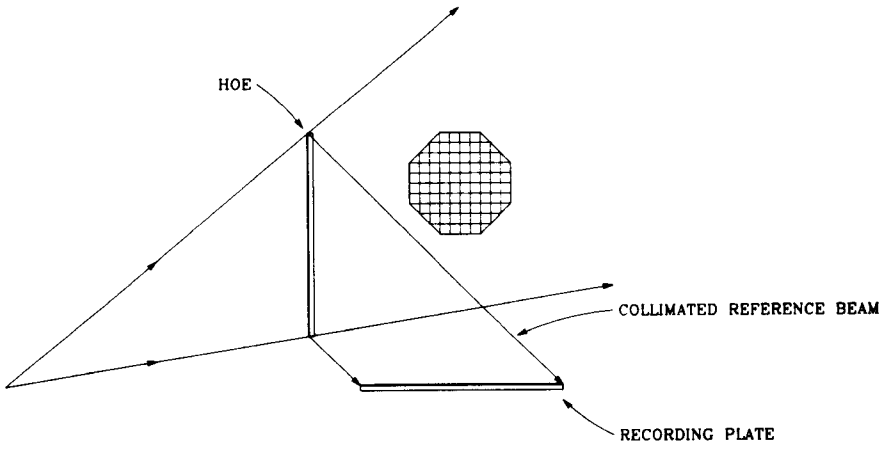

Fig. 3.4 An example of including a HOE in a recording system.

3.10 A VERSATILE SYSTEM FOR DISPLAY HOLOGRAPHY

Based on the above observations on the requirements of components in display holography we have designed and constructed a simple system which, within its limitations, is very simple to use and produces excellent holograms of most types, using both one-step and two-step techniques.

3.10.1 The Overall Concept

The system is designed to be used on a flat, stable iron or steel table top and comprises a number of simple components on permanent or switchable magnetic bases. The maximum size of the hologram to be made is 4″×5″, placed in 'landscape' mode—ie. with the longer edge horizontal—one edge being adjacent to the table. All beams travel horizontally, centred at 2″ above the table, and all components are centred at this height (Fig. 3.5). We shall consider each component in the system:

3.10.2 Laser

We have used a 5mW cylindrical He–Ne laser mounted such that its axis is precisely horizontal and at 2″ above the working surface. The laser is rotated in its mount such that the polarisation is horizontal.

3.10.3 Mirrors and Beamsplitters

Mirrors and beamsplitters are mounted on permanent magnets such that their surfaces are accurately vertical with respect to the base of the magnets. (The angular tolerance on the mounting is of the order of 1 mrad.) When these components are placed on the table, the reflected laser beams are automatically directed horizontally. Any small beam deviations can be corrected by the fine adjustments on the beam expanders.

3.10.4 Beam Expanders

Microscope objective and spatial filter assemblies are again mounted, this time on switchable magnetic bases with the optical axis horizontal and at 2″ above the table. Two fine adjustment screws on the objective holder allow correction of errors in mirror and beamsplitter assemblies.

3.10.5 Collimators

For collimation, $f/4$ plano-convex singlet lenses are used, with a diameter of 4″. These are mounted vertically, directly above the working surface.

3.10.6 Plateholders

We have chosen to hold the plates along one vertical edge, by pressing some 1/4″ of one edge against a milled flat surface, using a strong 'bulldog' clip. The horizontal edge of the plate rests on the table and the free vertical edge can be prevented from vibrating by putting a small magnet against it—this is usually found to be unnecessary.

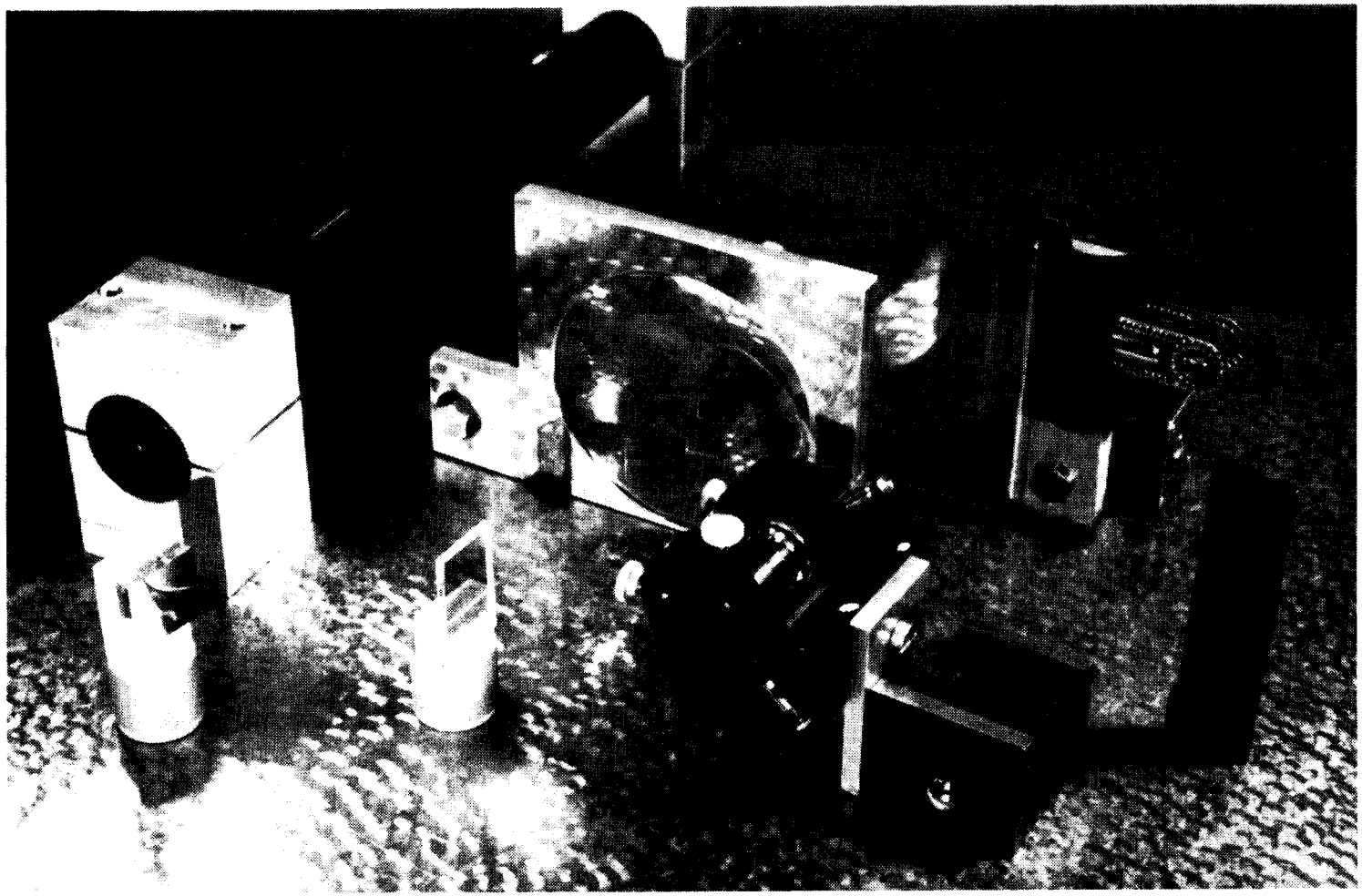

Fig. 3.5 A versatile system for display holography (§3.10). *Back row, left to right:* Laser, collimating lens, plateholder. *Front row, left to right:* mirror, beamsplitter, beam expander, baffle.

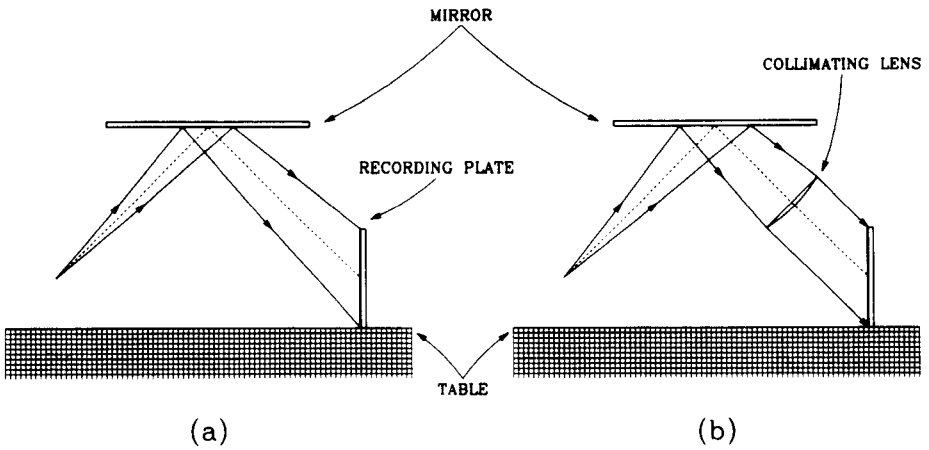

Fig. 3.6 Convenient methods of providing an overhead reference beam: (a) Diverging reference beam; (b) Collimated reference beam.

3.10.7 Baffles

Small black-anodised rectangular aluminium baffles are used, each held vertically by a small permanent magnet.

3.11 OVERHEAD REFERENCE BEAMS

It is convenient that holograms for display are illuminated from above or, less commonly, from below. This convention ensures that the observer is never in direct visual line of the illuminating light while moving in a display area and, in the case of reflection holograms, that the illuminating light is never impeded by the observer. This means that when the hologram is recorded, either the reference beam must travel in a vertical plane, or the objects must be placed on their side. Experience has shown that it is generally difficult and time consuming to use the latter method, and that if a recording set-up is to be used routinely to record such display holograms, it is worthwhile setting up an overhead reference beam. One important practical advantage is that space on the table is freed for complex illumination of the object using several illuminating beams.

There are, of course, many ways of providing an overhead reference beam. One method that reduces the height to which components must be raised is to 'fold' an expanded beam with a large mirror (Fig. 3.6*a*). For a collimated beam a plano-convex lens can be inserted (Fig. 3.6*b*). Such constructions are unorthodox on an optical table, and the stability of the raised components must be monitored carefully. Compensation of vibrations can be achieved to some extent by reflecting a part of the path of the object beam from the same mirror.

3.12 RECORDING MATERIALS

With the exception of dichromated gelatin (§8.5.3), The only material presently suitable for display holography is fine-grained silver halide emulsions, with a substrate of glass or flexible plas-

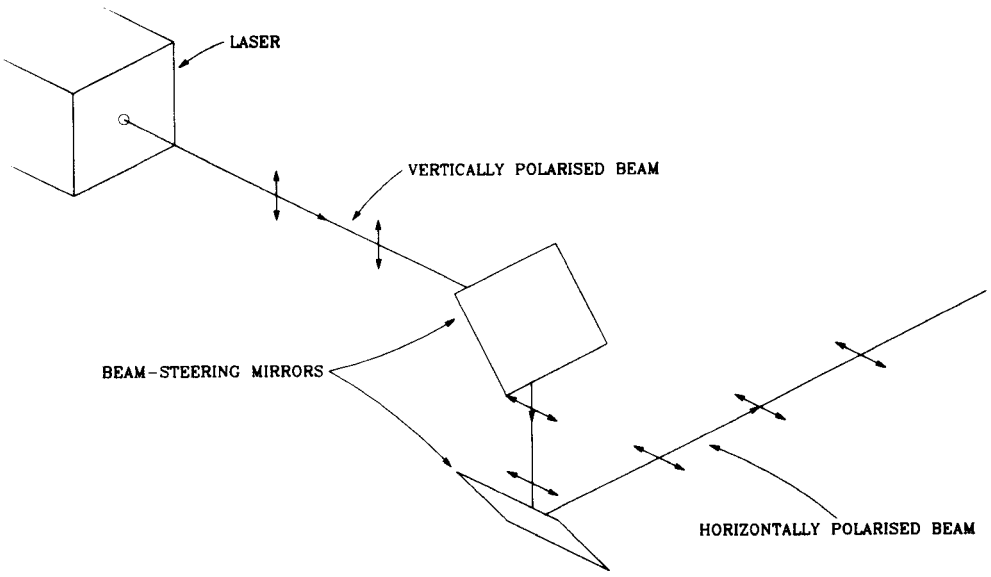

Fig. 3.7 Rotating the polarisation of a laser beam using two beam-steering mirrors.

tic. It is naturally far easier to hold a glass plate steady than flexible film, although the latter is gaining popularity because of the obvious handling advantages of the final hologram. Holographic emulsions are commercially produced by Agfa–Gevært and by Kodak, although other photographic companies such as Ilford and Fuji have recently shown interest.

In the United Kingdom only two emulsions are readily available for display holography, namely 8E75HD (red sensitive) and 8E56HD (blue-green sensitive), both made by Agfa–Gevært. At present no suitable panchromatic materials are commercially available.

3.13 ROTATING POLARISATION

The direction of polarisation of the laser beam can be controlled by several methods:

3.13.1 Rotating the laser

With small tubular lasers it is it is simplest merely to rotate the laser in situ until the desired polarisation is obtained. This is not convenient, however, if frequent polarisation control is required.

3.13.2 Beam-steering units

A 90°rotation of the polarisation can be obtained with a two-mirror beam-steering unit. This method is often convenient in rotating the normally vertical polarisation of powerful Ion lasers to obtain horizontal polarisation (Fig. 3.8).

3.13.3 1/2–wave plates

The most vesatile method of polarisation control is to use a 1/2–wave plate in a rotating mount. The polarisation can be continuously rotated by rotating the plate in its own plane.

CHAPTER 4

LASER TRANSMISSION HOLOGRAPHY

4.1 INTRODUCTION

A laser transmission hologram is defined as a transmission hologram which can only be satisfactorily viewed using a coherent light source such as a laser. It is the simplest type of display hologram to manufacture, and is produced in a single step. The image produced from a laser transmission hologram illuminated by a laser is sharp for any image depth.

The essential illumination requirements for the object and the recording plate are shown in Fig. 4.1. A diffusely reflecting object is illuminated by one or more expanded beams, and a reference beam illuminates the plate directly. Some variable parameters are the wavelength of the recording light, the angle of incidence of the reference beam at the plate—the reference angle, the state of polarisation of the beams, and the recording material.

4.2 RECORDING GEOMETRY

4.2.1 Single Object Beam

The precise geometry of the recording set-up for a laser transmission hologram is, of course, infinitely variable. We have investigated different possible configurations and we prefer a 'parallelo-

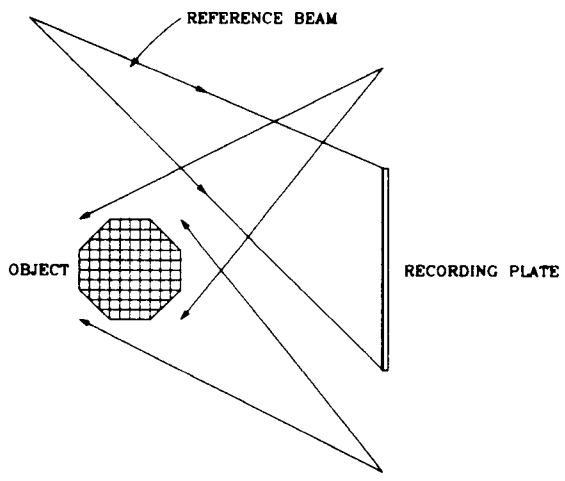

Fig. 4.1 Basic arrangement for recording a transmission hologram.

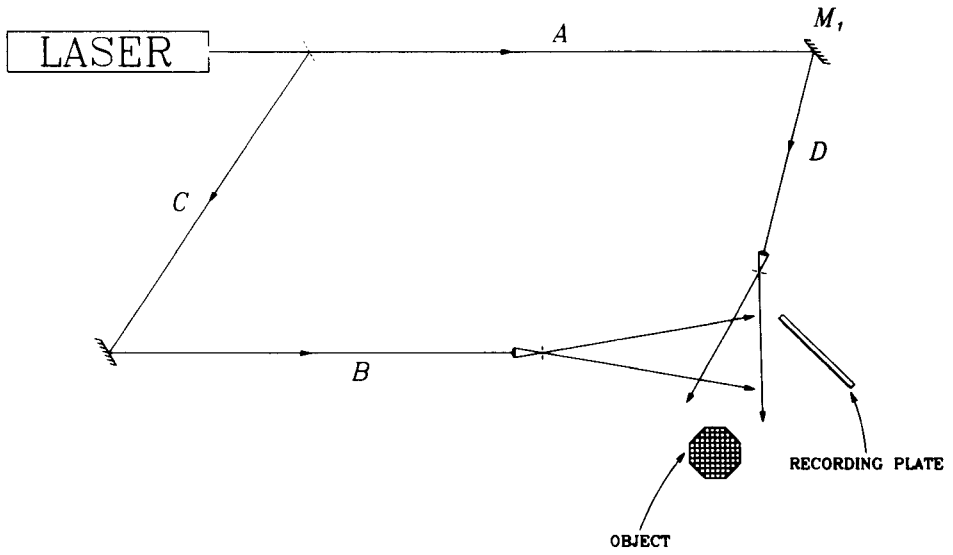

Fig. 4.2 The recommended 'parallelogram' arrangement for recording a transmission hologram.

gram' arrangement [24], as shown in Fig. 4.2, for the following reasons:

(a) Optical Components Required

The number of optical components required for this configuration is small, comprising, in the simplest case, one beamsplitter, two mirrors and two expanding lenses. The risk of failure due to vibration or movement of components is therefore minimised.

(b) Table Vibrations

If a rectangular metal table is used, one source of vibration in the optical system is resonance in the table-top. The simple modes of oscillation in a rectangular table-top have nodes and antinodes that lie parallel to its edges. In the parallelogram arrangement the optical path changes are roughly equal in the two arms of the set-up, and therefore roughly cancel. In Fig. 4.2 arm A cancels out such optical path changes in arm B and arm C cancels out those in arm D. If arms A and B are close to one another then the effects of air turbulence may also, to some extent, be compensated.

(c) Object Background

In the parallelogram arrangement of Fig. 4.2 there are no optical components behind the object, when the latter is viewed from the recording side. The background is therefore completely black. In most other arrangements baffles have to be strategically positioned to produce a black background.

(d) Matching Optical Paths

To obtain good fringe visibility on the hologram, the object and reference optical paths from the beamsplitter to the recording plate must not differ by more than the coherence length of the laser. In the parallelogram arrangement, due to symmetry, the optical paths are approximately matched automatically. Any mismatch can be corrected by moving the mirror M_1.

4.2.2 Double Object Beam

When good illumination of the object is required, one object illuminating beam is often insufficient, and extra illuminating beams are used. The optical path lengths of all the beams must be matched. The parallelogram arrangement can be easily modified to a double object beam set-up by placing an extra beamsplitter in the path of the original object-illuminating beam—Fig. 4.3. The advantage of deriving the extra object beam from the original object beam rather than from the reference beam is that if a different beam ratio is required, and the reflectance of BS_1 is varied, the ratio of the intensities of the two object-illuminating beams remains unchanged.

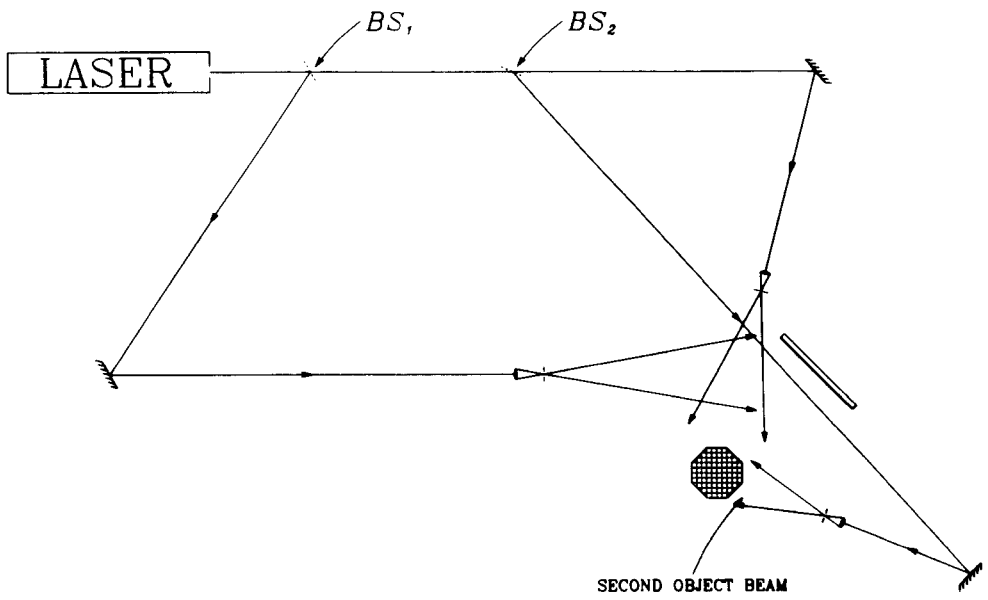

Fig. 4.3 Adaptation of the parallelogram arrangement for two-beam object illumination.

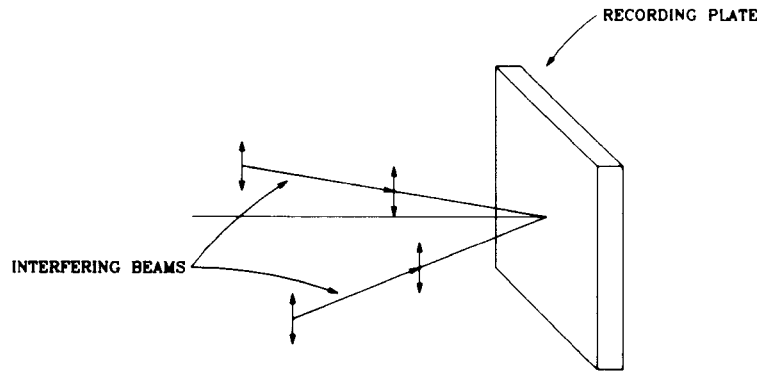

Fig. 4.4 Two beams in *s*–polarised mode.

4.3 POLARISATION

Two electromagnetic waves can only interfere if they are polarised in the same direction. If the polarisations of the two waves are mutually perpendicular, no interference takes place. The degree of interference, and hence the visibility of the fringes, is proportional to the cosine of the angle between the directions of polarisation of the interfering beams.

It is usually recommended that when recording a hologram, the beams should be *s*–polarised with respect to the recording plate. The reason for choosing this mode of polarisation is that the directions of polarisation of the two beams are then independent of the inter-beam angle—Fig. 4.4.

If the beams are *p*–polarised, the angle between the directions of polarisation is equal to the angle between the directions of propagation. If the beams are travelling at 90° to one another, no interference takes place. It is often incorrectly asserted that if the light beams are travelling in space at 90° to one another and are *p*–polarised with respect to the recording plate, then no interference fringes are recorded. In fact, although no interference is observed if the plate has unit refractive index, for any other refractive index, typically 1.54, the beams are refracted and are no longer mutually perpendicular (Fig. 4.5). We can define a polarisation attenuation factor F_{pol} which is equal to the cosine of the included angle in the recorded medium. Suppose two *p*–polarised beams are incident at θ_1 and θ_2 upon the recording medium which has a refractive index n. The corresponding angles in the medium are:

$$\theta_1' = \sin^{-1}\left(\frac{\sin\theta_1}{n}\right)$$

and

$$\theta_2' = \sin^{-1}\left(\frac{\sin\theta_2}{n}\right).$$

The attenuation factor is then given by

$$F_{\text{pol}} = \cos\left[\sin^{-1}\left(\frac{\sin\theta_1}{n}\right) - \sin^{-1}\left(\frac{\sin\theta_2}{n}\right)\right]. \tag{4.1}$$

We now consider two *p*–polarised beams travelling at 90° to one another in free space, and incident symmetrically upon a recording medium such that $\theta_1 = -\theta_2 = 45°$. If $n = 1.54$ then $F_{\text{pol}} = 0.58$. The fringe visibility is therefore only reduced by some 40%. Fig. 4.6 shows the variation of F_{pol} with the included angle in air for two *p*–polarised beams symmetrically incident upon the recording medium. A minimum F_{pol} of 0.16 occurs when both beams are at grazing incidence.

When using *p*–polarised light to record a hologram of an extended diffuse object, there is no fixed angle of incidence for the light impinging on the hologram from the object. In Fig. 4.7, for example, the minimum and maximum angles of incidence are shown as θ_{min} and θ_{max}. F_{pol} is variable accross the hologram, and for each object point considered. The brightness of the image upon reconstruction is therefore also variable. To obtain an expression for the maximum and minimum F_{pol}, let us consider the simplified arrangement in Fig. 4.8. We assume that the reference beam is collimated and is incident at angle θ_r, and that the object is only extended laterally and is of dimension S_O. If S_H is the size of the holographic recording plate, and it is separated from the object by a distance D, then

$$\theta_{max} = \tan^{-1}\left(\frac{S_H + S_O}{2D}\right)$$

and

$$\theta_{min} = -\theta_{max}.$$

Then

$$(F_{\text{pol}})_{max} = \cos\left[\sin^{-1}\left(\frac{\sin\theta_r}{n}\right) - \sin^{-1}\left(\frac{\sin\theta_{max}}{n}\right)\right]$$

and

$$(F_{\text{pol}})_{min} = \cos\left[\sin^{-1}\left(\frac{\sin\theta_r}{n}\right) - \sin^{-1}\left(\frac{\sin\theta_{min}}{n}\right)\right].$$

In a typical set-up where $\theta = 45°$, $S_H = 20\text{cm}$, $S_O = 10\text{cm}$ and $D = 30\text{cm}$,

$$(F_{\text{pol}})_{min} = 0.72 \quad \text{and} \quad (F_{\text{pol}})_{max} = 0.98.$$

The maximum variation accross the hologram is therefore some 25%, which can be acceptable in display work. The advantages of using p–polarisation are discussed in §4.6.

4.4 DEPOLARISATION BY OBJECT

Most diffusing objects depolarise any incident polarised radiation, while metallic and other specularly reflecting objects retain the original polarisation. Depolarisation reduces the fringe visibility on the hologram. The diffused light can be repolarised in the original direction by placing a polarising screen between the object and the plate, although this is rarely convenient and leads to more problems arising from reflections from the surfaces of the polarising screen, and the degradation of the image due to imperfections in the screen. The depolarised light contributes only to fogging the plate. As the diffused object beam is normally much less intense than the reference beam, the effect is usually negligible.

Such depolarisation can be used to advantage in display holography to change the apparent texture of the object. Most objects have areas which reflect the light in the original polarisation—'shiny' areas, and those which depolarise—'matt' areas. If we choose an object illuminating beam which has a polarisation orthogonal to that of the reference beam, then the 'shiny' areas are eliminated, as the specularly reflected component does not interfere with the raference beam. The object then appears completely matt in the reconstructed image. Quite dramatic changes in object appearance can be obtained with very shiny objects.

4.5 BEAM RATIO

The beam ratio, K, is defined as the ratio of the intensity of the reference beam to that of the object beam, as measured at the recording plate ($K = I_R/I_O$). The visibility of the interference fringes recorded on a hologram is maximum when the beam ratio is equal to unity. When the object beam is purely specular, eg. when making a holographic optical element, a unit beam ratio is usually the best to use. With diffuse objects, however, the problem of intermodulation noise arises. This is

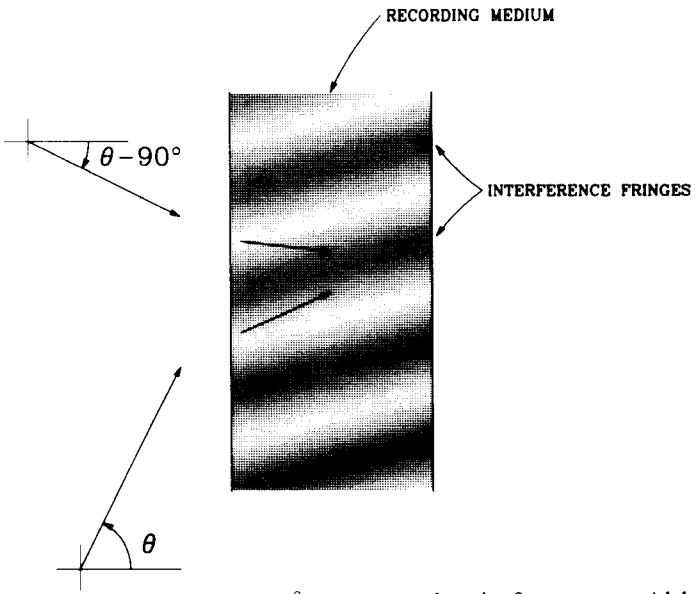

Fig. 4.5 Two *p*–polarised beams travelling at 90° to one another in free space. Although they cannot interfere in free space, in a recording medium they are refracted so that interference can take place.

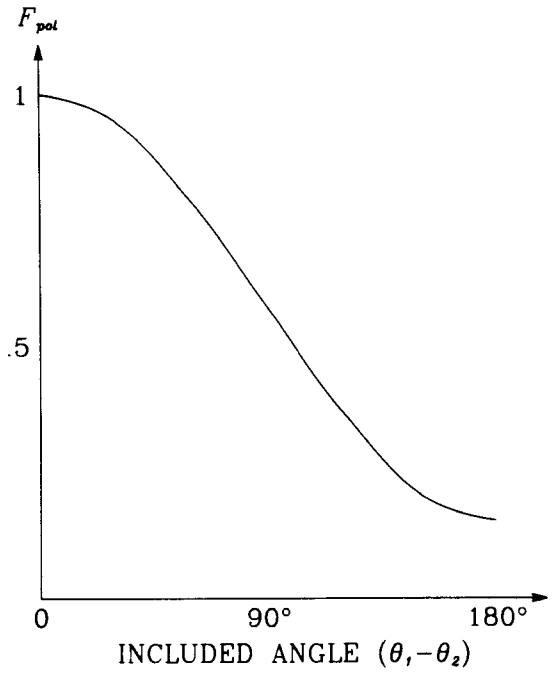

Fig. 4.6 Dependence of the polarisation attenuation factor F_{pol} (see §4.3) on the included angle between two *p*–polarised beams.

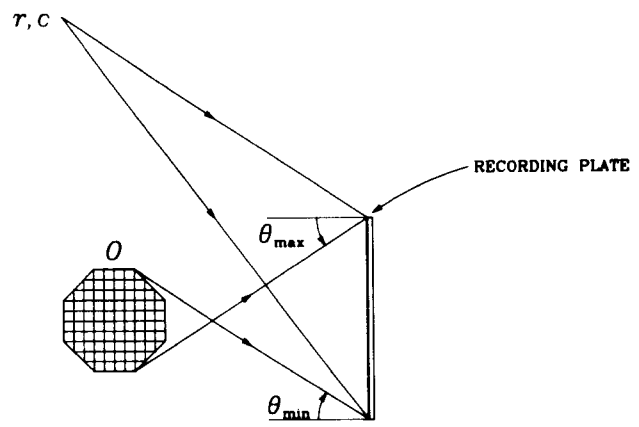

Fig. 4.7 Minimum and maximum angles of incidence of an object at a recording plate.

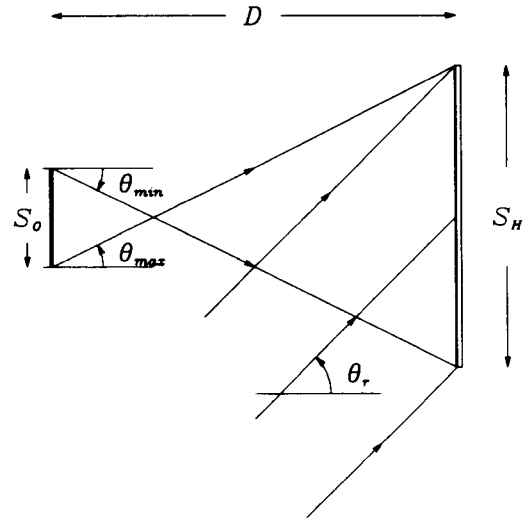

Fig. 4.8 Arrangement for calculating minimum and maximum F_{pol} for an extended diffuse object.

due to significant self-interference between different parts of the object. In amplitude holograms this normally results in a low-frequency component hologram, and the noise produced is confined to haze around the reference beam. In phase holograms the noise is more problematic, and one component of it surrounds the image [25]. This noise can be reduced by increasing the beam ratio. The exact beam ratio used is a compromise between brightness—low K—and low noise—high K.

Another argument for using a beam ratio greater than unity is that the linear part of the transmittance–Exposure (t–E) curve is used and so the transmittance is sinusoidally varying. Such a variation has the property that only first order diffraction occurs in reconstruction. In most cases in display holography, however, this argument does not apply— firstly, most display holograms are

bleached and are therefore primarily phase holograms which are *inherently* non-linear [25], and secondly, even when unbleached holograms are used, at the usually large reference angles higher order diffraction orders *and* the -1 order (conjugate wave) are either imaginary or are suppressed by Bragg angle violation.

The beam ratio we normally use in laser transmission work is between 3 and 10.

4.6 ELIMINATION OF UNWANTED REFLECTIONS

When a transmission hologram is recorded on a photographic plate, part of the transmitted reference beam may be reflected from the back of the plate. This results in course interference fringes on the emulsion which can be distracting when the image is viewed. If the recording plate has an anti-halation backing the back-surface reflection is eliminated. However, most commercial holographic recording materials have no such backing (so that they can be used in reflection holography).

To eliminate unwanted reflections the back surface of the plates can be index-matched to a black material. One way to achieve this is to coat the back of the plate with black paint and to scrape it off after exposure. More convenient methods are to use a lacquer paint that can be peeled off easily [26], or to adhere black PVC masking tape to the rear side of the plate [27].

Another way to reduce unwanted back-surface reflections is to p–polarise the object and reference beams. The intensity of the reference beam on the plate is normally much greater than that of the object beam and the back-surface reflections due to the object beam can be neglected. The reflections due to the reference beam are smaller when p–polarised. If the reference beam impinges on the the recording plate at incidence angle θ, then the angle of refraction in the glass substrate is θ', such that

$$n \sin\theta' = \sin\theta,$$

where n is the refractive index of the glass. If the intensity of the light incident on the glass–air interface is I_i and the intensity reflected is I_r, then the reflectance R is defined as

$$R = \frac{I_r}{I_i}.$$

For p–polarised light the reflectance is [28]

$$R_p = \frac{\tan^2(\theta - \theta')}{\tan^2(\theta + \theta')}, \tag{4.2}$$

and for s–polarised light it is

$$R_s = \frac{\sin^2(\theta - \theta')}{\sin^2(\theta + \theta')}. \tag{4.3}$$

If we let $n = 1.5$ and $\theta = 45°$, then $R_p = 0.01$ and $R_s = 0.09$, so that for p–polarisation only 1% of the transmitted reference beam is reflected. The unwanted interference fringes now have negligible visual effect. We have found that this advantage of p–polarised light outweighs the disadvantages discussed in §4.3. In all of our display work we have therefore adopted p–polarisation.

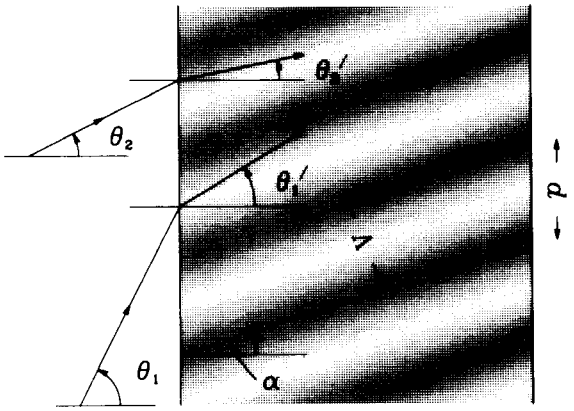

Fig. 4.9 Calculation of the resolution required of the recording material (§4.7).

4.7 RESOLUTION OF THE RECORDING MEDIUM

Fig. 4.9 shows two phase-related collimated beams of wavelength λ interfering, the fringes being recorded in a medium of refractive index n. The beams are incident at angles θ_1 and θ_2 and are refracted to θ_1' and θ_2' respectively. If $\lambda' = \lambda/n$ is the wavelength of the light in the medium, the spacing between the fringes in the recording medium is

$$\Lambda = \frac{\lambda'}{2\sin\left(\frac{\theta_1'-\theta_2'}{2}\right)}$$

$$= \frac{\lambda}{2n\sin\frac{1}{2}\left[\sin^{-1}\left(\frac{\sin\theta_1}{n}\right) - \sin^{-1}\left(\frac{\sin\theta_2}{n}\right)\right]}. \tag{4.4}$$

As an example, if $n = 1.5$, $\lambda = 550$nm, and θ_1 and θ_2 are 45° and 0° respectively, then $\Lambda = 7.55 \times 10^{-4}$mm. The resolution of the plate must be greater than $1/\Lambda$, ie. 1325 lines/mm. Most commercial recording materials have resolutions well above this value.

The orientation of the fringes inside the recording medium is

$$\alpha = \frac{\theta_1' + \theta_2'}{2}.$$

If the recording medium is thin, then the effective fringe spacing is

$$d = \frac{\Lambda}{\cos\alpha}$$

$$= \frac{\lambda'}{2\sin\left(\frac{\theta_1'-\theta_2'}{2}\right)\cos\left(\frac{\theta_1'+\theta_2'}{2}\right)}$$

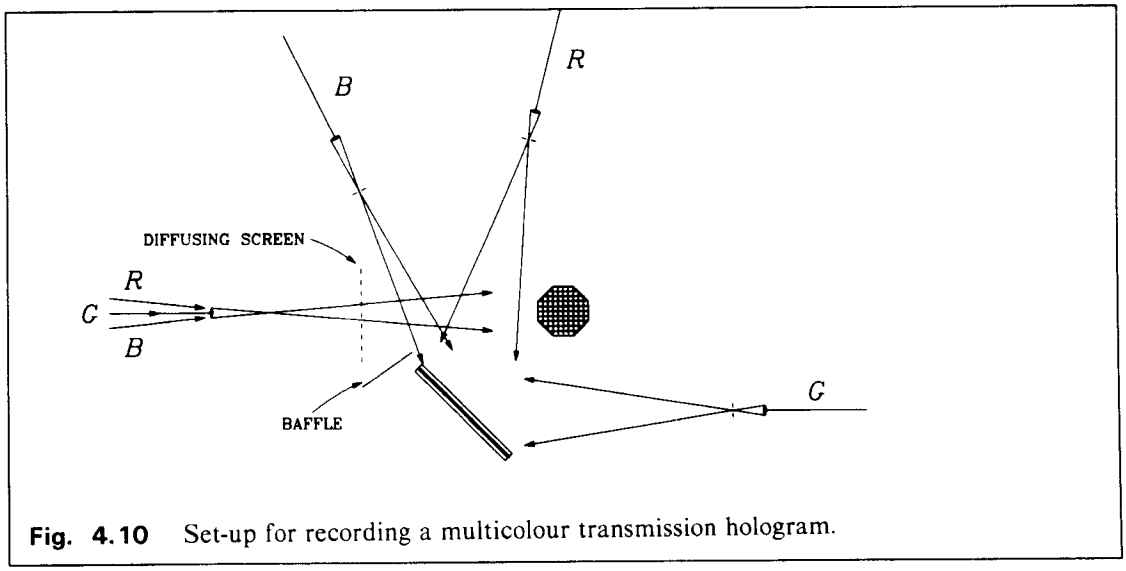

Fig. 4.10 Set-up for recording a multicolour transmission hologram.

$$= \frac{\lambda'}{\sin\theta_1' - \sin\theta_2'}$$

$$= \frac{\lambda}{\sin\theta_1 - \sin\theta_2}. \tag{4.5}$$

The effective grating fringe spacing is therefore independent of the refractive index of the recording medium, and when a symmetrical arrangement is used, ie. when $\theta_2 = -\theta_1$,

$$d = \frac{\lambda}{2\sin\theta_1}. \tag{4.6}$$

In this case $\alpha = 0^\circ$ and the fringes are perpendicular to the emulsion surface.

4.8 PROCESSING CHEMISTRY

The processing chemistry for exposed holographic emulsions is a young field and progress is rapidly being made. We have tried several published processes and we have standardised on one that seems to be reliable and produces good results. The process we use is published by Agfa–Gevært [29] for processing their emulsions. It is based on the original work of Phillips et al. [30]. For transmission work we expose the plates to a density of about 1.5 before bleaching.

4.9 MULTICOLOUR HOLOGRAMS

Laser transmission holography can be used to produce very high quality multicolour images. The simplest method is to superimpose several monochromatic holograms, each recorded with a different wavelength, but with identical recording geometries. The disadvantage is the production of unwanted spurious images due to each wavelength being diffracted from all component holograms during reconstruction ('cross-talk'). This can be avoided by using different reference beam angles for each wavelength—see ref. [8] for detailed bibliography. We have produced high quality multicolour images using this technique. The arrangement used is shown in Fig. 4.10. Three wavelengths

were used, namely 476.5nm, 514.5nm and 632.8nm. The respective reference beam angles were 70°, −45° and 30°. These angles were carefully chosen so as to minimise 'cross-talk' between different wavelengths—eg. the combined effect of angle and wavelength difference between the red and blue beams makes cross-talk less likely than if the reference angles were identical, the Bragg mismatch being greater in the former case.

The recording meterials used were Agfa–Gevært 8E75HD and 8E56HD plates, sandwiched emulsion to emulsion. After simultaneously exposing the plates they were separated, processed, and replaced in register in their original positions. Some examples of the results achieved are shown in Plate II.

CHAPTER 5

IMAGE-PLANE HOLOGRAPHY

5.1 INTRODUCTION

Image-plane holography—also called focused-image or full-aperture holography—is the technique of recording a transmission hologram with the recording medium lying within a shallow real image projected by an optical system. The optical system may be a conventional one [31–33], comprising lenses and/or mirrors (one-step image-plane holography) or may itself be a hologram [34]—two-step image-plane holography.

Because the recorded image points are close to the surface of the hologram, spatial and temporal coherence requirements on the light source are relaxed. For image depths of say 2cm, a quasi-point source of white light can be used for image reconstruction.

5.2 ONE-STEP IMAGE-PLANE HOLOGRAPHY

The basic arrangement for one-step image-plane holography is shown in Fig. 5.1. In the simplest

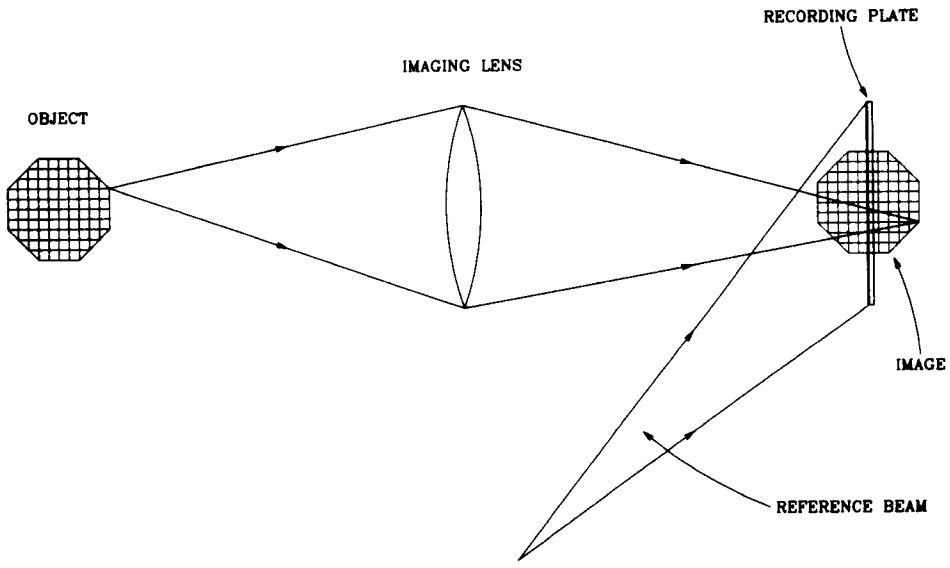

Fig. 5.1 Basic arrangement for recording a one-step image-plane hologram.

case a converging lens is used to form a real image of the object in the vicinity of the recording plate. We shall later consider other arrangements using spherical mirrors (§§5.2.2–5.2.3).

5.2.1 Vignetting and Field of View

The image produced by a one-step image-plane hologram normally exhibits severe vignetting.

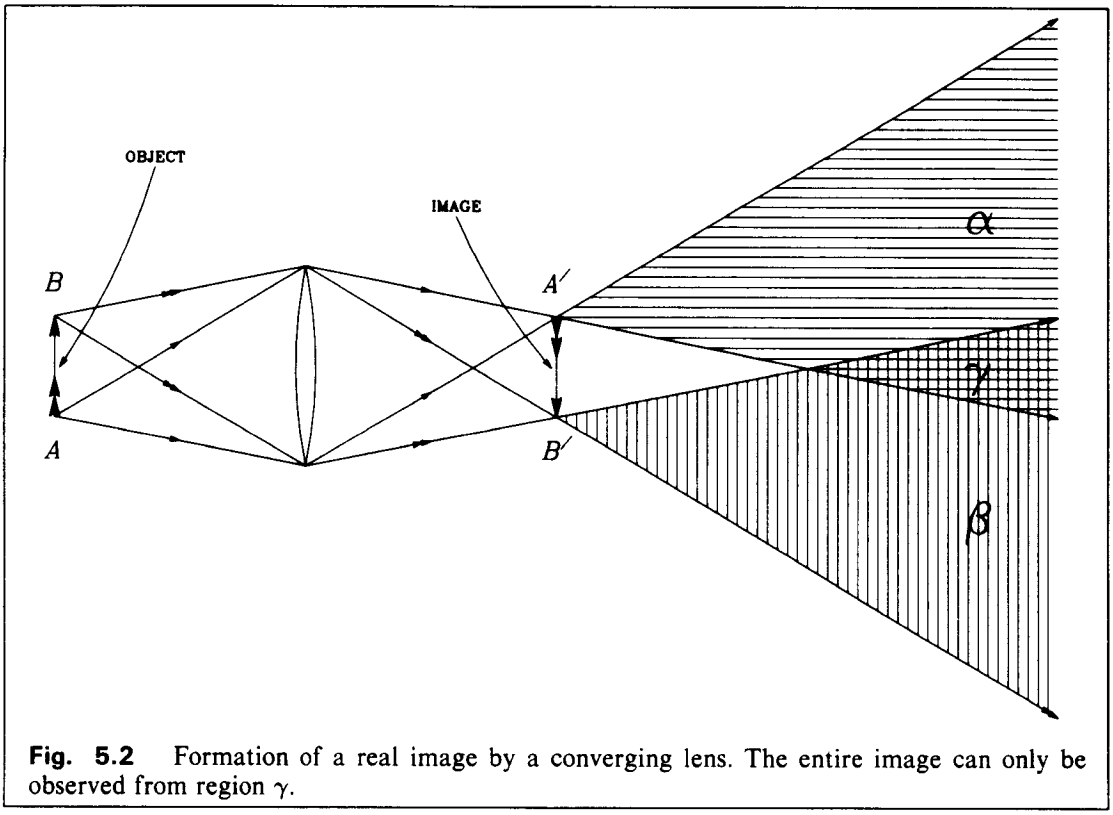

Fig. 5.2 Formation of a real image by a converging lens. The entire image can only be observed from region γ.

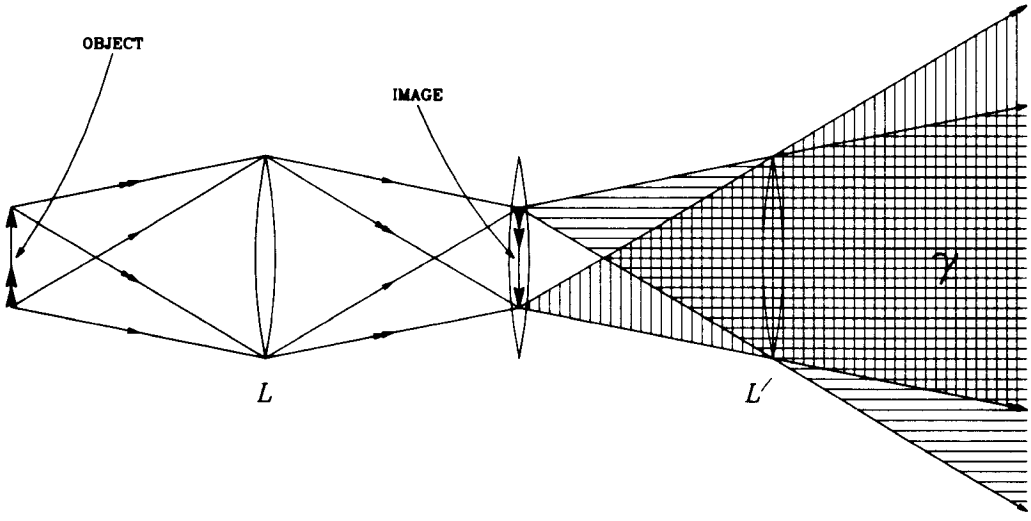

Fig. 5.3 Increasing the field of view by using a field lens in the image plane.

This can be appreciated by considering the imaging system in Fig. 5.2. A converging lens L produces a real image I of the object O. If the image is viewed by an observer to the right of I, the whole of the image can only be simultaneously viewed from certain positions [35–36]. The extremity A of the object, which is imaged onto A', can only be viewed when the observer is in the region α, and analogously, B' can only be viewed from region β.

To observe simultaneously both extremities and thus the whole of the image, the observer must be positioned in the narrow region γ. Such constraint is not normally desirable. One solution is to place a field lens in the image plane, prior to the photosensitive plate [37, 38]. This lens produces a real image L' of the imaging lens L, through which the whole of the image is observable (Fig. 5.3). The region γ is now much larger than before and the projected image can comfortably be viewed when both eyes are in this region. A further advantage of using a field lens is that the longitudinal magnification produced by the imaging system is reduced. A serious disadvantage is that the reference beam must pass through the field lens to reach the hologram, and off-axis aberrations are thus introduced.

Another elegant method of eliminating vignetting is to use a short reference beam and a long reconstruction beam [38, 39] (Fig. 5.4). The change in beam divergence has a focusing effect which produces similar results to the previous method. We have found that this method works well and is convenient, in that collimating optics in the reference beam are not required during recording. One problem, however, is that the change in reconstruction angles near the edges of the plate may violate the Bragg condition, and thus some wavelengths may be preferentially diffracted. For example, the centre of the image can appear achromatic while the upper portion has a reddish tint and the lower portion has a bluish tint. It is recommended, therefore, that the imaging lens has a large diameter and focal length so that smaller adjustments to the reconstruction beam are necessary.

5.2.2 Concave Mirror Imaging System

Large lenses with small f–numbers are cumbersome and expensive, and there is therefore a limit to the field of view attainable with a converging lens system. It is possible to increase the field of view by using large spherical mirrors. The mirror is used at unit magnification, slightly off-axis (Fig. 5.5). As the imaging properties are wavelength-independent, the system is ideal for multicolour holography [40]. The techniques for increasing the field of view outlined in §5.2.1 are, of course, applicable to mirror imaging systems.

The disadvantages of the single-element mirror system are that the image is mirror-reversed in the final hologram, and that some off-axis aberrations are present.

5.2.3 Mirror-Beamsplitter Imaging Systems

An imaging system that produces a low-aberration, non-reversed image is the spherical mirror-beamsplitter system shown in Fig. 5.6. The image is produced on-axis, and the aberrations are therefore small, but because of the beamsplitter component the maximum transmission through the system is 25%.

5.3 TWO-STEP IMAGE-PLANE HOLOGRAPHY

To obtain an image with less distortion and larger field of view than in the previous method, a two-step technique is used. This involves the production of a 'master' hologram, the real primary image from which is holographically recorded in or near the plane of a secondary plate [34]—

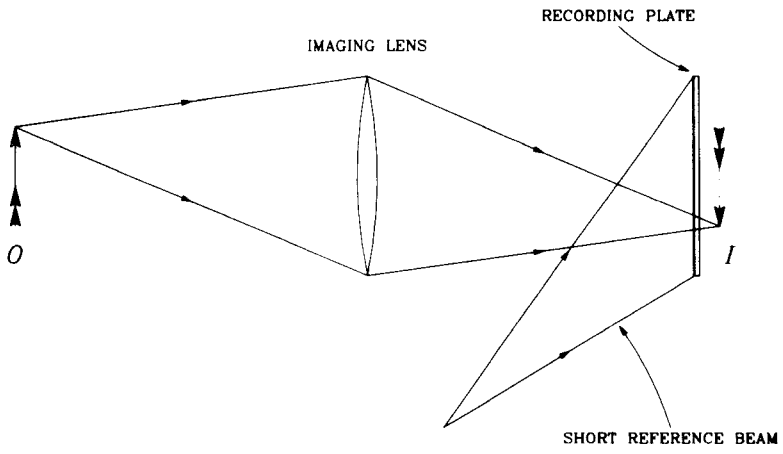

Fig. 5.4*a* Using a short reference beam to record an image-plane hologram.

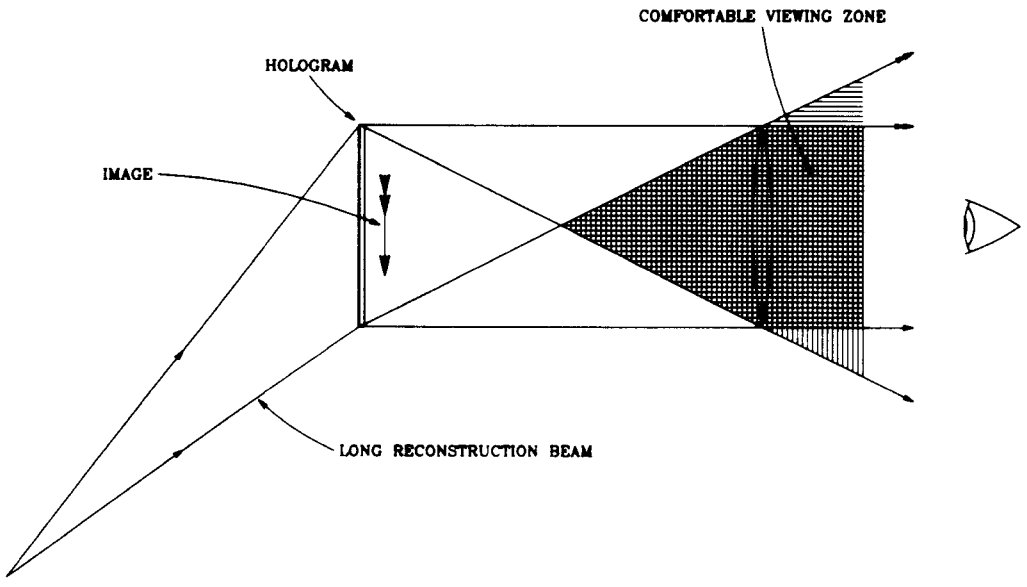

Fig. 5.4*b* Increasing the field of view by using a long reconstruction beam.

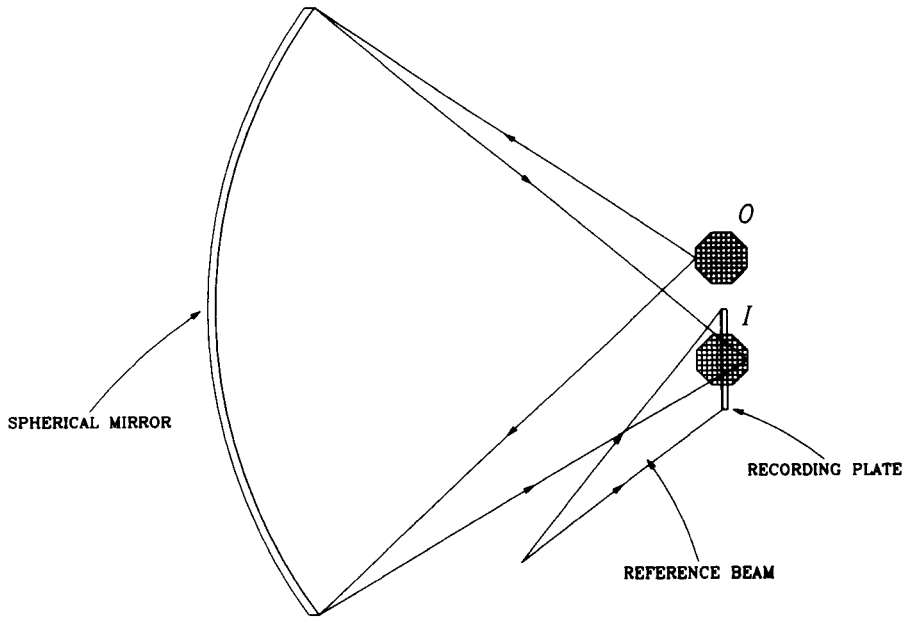

Fig. 5.5 Using a spherical mirror to form a real image.

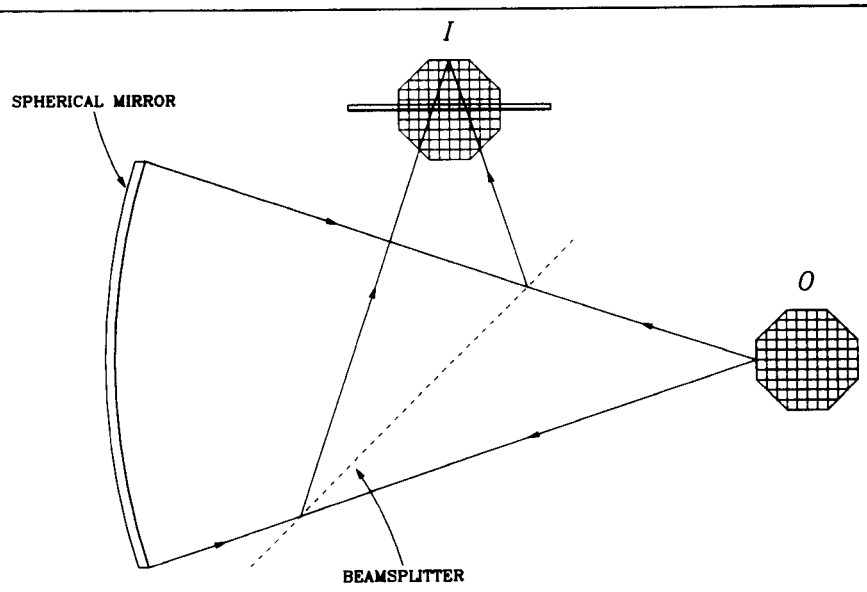

Fig. 5.6 Using a mirror-beamsplitter system to form a real image with low aberrations.

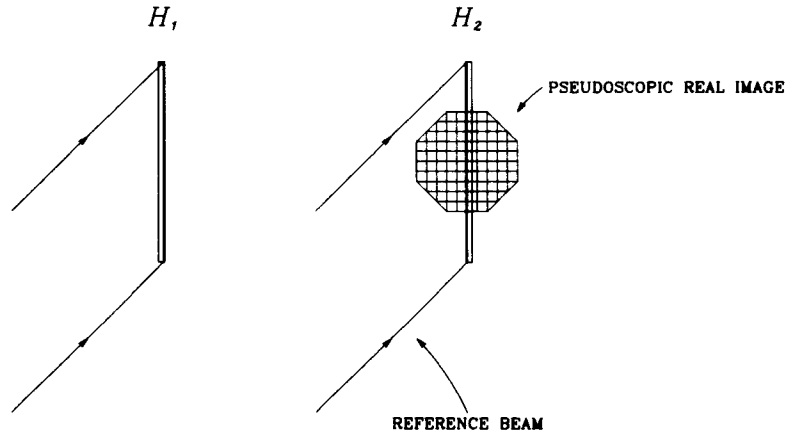

Fig. 5.7*a* Recording a two-step image-plane hologram.

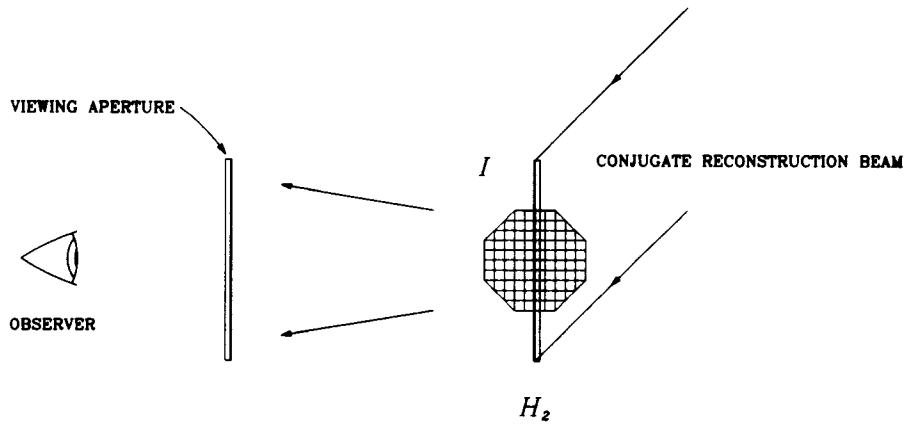

Fig. 5.7*b* Viewing a two-step image-plane hologram.

Fig. 5.7*a*. The projected image from the first hologram, H_1, is pseudoscopic, and therefore the final reconstruction beam on H_2 must be the conjugate of its original reference beam to obtain an orthoscopic final image (Fig. 5.7*b*).

The problem of vignetting no longer arises, because a real viewing aperture is automatically produced. The field of view is determined by the angle subtended by H_1 at H_2. For convenience all reference and reconstruction beams are collimated, although those on H_1 are much more critical than those on H_2, as the image points are further from the hologram. Controlled departure from collimation on H_1 can lead to interesting results [41, 42]—see § 5.7.

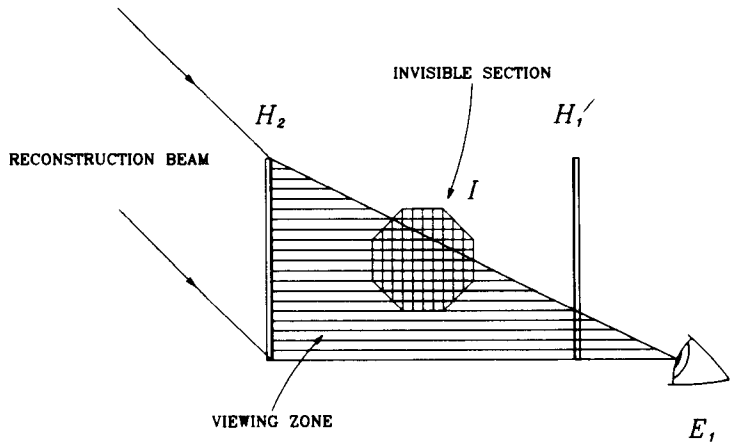

Fig. 5.8 Image cut-off by a 'virtual window'.

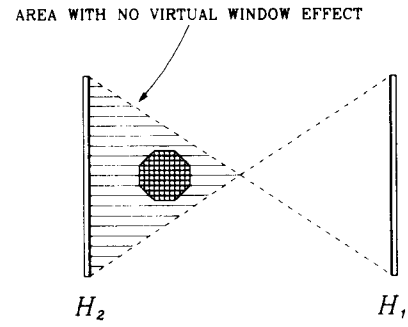

Fig. 5.9 Area in which the image is first cut off by the boundaries of H_1, thus exhibiting no 'virtual window' effect.

5.3.1 The 'Virtual Window' Effect

One form of vignetting which can arise in two-step image-plane holography is the 'virtual window' effect which occurs when the final image is projected a long way forward. Images formed in image-plane holography are normally of shallow depth and the problem rarely arises, but the principle applies to other two-step techniques such as in two-step reflection holography. Consider the arrangement in Fig. 5.8. An intermediate image is recorded on H_2 such that the final image I is a long distance in front of H_2. The observer views the image through the projected window H_1' which is the image of H_1. In order that the image is visible, the observer's line of sight must simultaneously intersect a part of H_1' and of H_2. Consider an observer in position E_1. A portion of the image is invisible because the observer's line of sight does not intersect H_2.

The visual effect is especially disconcerting because it appears that the image is bounded by a window which lies *behind* it—an effect never encountered with real objects. We have found that this effect is a particularly strong visual depth cue, and tends to suggest that the image lies behind H_2, whereas other visual depth cues such as stereopsis, convergence, etc. suggest that it is in front. We have found that when the effect simultaneously occurs on two or more sides of the image, the image is perceived as being just behind H_2, even for long projection distances. To avoid the 'virtual window' effect the image must lie in the zone shown in Fig. 5.9, thereby ensuring that the image is first 'cut off' by H_1—an apparently normal window in front of the image.

5.4 BEAM RATIO

In simple off-axis transmission holography the beam ratios used are normally between 3:1 and 10:1 (ie. 3 or 10 times more intensity in the reference beam than in the object beam). Beam ratios near 1:1 produce bright images, but usually the images are accompanied by background haze due to intermodulation noise. In image-plane holography, if the image is shallow, each part of the image is recorded only on a small part of the hologram, and can be treated independently. Any intermodulation noise is therefore localised and not noticeable [43]. We can therefore use beam ratios near 1:1 and obtain very bright images. As the image is focused onto the recording plate, the beam ratio is non-uniform. We have found that for shallow images—say 5mm total depth—a beam ratio of 1:1 for the brightest parts of the object beam produces good results. As image depth is increased, intermodulation noise from the bright areas overlap with the darker areas of the image, and higher ratios must be used.

When the two-step technique is used with the low beam ratios, the master hologram should be a particularly clean one, as background noise tends to be exaggerated. We often use unbleached master holograms to reduce final background noise.

5.5 IMAGE BLUR

The image observed in an image-plane hologram shows blurring due to the reconstruction source size—source size blur—and to transverse chromatic aberration—chromatic blur.

5.5.1 Source Size Blur

The angular blur produced by an illuminating source of finite angular extent is equal to the angular subtence of the light source at the hologram. If the light source subtends an angle θ_c, and the image point is at a distance D from the hologram, then the angular blurring is

$$\theta_c = \frac{\delta}{D}$$

where δ is the lateral blurring of the image point. So

$$\delta = D\theta_c. \tag{5.1}$$

The lateral blurring is therefore proportional to the distance of the image point from the hologram, D.

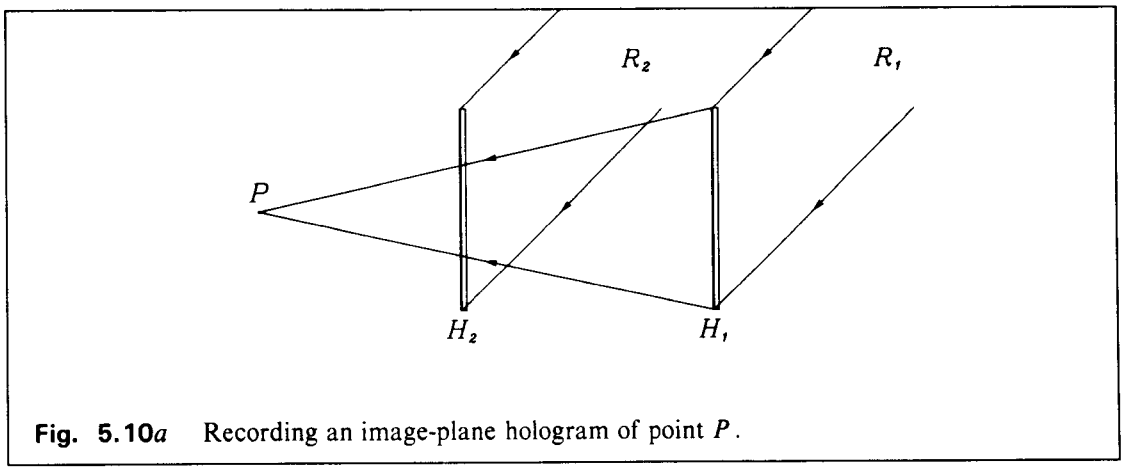

Fig. 5.10*a* Recording an image-plane hologram of point P.

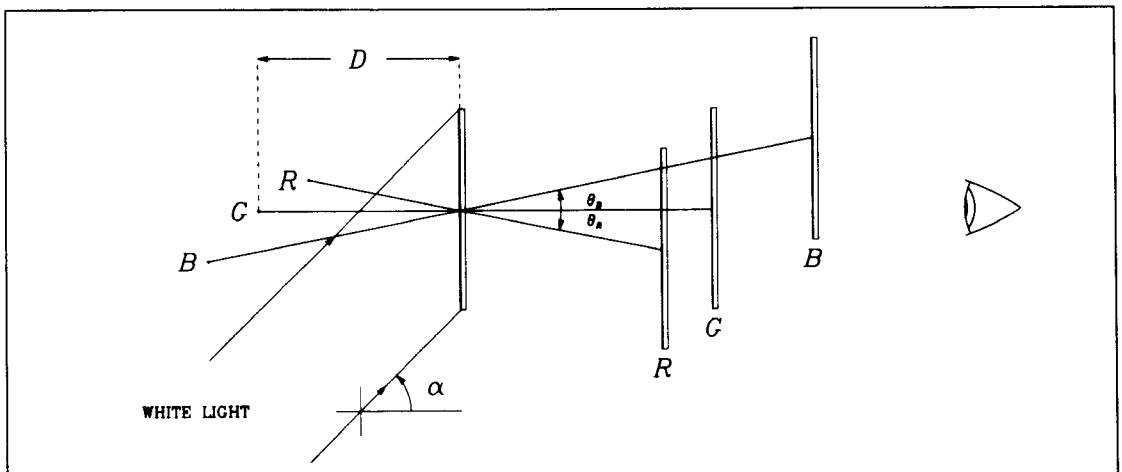

Fig. 5.10*b* Chromatic aberration in an image-plane hologram.

5.5.2 Chromatic Blur

Let us consider an image-plane hologram recorded from a master hologram according to Fig. 5.10*a*. The collimated beam R_1 projected an undistorted image I within which H_2 is positioned. R_2 is a collimated reference beam for H_2. P is a point on the image being recorded. The hologram is recorded with wavelength λ_G which is near the centre of the visible spectrum. If the hologram is subsequently reconstructed with collimated white light (Fig. 5.10*b*), an undistorted image of the point P and the master hologram H_1 is produced by wavelength λ_G. Other wavelengths produce longitudinally and transversely displaced images of P and of H_1. If R_2 records the image from H_1 at reference angle α, then the average fringe spacing on H_2 is

$$d = \frac{\lambda_G}{\sin\alpha}.$$

Upon reconstruction with white light,

$$\sin\alpha - \sin\theta_R = \frac{\lambda_R}{d}$$

and

$$\sin\alpha - \sin\theta_B = \frac{\lambda_B}{d}$$

where θ_R and θ_B are the angular deviations of the image of P reconstructed by the longest and the shortest visible wavelengths respectively. If θ_R and θ_B are assumed to be small, then

$$\theta_R \approx \sin\theta_R = \sin\alpha - \frac{\lambda_R}{d},$$

and

$$\theta_B \approx \sin\theta_B = \sin\alpha - \frac{\lambda_B}{d}.$$

Therefore

$$\begin{aligned}\Delta\theta &= \theta_B - \theta_R \\ &\approx \frac{\lambda_R - \lambda_B}{d} \\ &= \frac{\Delta\lambda}{\lambda_G}\sin\alpha,\end{aligned}$$

$\Delta\lambda$ being the total visible wavelength spread in the reconstruction beam. If the point P is at a distance D from the hologram plate H_2, the transverse image blur is

$$\Delta x = D\sin\alpha\left(\frac{\Delta\lambda}{\lambda_G}\right). \tag{5.2}$$

In the above analysis we have assumed that the observer sees the image point P in all wavelengths of the visible spectrum, ie. he perceives a black and white image. This is usually true, unless the master hologram has a limited height, as in the case of a rainbow hologram (Chapter 6). The results derived also apply to one-step image-plane holograms.

A review of image-plane holography has been published by Brandt [35]. In his analysis of image blur he has obtained a result very different from ours. We believe that our analysis is correct for the case of diffuse objects. Brandt has assumed that the observer sees the image in only a narrow band of wavelengths, determined by the chromatic dispersion of the hologram. This is only the case for specular objects, such as a transparency back-illuminated with a collimated reference beam, or when the imaging aperture has a limited height, ie. in the case of a rainbow hologram. In fact Brandt's formula for image blur is identical to that given by Wyant [44] for the optimum case in a rainbow hologram.

5.6 EFFECT OF EMULSION THICKNESS

It is normally assumed that in an image-plane hologram all visible wavelengths are diffracted with equal efficiency. With thick emulsions, however, particularly when high refractive index modulation is present, Bragg selection may prevent achromatic reconstruction. It is, in fact, possible to produce multicolour images of low saturation by superposing several holograms made with different wavelengths, but with identical geometries.

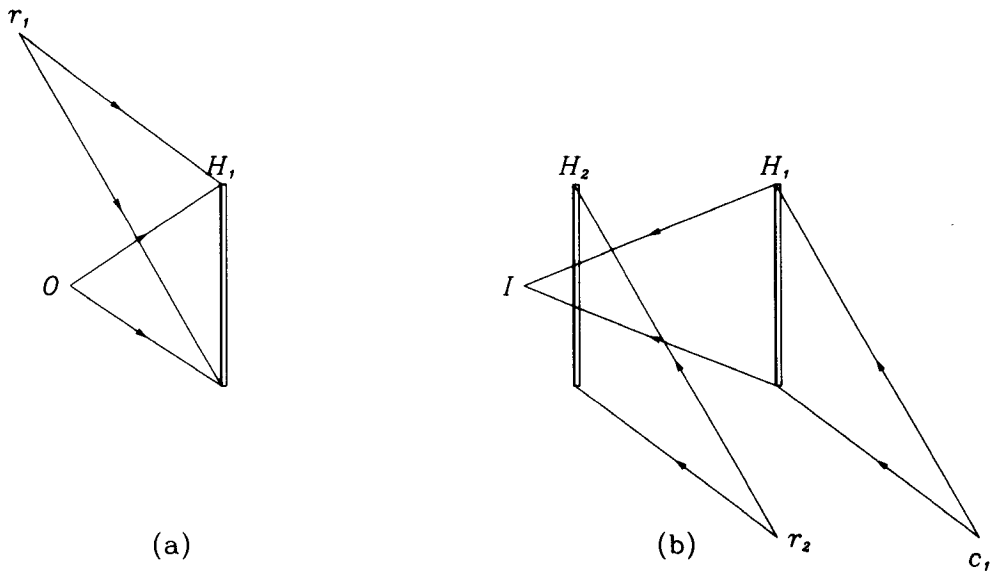

Fig. 5.11 (*a*) Recording and (*b*) reconstruction arrangements for studying the effect of astigmatism (§5.7).

5.7 EFFECT OF ASTIGMATISM

We have discovered that the controlled introduction of aberrations in image-plane holography can result in interesting visual effects [41]—see Appendix. In particular, in the two-step technique, by altering the divergence of the conjugate reconstruction beam used to project the intermediate image, the image produced is astigmatic, and the final hologram can have an apparent plane of greatest sharpness which does not lie in the image plane [41, 42].

Fig. 5.11 shows the geometry used in our experiments. A 'master' hologram H_1 is recorded of the object O, using a diverging reference beam R_1. The hologram is re-illuminated to produce a real image I, using a reconstruction beam C that is directionally the conjugate of R, but is again diverging. The image I is therefore aberrated. A second hologram H_2 is recorded by placing a second recording plate within I. The recording and reconstruction beams for H_2 are identical to those for H_1, ie. both diverging. A second set of aberrations are thus introduced into the final image. In the second step, however, the image points are much closer to the hologram plane than in the first, and the aberrations introduced are correspondingly smaller. We therefore restrict our analysis of the aberrations to those introduced through H_1.

Let us consider a specific example: A hologram is recorded of an object comprising a plane parallel to, and placed 50mm from the recording plate. The reference beam is a diverging beam emanating from a point 500mm from the centre of the recording plate, and impinging on it with a reference angle of 80°. The reconstruction beam is a diverging beam falling onto the plate from the opposite direction to the reference beam, emanating from a point 500mm from the centre of the plate. Both reference and reconstruction sources are in the x–z plane. Using the terminology in §2.3,

$$x_O = -80 \quad \cdots + 80\text{mm}$$

$$y_O = -80 \quad \cdots + 80\text{mm}$$

$$z_O = -50\text{mm}$$

$$R_r = -500\text{mm} \qquad \theta_r = -80^\circ$$
$$R_c = +500\text{mm} \qquad \theta_c = -80^\circ$$

where θ_r and θ_c are the reference and reconstruction beam angles of incidence. We assume that the recording and reconstruction wavelengths are equal. Using Eqn. 2.9, we find that the gaussian image distance is $R_I = -62.5$mm when $x_O = y_O = 0$ so that the centre of the hologram is the imaging area. This figure is approximately constant over the entire area of the image, and the corresponding area on the hologram. (We assume that the observer is at a long distance from the hologram so that the direction of observation is parallel to the z-axis.)

The aberrations of the image can be ascertained using Eqns. 2.13–2.18 and the procedure outlined in § 2.3.4. When $x_O = y_O = 0$ we find that

$$C_x = C_y = A_y = A_{xy} = 0,$$

$$S = -3.9 \times 10^{-6}\text{mm}^{-3}$$

and

$$A_x = 3.9 \times 10^{-3}\text{mm}^{-1}.$$

Looking at other points in the image, A_x is approximately constant over the entire image and varies by no more than some 3%. A_y and A_{xy} are both of the order of 10^{-5}mm^{-1}, and C_x and C_y are of the order of 10^{-6}mm^{-2}.

We can substitute these aberrations into Eqn. 2.12 to obtain the magnitude of the aberrations observed. Let us assume that the image is viewed from a distance of 500mm and that the effective viewing aperture at the observing position is 50mm—ie. equal to the interocular spacing. The wavefront aberrations for $x_O = y_O = 40$mm, for example, are:

$$W_S = 0.06\lambda$$

$$W_{C_x} = -0.2\lambda$$

$$W_{C_y} = -0.2\lambda$$

$$W_{A_x} = -30\lambda$$

$$W_{A_y} = -.005\lambda$$

$$W_{A_{xy}} = 0.9\lambda.$$

The major contributor to aberrations is clearly A_x, and we shall examine its effect. Fig. 5.12 shows schematically the formation of a point image when viewed along the z-axis. The dashed curve is the gaussian reference sphere which forms the first order image I. The solid curve is the aberrated wavefront which forms the third order image at I'. The radius of the contributing area is ρ. If h_I is the distance of the reference sphere from the hologram, as shown in Fig. 5.12, the two-dimensional equation for the reference sphere can be written as:

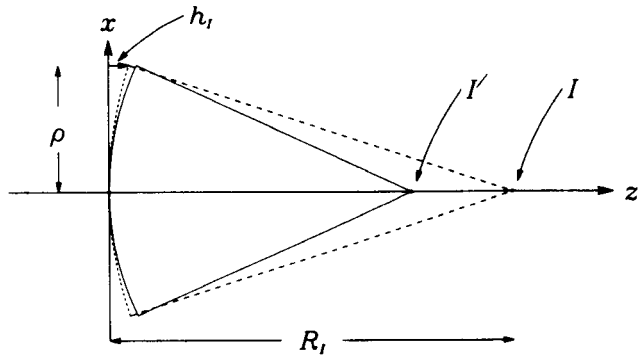

Fig. 5.12 Image shift caused by astigmatism.

$$(R_I - h_I)^2 + \rho^2 = R_I^2,$$

therefore

$$h_I^2 + \rho^2 - 2R_I h_I = 0.$$

If $h_I \ll R_I$, then

$$2R_I h_I = \rho^2$$

or

$$h_I = \frac{1}{2R_I}\rho^2. \tag{5.3}$$

From Eqn. 2.12, the wavefront aberration contributed by A_x is

$$\phi_{3A_x} = -\frac{\pi}{\lambda_c}\rho^2 \cos^2\theta A_x.$$

When $\theta = 0$, the path difference Δh contributed to the image-forming wavefront is therefore

$$\Delta h = \frac{\lambda_c}{2\pi}\phi_{3A_x}$$

$$= -\frac{1}{2}A_x\rho^2. \tag{5.4}$$

The radius of curvature of the image-forming sphere can be formed by adding the extra term to the equation of the reference sphere:

$$h_I' = h_I + \Delta h$$

$$= \frac{1}{2R_I}\rho^2 - \frac{1}{2}A_x\rho^2$$

$$= \frac{1}{2R_I'}\rho^2$$

where R_I' is the distance of the tangential image point. Therefore

$$\frac{1}{R_I'} = \frac{1}{R_I} - A_x \tag{5.5}$$

Substituting $R_I = -62.5\text{mm}$ and $A_x = 3.9 \times 10^{-3}\text{mm}^{-1}$,

$$R_I' = -50.25\text{mm}.$$

Applying the same procedure to find the sagittal image—by substituting A_y—we find that the image position is shifted by less than 1% at the extremities of the image and, of course, unchanged at the centre. The sagittal image distance is therefore about −62.5mm.

The results derived predict that when the eyes of the observer are aligned parallel to the x–axis, the image position is almost unchanged from that of the original object position, but when the eyes are aligned parallel to the y–axis, there is a considerable image shift—in this case some 12mm.

5.7.1 Experimental Verification

We have recorded and reconstructed holograms using the data used in the preceding analysis. The corresponding image distances were found to be −51mm and −62mm.

A second object plane was placed at 70mm from the hologram. The corresponding results were as follows:

Theoretical	experimental
−70.5mm	−71mm
−97.2mm	−97mm

The results show good agreement with theory, with $< 1\%$ error.

5.7.2 Effect in Image-plane Holograms

If an image-plane hologram is recorded using a master hologram with the aberrations described, an interesting effect is observed when the eyes are aligned parallel to the y–axis, namely that the plane of least dispersion lies behind the hologram plane not, as usually observed, coincident with it. Although the total image depth attainable is still restricted by chromatic dispersion, the image-shifting capability extends the versatility of the technique.

CHAPTER 6

RAINBOW HOLOGRAPHY

6.1 INTRODUCTION

Rainbow or 'Benton' holography [45] is a derivative of image-plane holography in which vertical motion parallax is sacrificed in return for greater image depth. Analogously to image-plane holography, rainbow holography can be performed using both one-step and two-step techniques, with similar advantages and disadvantages. Rainbow holograms produce extremely bright, sharp images and are therefore popular in display holography.

6.2 ONE-STEP RAINBOW HOLOGRAPHY

The simplest arrangement for recording a one-step rainbow hologram is shown in Fig. 6.1*a*. The arrangement is identical to that for making a one-step image-plane hologram (§5.2), except that a long, narrow slit is placed in the imaging system [46,47]. A hologram is recorded by introducing a reference beam as shown. When the image is reconstructed using white light spatially conjugate with the reference beam (Fig. 6.1*b*), a bright image is observed in the original recording wavelength when the eyes are placed within the projected image of the slit aperture. As the eyes

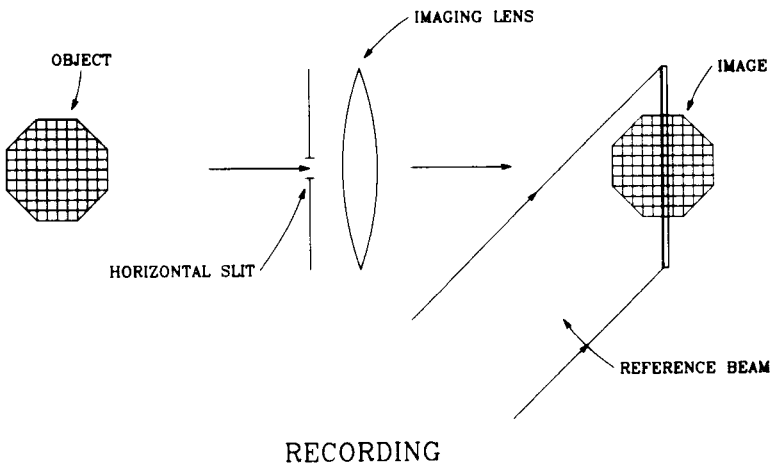

Fig. 6.1*a* Recording a one-step rainbow hologram.

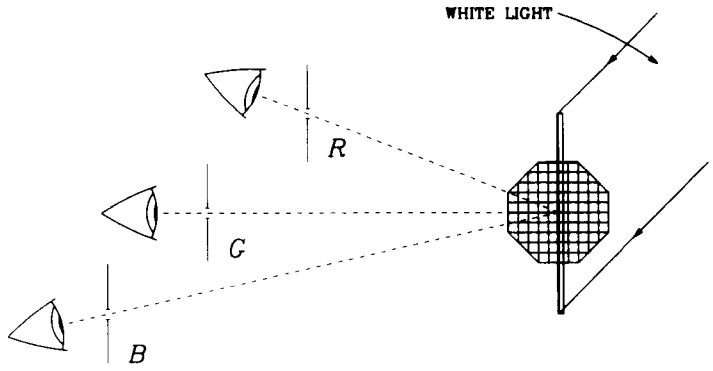

Fig. 6.1*b* Viewing the image of a one-step rainbow hologram.

are moved vertically, ie. perpendicular to the direction of the slit aperture, the image appears in a different colour corresponding to the wavelength in which the image of the slit is formed at that position. The restricted height of the slit prevents the observer viewing the image in a broad spread of wavelengths, thus reducing the chromatic blur in the image.

The image observed in the previous case is pseudoscopic. The orthoscopic image, formed when the reference and reconstruction beams are directionally identical, suffers from vignetting for the same reasons as in §5.2. One way to overcome the vignetting is to place the slit in such a position that a real image of it is produced during recording [46] —Fig. 6.2. A method that produces less aberrations in the final image is to use a short reference and a long reconstruction beam [39, 38]— see §5.2.1. Other imaging elements such as spherical mirrors [40] may be used, as in the case of image-plane holography.

The view observed through each slit image is identical, save aberrations produced. The observer therefore cannot look over and under foreground objects as the eyes are moved up and down— a rainbow hologram therefore only displays horizontal motion parallax. (A convincing demonstration is to align the eyes vertically, such that each eye sees the image through a different coloured slit; the image thus observed is two-dimensional and seems photographic.)

6.3 TWO-STEP RAINBOW HOLOGRAPHY

The two step version of rainbow holography is the exact analogue of two-step image-plane holography. The master hologram, in this case, is long and narrow, and is the equivalent of the slit aperture in the one-step case. Fig. 6.3 shows the steps used in recording and reconstructing a two-step rainbow hologram. The final image observed is orthoscopic.

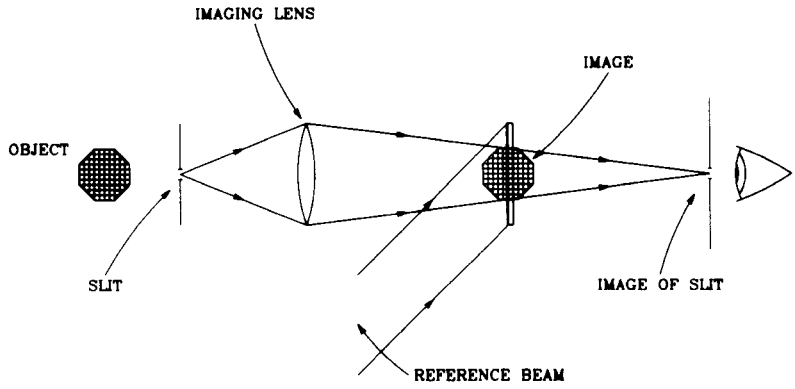

Fig. 6.2 Arrangement for recording a one-step rainbow hologram with an orthoscopic image.

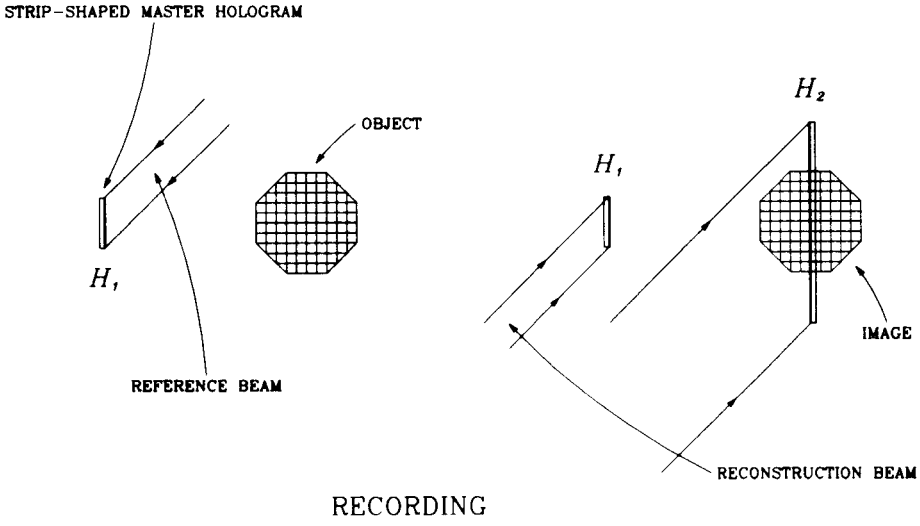

Fig. 6.3*a* Steps in recording a two-step rainbow hologram.

6.4 LOCUS OF PROJECTED VIEWING SLITS

Let us consider a rainbow hologram recorded according to Fig. 6.4, with a recording wavelength of 550nm and a collimated reference beam incident at 45°. The hologram is illuminated with white light which is spatially conjugate with the reference beam (Fig. 6.5). To calculate the positions of the viewing slits for different wavelengths, we need to use a similar procedure to that used in Chapter 5. Using the procedure of §5.7, we obtain

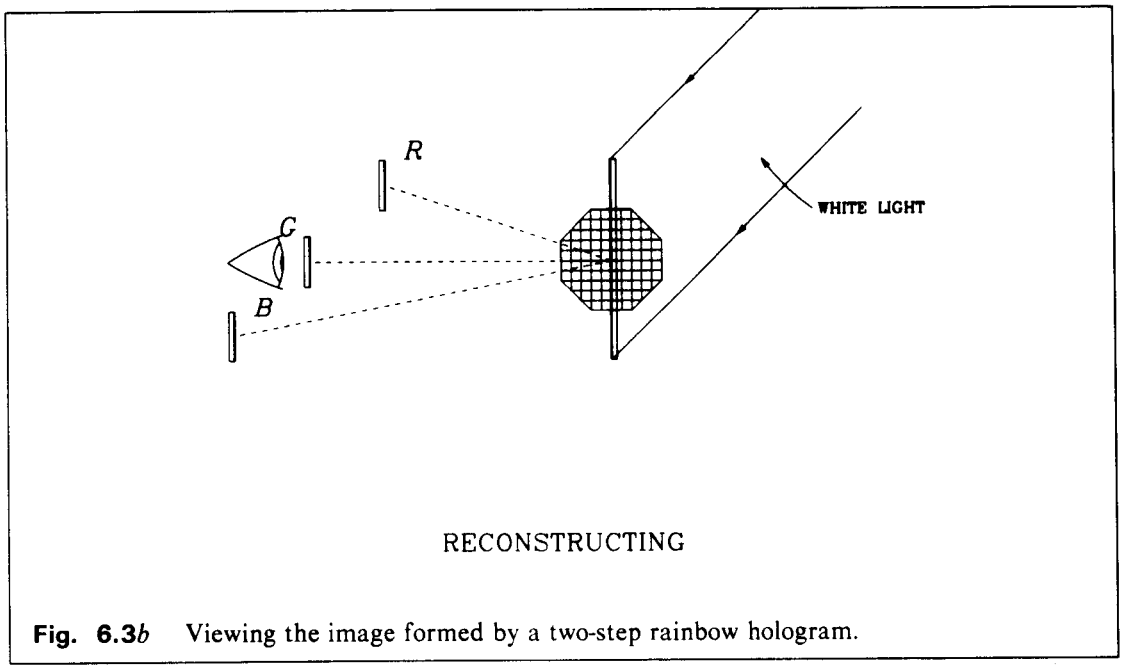

Fig. 6.3*b* Viewing the image formed by a two-step rainbow hologram.

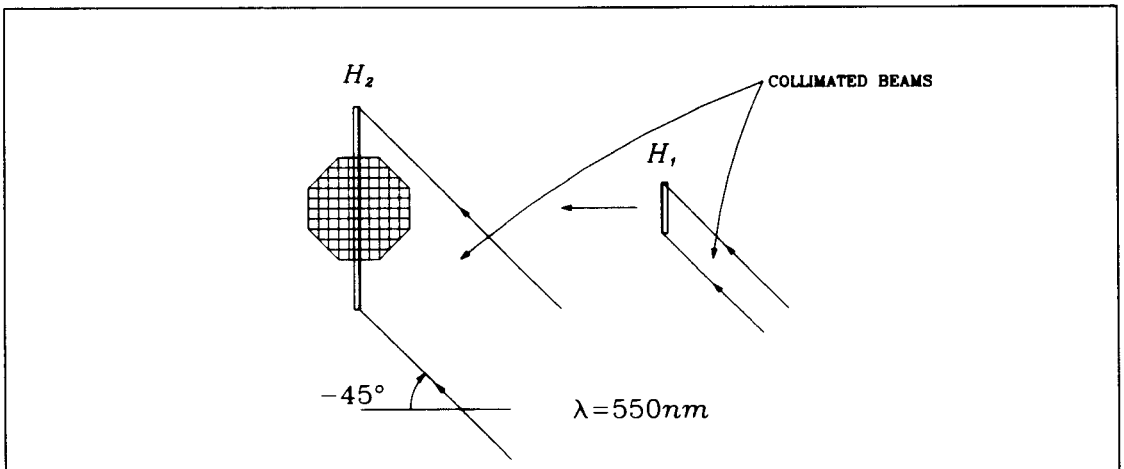

Fig. 6.4 Arrangement for recording a two-step rainbow hologram for the calculations in §6.4.

$$\frac{1}{R_{\text{Tan}}} = \frac{1}{R_I} - A_x \tag{6.1}$$

and

$$\frac{1}{R_{\text{Sag}}} = \frac{1}{R_I} - A_y \tag{6.2}$$

where R_{Tan} and R_{Sag} are the tangential and sagittal image distances. In the x–z plane A_y vanishes (Eqn. 2.17), and therefore $R_{\text{Sag}} = R_I$. Substituting Eqn. 2.16 into 6.1 we obtain

$$\frac{1}{R_{\text{Tan}}} = \frac{1-\sin^2\theta_c}{R_c} + \mu\left[\frac{1-\sin^2\theta_O}{R_O} - \frac{1-\sin^2\theta_r}{R_r}\right] + \frac{\sin^2\theta_I}{R_I}$$

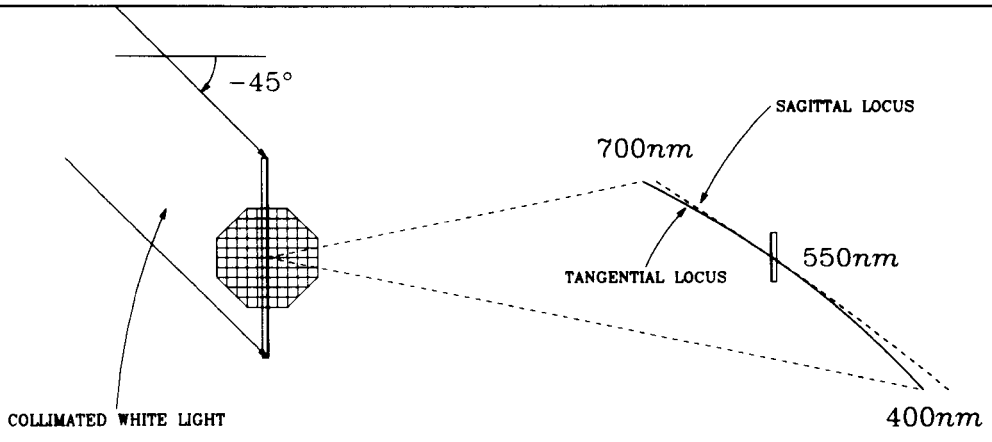

Fig. 6.5 Sagittal and tangential loci of viewing slits of a rainbow hologram.

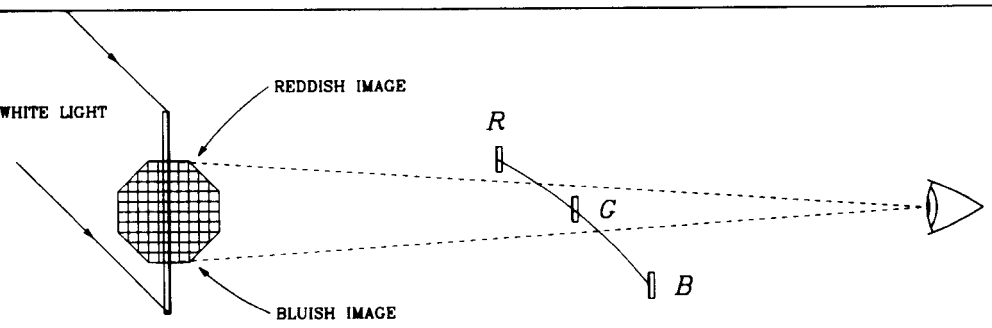

Fig. 6.6 Observation of a rainbow image from a non-optimal viewing position. Each part of the image is observed in a different spectral colour.

where θ_c, θ_O, θ_r and θ_I are the polar angles of the reconstruction, object, reference and image points, according to the coordinate system used in Chapter 2. θ_I can be found using Eqn. 2.10.

Let us consider the point of intersection of the slit image with the x–z plane. Fig. 6.5 shows the loci of the images of the point for all wavelengths in the visible spectrum, and for both sagittal and tangential cases. Since the slit is parallel to the y–axis, the tangential locus is the appropriate one to consider. (When the image is viewed from one of the slit image positions, however, Sagittal focusing is observed!) The image is seen monochromatically only if the eyes are placed on the tangential locus. Plate III shows different views from different slit image points. The perspective is identical, but each image is in a different spectral colour. When the image is viewed from a position in space not on the tangential locus (Fig. 6.6) each part of the image is seen in a different spectral colour (Plate IV).

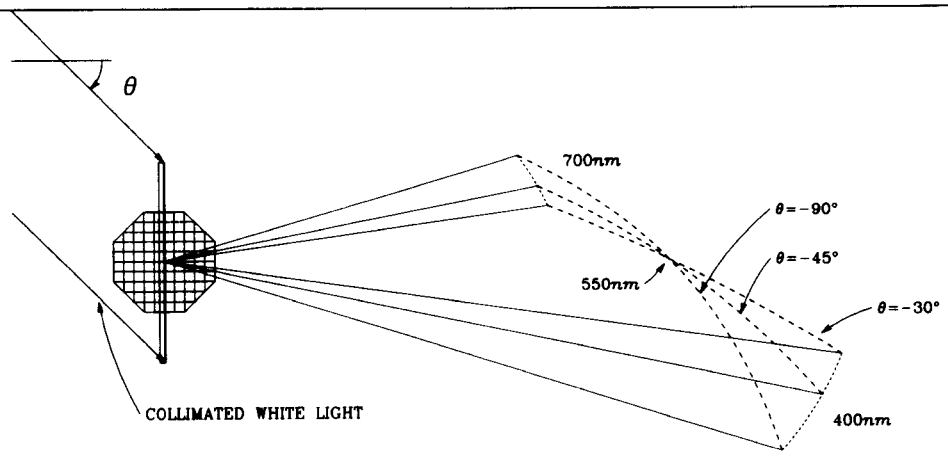

Fig. 6.7 Variation of the locus of projected viewing slits with reconstruction angle.

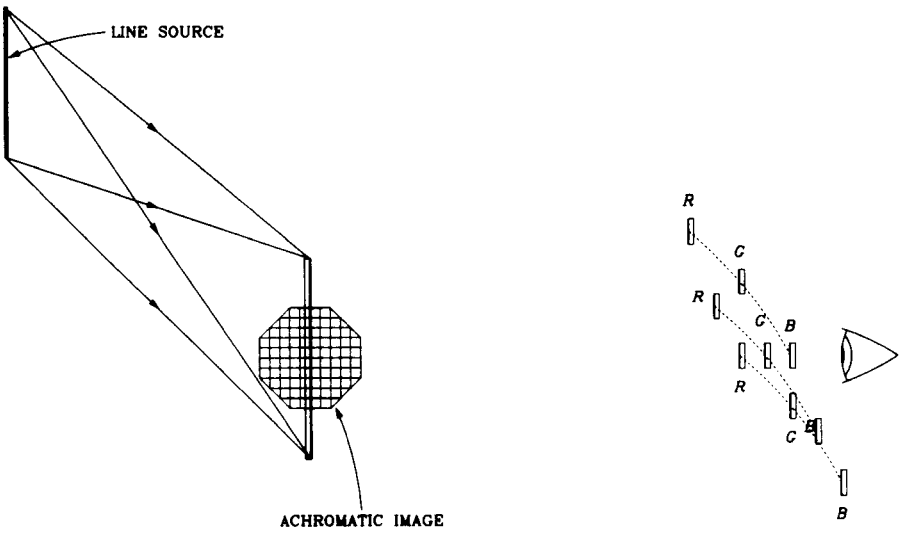

Fig. 6.8 A simple method for producing an achromatic image from a rainbow hologram.

6.5 FIELD OF VIEW

The horizontal field of view is determined by the angle subtended by the length of the slit master hologram at the centre of the final hologram during the second recording stage—cf. §5.3. The vertical field of view, however, is dependent on the bandwidth of the reconstruction source and on the dispersive power of the hologram. The dispersive power of the hologram depends on the fringe spatial frequency, which is a function of the inter-beam angle during recording.

Suppose that the image of a rainbow hologram with fringe spacing d is reconstructed using a

collimated reconstruction beam of bandwidth $\Delta\lambda$, and that the hologram has been recorded such that the central wavelength of the spectrum, λ_G, emerges normally to the hologram. If the reconstruction angle is θ, then the fringe spacing is given by

$$d = \frac{\lambda_G}{\sin\theta},$$

and the diffraction angle ϕ for any wavelength λ is (§2.2):

$$\sin\phi = \sin\theta - \frac{\lambda}{d}.$$

In particular, the maximum and minimum angles of diffraction are given by

$$\sin\phi = \sin\theta - \frac{\lambda_G \pm \Delta\lambda}{2d}$$

$$= \pm\frac{\Delta\lambda}{2\lambda_G}\sin\theta.$$

The total field of view is therefore

$$\phi = 2\sin^{-1}\left\{\frac{\Delta\lambda}{2\lambda_G}\sin\theta\right\}. \tag{6.3}$$

Substituting 550nm and 300nm for λ_G and $\Delta\lambda$ respectively, and assuming a reference angle of 45°, the field of view is 22.2°, ie. 11.1° above and below the normal to the plate. The maximum field of view is obtained for the limiting case of $\theta = 90°$ in which case $\phi = 31.7°$. Fig. 6.7 shows the tangential loci of slit images for several different reference beam angles θ.

6.6 ACHROMATIC IMAGES

The simplest way of obtaining an achromatic image from a rainbow hologram is to reconstruct the hologram with a line source, thus reconstructing a continuum of overlapping sets of slit images (Fig. 6.8). An observer at any position within a limited zone sees the image simultaneously in all wavelengths of the spectrum.

A more elegant approach is to incorporate the multi-slit effect into the hologram at the recording stage. Several variations on this technique are possible [eg. 48, 49].

6.7 MULTICOLOUR IMAGES

Multicolour images can be formed by superimposing two or more rainbow holograms made with different wavelength, using identical recording geometries. At the correct vertical position three superimposed images are observed, each in the original colour of the laser used in the recording, thus forming a multicolour image. As the eyes are moved vertically, all colours are distorted. The method can be applied to both one-step [50, 38] and two-step [51] rainbow holography.

CHAPTER 7

DISPERSION COMPENSATION

7.1 INTRODUCTION

The aim of all white-light reconstruction techniques in holography is to overcome the chromatic dispersion, and hence the image blur, inherent in the diffractive mechanism. Reflection holography, for example, improves image sharpness by discarding all but a narrow band of wavelengths from the recontruction beam, with the disadvantage of loss of image luminance. The rainbow or 'Benton' technique relies on distributing the diffracted light such that only a narrow band of wavelengths reaches the observer from any image point. The image luminance is retained, but vertical parallax is sacrificed. One method that retains luminance *and* full parallax is dispersion compensation, which can produce sharp achromatic images with the low dispersive properties of a Gabor in-line hologram. The disadvantage of the system is that an auxiliary diffracting structure must be used for reconstruction, but this can be compact and convenient to use [52]—see §7.8.

7.2 PRINCIPLES

Consider the hologram of a point object (Fig. 7.1). When illuminated by coherent light, a sharp image is reconstructed. Using white light, however, a chromatically blurred image is reconstructed (Fig. 7.2*a*). If the white light is first diffracted through a diffraction grating with spatial frequency equal to the average spatial frequency of the hologram, the dispersion in the resultant image is, in the first approximation, compensated, and a quasi-achromatic image is observed (Fig. 7.2*b*). Plate V shows a white-light reconstructed holographic image with and without dispersion compensation.

Dispersion compensation was first proposed by Paques [53] and then by Burckhardt [54] and de Bitetto [55]. To prevent the image being 'washed out' by the undiffracted portion of the original reconstruction beam Burckhardt proposed the use of a miniature Venetian blind structure between the diffracting elements (Fig. 7.3). First order Chromatic correction is achieved in whichever order the diffracting elements are placed. As will be shown in the next section, however, it is preferable that the diffraction grating be placed first.

7.3 CHOICE OF FIRST DIFFRACTING ELEMENT

As the average fringe spatial frequency of the hologram is equal to the spatial frequency of the compensating grating, first order correction of dispersion is achieved in whichever order the two elements are placed. A simple ray-trace through the two elements shows that if the elements are separated, the image is sharper if the grating is placed before the hologram. Let us consider a

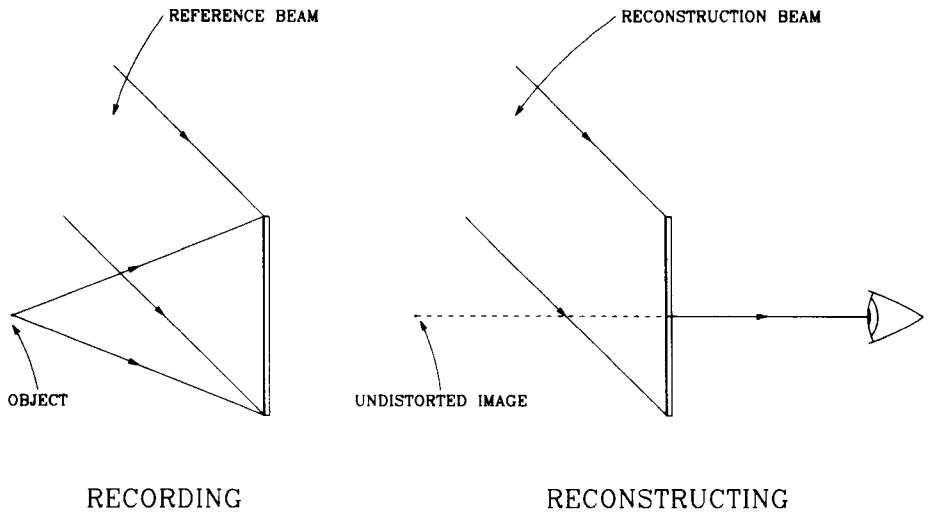

Fig. 7.1 Reconstruction of a sharp, undistorted image by a coherent reconstruction beam.

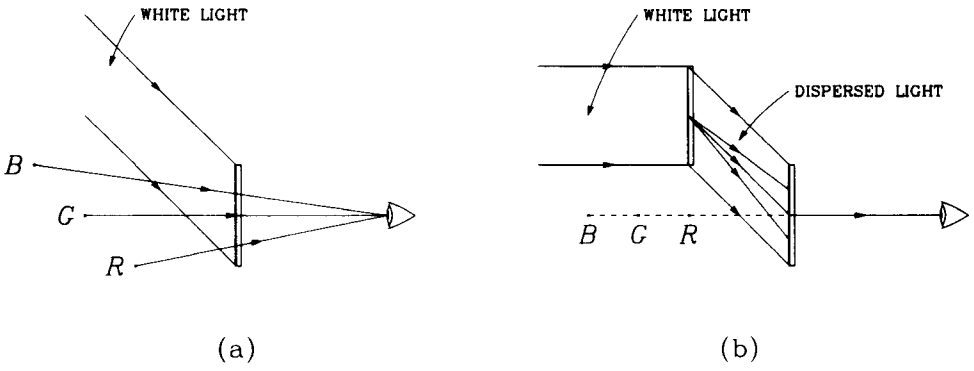

Fig. 7.2 Image reconstruction by a polychromatic reconstruction beam (*a*) without and (*b*) with a compensating grating.

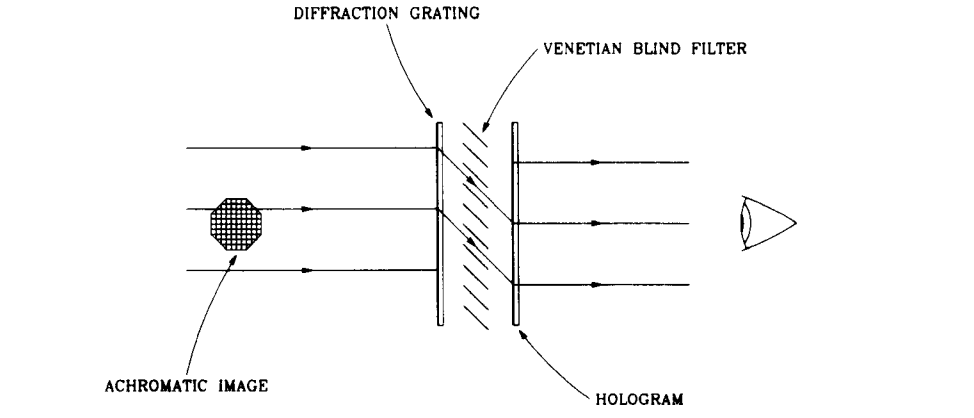

Fig. 7.3 Prevention of the undiffracted reconstruction beam reaching the observer by using a 'Venetian blind' structure according to Burckhardt [54].

hologram of a point P, which lies at distance D_P from the hologram H (Fig 7.4*a*). The hologram is formed using a collimated reference beam of wavelength 550nm incident at 45°. A correcting grating for this hologram is made with two collimated reference beams at 0° and 45° to the normal, using the same wavelength (Fig. 7.4*b*). The fringe spatial frequency of the grating is equal to the average spatial frequency of the hologram, and therefore a quasi-achromatic image can be formed by dispersion compensation. The grating can be placed either before or after the hologram.

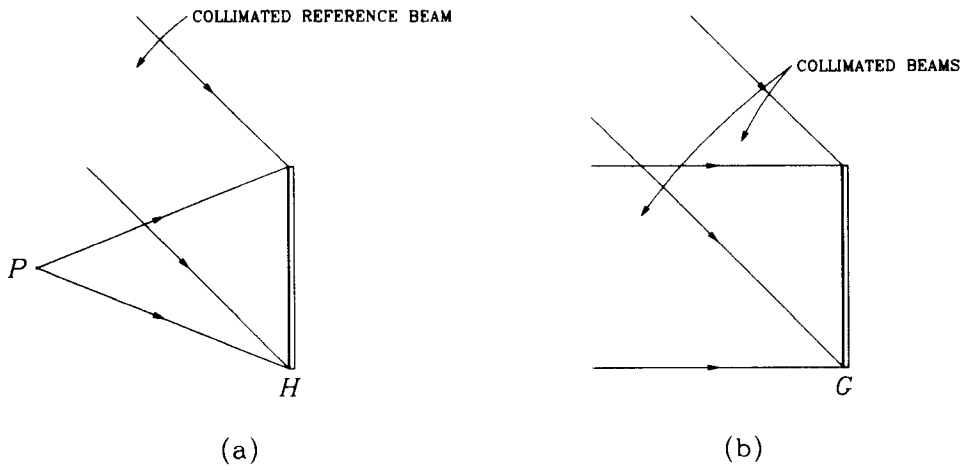

Fig. 7.4 Arrangement for recording a hologram of a point P and the corresponding compensating grating.

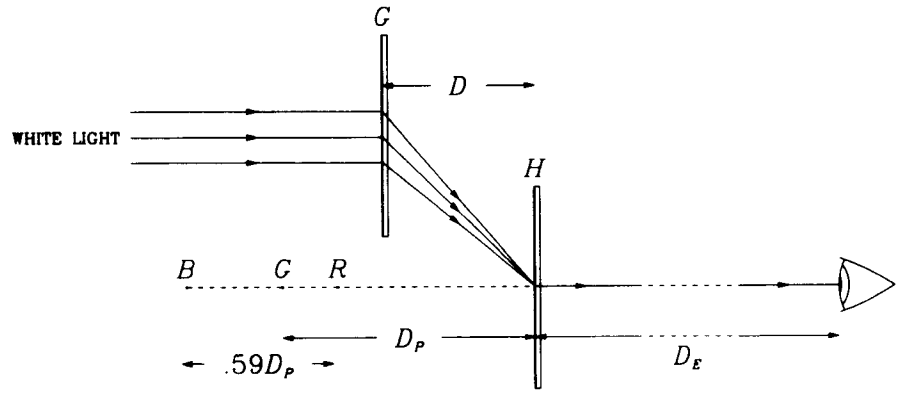

Fig. 7.5 Production of a quasi-achromatic image by placing the grating *before* the hologram.

7.3.1 Grating Placed Before the Hologram

Fig. 7.5 shows the arrangement for obtaining a dispersion compensated image from the system. A collimated beam of white light is incident normally on the grating G. The first order diffracted beam is a continuous spectrum, each wavelength being collimated. The hologram H is placed such that it is illuminated by all wavelengths and that the portion of the spectrum at 550nm is incident at 45° and therefore reconstructs an undistorted image of P. The image of P reconstructed by other wavelengths will be displaced and aberrated. We assume that the observer is looking normally through the centre of H, and that the observer distance $D_E \gg D_P$.

To ascertain the position of the image P' for any wavelength, we choose two rays about the principal ray. The angular separation of each ray from the principal ray is kept small so that the effects of aberrations are minimised. The distance D between H and G does not affect the ray-tracing calculation so long as it is small enough for all wavelengths to intercept the hologram. A range of wavelengths between 400nm and 700nm are chosen and ray-tracing shows that there is no residual lateral chromatic aberration. The total displacement between the blue (400nm) and red (700nm) images is $.59D_P$.

7.3.2 Grating Placed After the Hologram

In this arrangement (Fig. 7.6) the hologram is illuminated with a collimated reconstruction beam at an angle identical to that of the original reference beam, namely 45°. A spectrally smeared image P' is formed by first order diffraction. The diffracted rays fall on the correcting grating G and are again diffracted, forming a virtual, quasi-achromatic image P''. A procedure similar to that in the previous case is used, and a narrow bundle of rays are traced to form each spectral image, the central ray always being that passing through the centre of H. In this way all central rays undergo two equal and opposite deflections and emerge parallel. If we assume that $D_E \gg D_P$, then these rays can be regarded as the principal rays. The separation D between the diffracting elements is now significant and the colour smear at P'' increases with increasing separation.

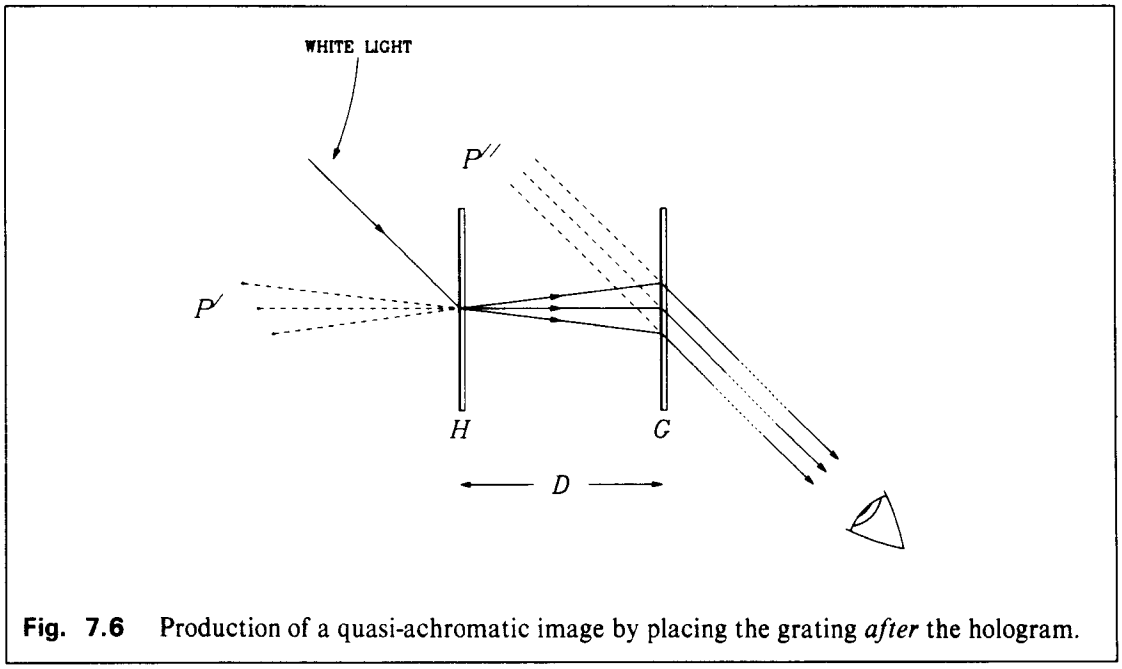

Fig. 7.6 Production of a quasi-achromatic image by placing the grating *after* the hologram.

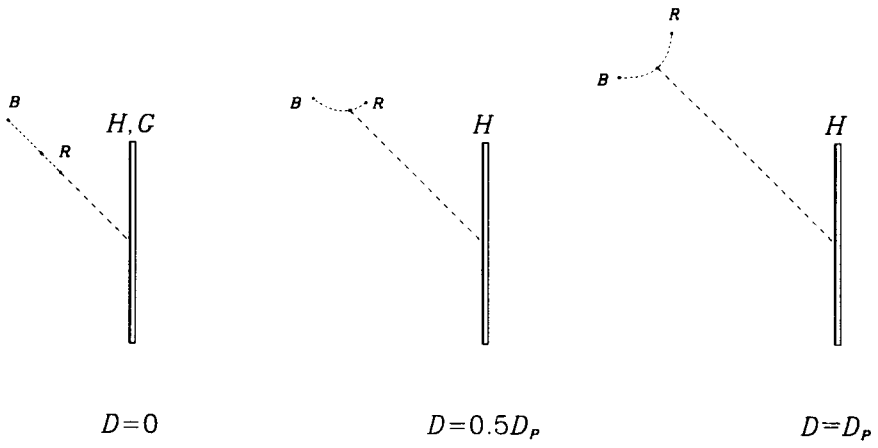

Fig. 7.7 Variation of the locus of image points produced in the reconstruction arrangement of Fig. 7.6 as a function of the hologram–grating separation D.

Fig. 7.7 shows the calculated shape and size of the smeared image for various values of D. For infinitesimal separation there is no transverse smear, only longitudinal smear. In this case the distance of the green (550nm) image from the centre of the grating is exactly $0.5P$. As the separation of the diffracting elements increases, the image distance increases and the image has increasing lateral smear. In practice, D must have a minimum value such that the undiffracted light from the first element is not superimposed on the final image P''.

7.3.3 Conclusion

The lateral colour smear produced when the hologram is placed before the grating is unacceptable when polychromatic illumination is used. Furthermore, the image is distorted and aberrated. Placing the grating before the hologram produces no lateral smear and the image is negligibly aberrated for wavelengths near the original recording wavelength.

7.4 USING A VENETIAN BLIND STRUCTURE

The system shown in Fig. 7.2*b* produces images of excellent quality. The main disadvantage is that the diffraction grating and the hologram must be spatially separated so that the undiffracted portion of the original white light does not overlap with the image. A technique that allows the two elements to be placed close to one another involves placing a miniature Venetian blind structure between the elements [54], thus allowing only the first order diffracted beam from the grating to pass through to the hologram, and blocking the undiffracted portion of the white light (Fig. 7.3). The individual louvres must be small enough so that they are not visible to the observer. If they are too small, on the other hand, diffraction effects may impair the image. A product that is excellent for this purpose is commercially manufactured [56] and has a louvre spacing of some 0.1mm.

7.5 PRODUCTION OF A COMPENSATING GRATING

To produce a diffraction grating with predictable performance, careful consideration must be given to the recording and reconstruction parameters. In this section we investigate the properties of a typical compensating grating.

Let us assume that we are using a dispersion-compensating system as shown in Fig. 7.3. A compensating grating and a hologram are separated by a miniature Venetian blind screen with a louvre angle of 45°. What is the best angle to choose for the diffracting elements? It is best to choose a central wavelength at, say, 550nm to be diffracted through 45° when the beam is incident normally on the grating—this will ensure that the portion of light with the highest luminosity passes through the system with the minimum attenuation. We wish to optimize the grating for this wavelength. If the grating is to be made using light of wavelength 632.8nm, then we must use the equations derived in §2.4.2.5 to calculate the angles of incidence of the two interfering beams. Assuming negligible change in emulsion thickness and refractive index, the two beams must be incident at 49.2° and −3.3°.

From the formulæ in §2.4.2.5, $\theta_f = 13.48°$, $\Lambda = 756.2$nm, and hence the effective thin grating fringe spacing is

$$d_{\text{eff}} = \frac{\Lambda}{\cos\theta_f} = 777.7\text{nm}.$$

We can now use the *thin* grating diffraction formula to predict the angle of diffraction at other wavelengths. Eg. for blue (400nm) and red (700nm),

$$\theta_B = \sin^{-1}\frac{400}{777.7} = 31.0°,$$

and

$$\theta_R = \sin^{-1}\frac{700}{777.7} = 64.2°.$$

Wavelengths other than the central 550nm will not, of course, satisfy the Bragg condition, and will therefore be diffracted with a lower diffraction efficiency. In practice, using silver halide recording materials, the diffracted bandwidth is acceptable, and an achromatic image is observed.

7.6 DISTORTIONS AND THIRD ORDER ABERRATIONS

7.6.1 Third Order Aberrations

7.6.1.1 'On-axis' Points

Let us consider a hologram of a point-object lying along the z-axis (according to the coordinate system in Fig. 2.4), recorded using a collimated reference beam of wavelength λ_r, incident at angle θ_r. The image is reconstructed with a collimated beam of wavelength λ_c incident at angle θ_c. All points of interest lie in the x–z plane and all $y_q = 0$. Using Eqns. 2.9–2.18,

$$\frac{1}{R_I} = \frac{\mu}{R_O},$$

$$\sin\theta_I = \sin\theta_c - \mu\sin\theta_r,$$

$$y_I = 0,$$

$$S = \frac{\mu}{R_O^3} - \frac{1}{R_I^3},$$

$$C_x = -\frac{x_I}{R_I^3},$$

$$A_x = -\frac{x_I^2}{R_I^3},$$

$$C_y = A_y = A_{xy} = 0.$$

The only aberrations present are S, C_x and A_x. If dispersion is compensated during reconstruction, ie. if $\theta_I = \theta_O = 0$, then

$$\mu = \frac{\sin\theta_c}{\sin\theta_r},$$

and

$$C_x = A_x = 0.$$

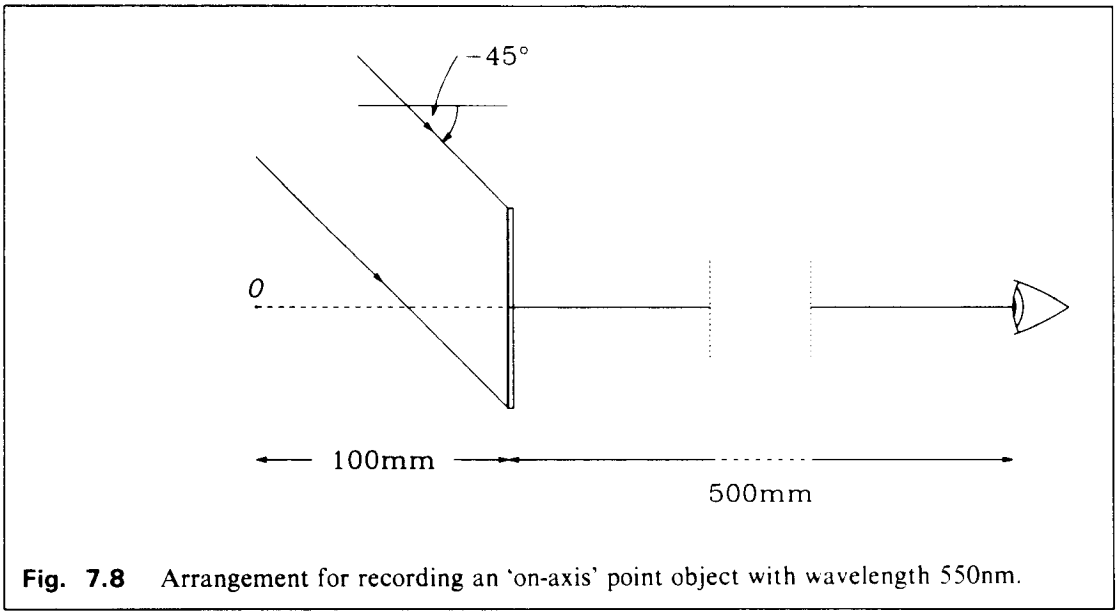

Fig. 7.8 Arrangement for recording an 'on-axis' point object with wavelength 550nm.

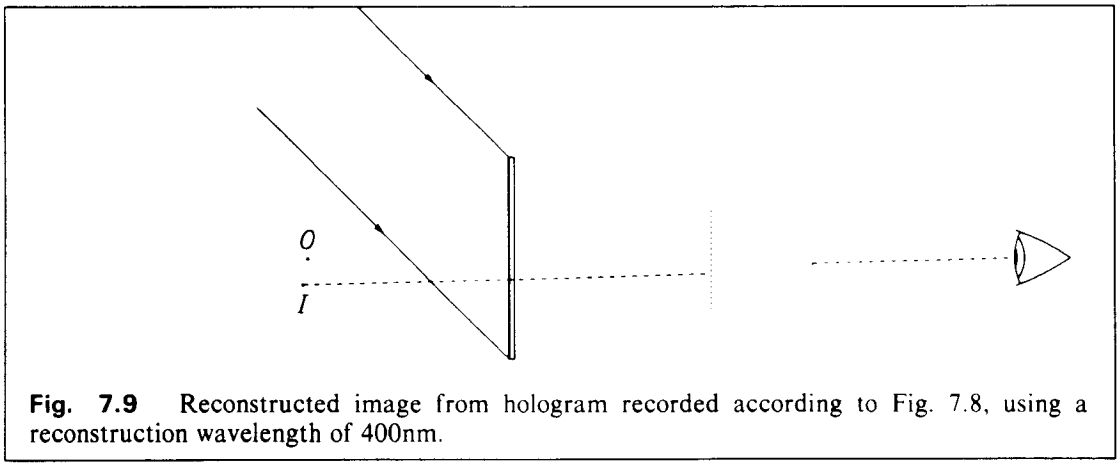

Fig. 7.9 Reconstructed image from hologram recorded according to Fig. 7.8, using a reconstruction wavelength of 400nm.

The only aberration remaining in this case is Spherical aberration. Let us now examine the magnitude of these aberrations as a function of the reconstruction angle. Consider the recording geometry in Fig. 7.8. A point-object O is on the z–axis, and at 100mm from the recording plate. A collimated reference beam of wavelength 550nm falls onto the plate with an angle of incidence of $-45°$. The image I is reconstructed with a collimated reconstruction beam of wavelength 400nm and angle of incidence $-45°$ (Fig. 7.9), and is viewed by an observer placed along the z–axis at 500mm from the origin. Setting the diameter of the exit pupil equal to the interocular separation, say 50mm, and using the procedure of §2.3 we obtain

$$x_I = 27.1\text{mm}, \qquad z_I = -140.4\text{mm}.$$

The Seidel aberration coefficients are

$$S = -3.2\times 10^{-7}\text{mm}^{-3},$$

$$C_x = 1.7\times 10^{-5}\text{mm}^{-2},$$

and

$$A_x = -2.9\times 10^{-4}\text{mm}^{-1}.$$

The corresponding wavefront aberrations are

$$W_S = 0.1\lambda,$$

$$W_{C_x} = 3.4\lambda,$$

and

$$W_{A_x} = 11.0\lambda.$$

We now change the reconstruction beam angle as if to compensate for transverse chromatic aberration. If the new angle is θ_c then

$$\sin\theta_c = \frac{\lambda_c \sin\theta_r}{\lambda_r} = \frac{400\sin 45°}{550}$$

$$\Rightarrow \qquad \theta_c = -30.9°.$$

The new image location is at

$$x_I = 0\text{mm}, \qquad z_I = -137.5\text{mm}.$$

The accompanying aberrations are:

$$S = -3.4\times 10^{-7}\text{mm}^{-3} \qquad W_S = 0.1\lambda$$

$$C_x = 0 \qquad W_{C_x} = 0$$

$$A_x = 0 \qquad W_{A_x} = 0$$

The Spherical aberration observed is small, and C_x and A_x are eliminated. Fig. 7.10 shows how these aberrations change with reconstruction angle.

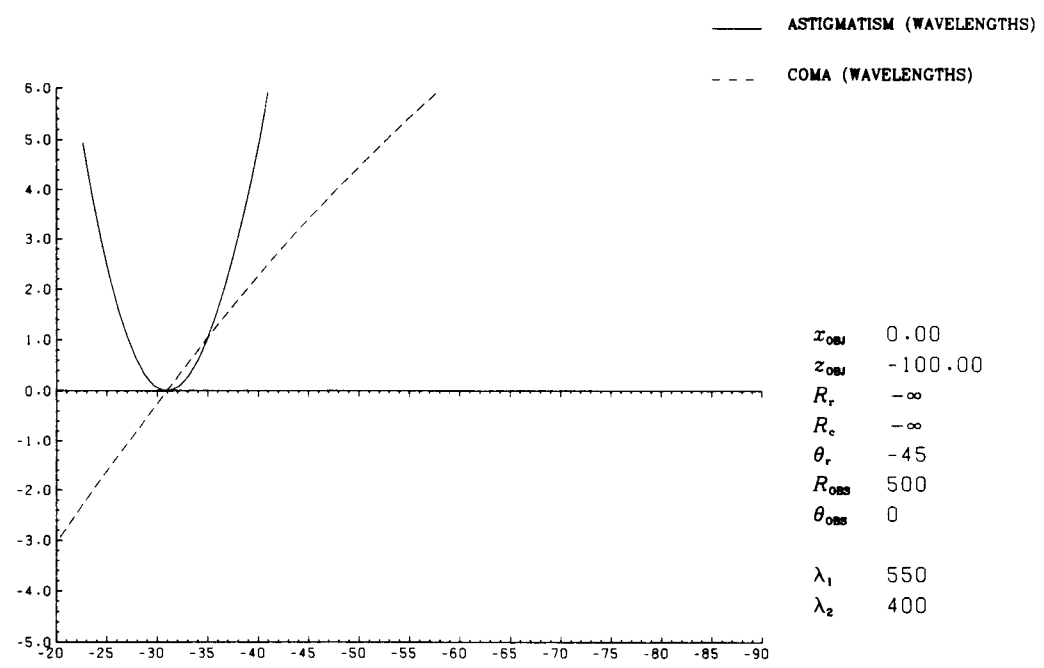

Fig. 7.10 Variation of Coma and Astigmatism in the reconstructed image of an 'on-axis' object. Both aberrations vanish at the 'dispersion-compensated' angle, 30.9°.

7.6.1.2 'Off-axis' Points

Let us consider a recording geometry identical to that in the previous section, but with $x_O \neq 0$, ie. an object point 'off-axis'. If $x_O = 50\text{mm}$ and $z_O = -100\text{mm}$, reconstructing the image with 400nm light at the 'dispersion-compensated' angle,

$$x_I = 50.0\text{mm}, \qquad z_I = -137.9\text{mm}.$$

The accompanying aberrations are:

$$S = -3.4 \times 10^{-7}\text{mm}^{-3}, \qquad W_S = 0.1\lambda,$$

$$C_x = -3.6 \times 10^{-6}\text{mm}^{-2}, \qquad W_{C_x} = -0.7\lambda,$$

$$A_x = -3.9 \times 10^{-5}\text{mm}^{-1}, \qquad W_{A_x} = 1.4\lambda.$$

Fig. 7.11 shows the dependence of C_x and A_x on the reconstruction angle for the off-axis case. It is clear that the aberrations are minimised near the dispersion-compensated angle. Fig. 7.12 shows the curves for $z_O = -100\text{mm}$, and $x_O = -50$, 0, and $+50\text{mm}$. All aberrations are small near $\theta_c = -30.9°$. Figs. 7.13–7.15 show the corresponding curves for other wavelengths.

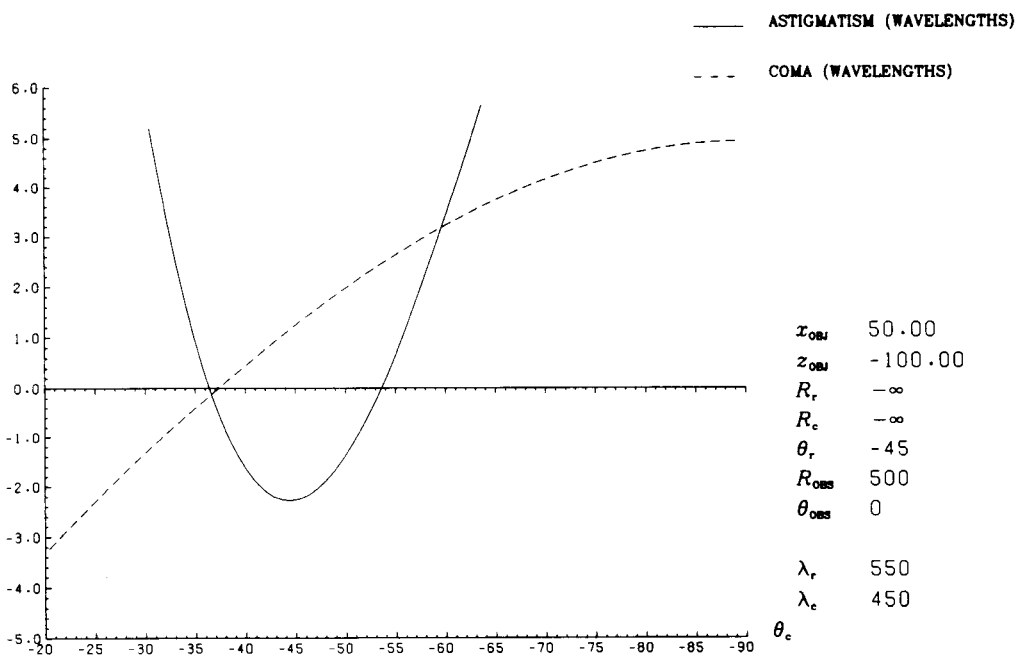

Fig. 7.11 Variation of Coma and Astigmatism in the reconstructed image of an 'off-axis' point. Both aberrations are small near the 'dispersion-compensated' angle.

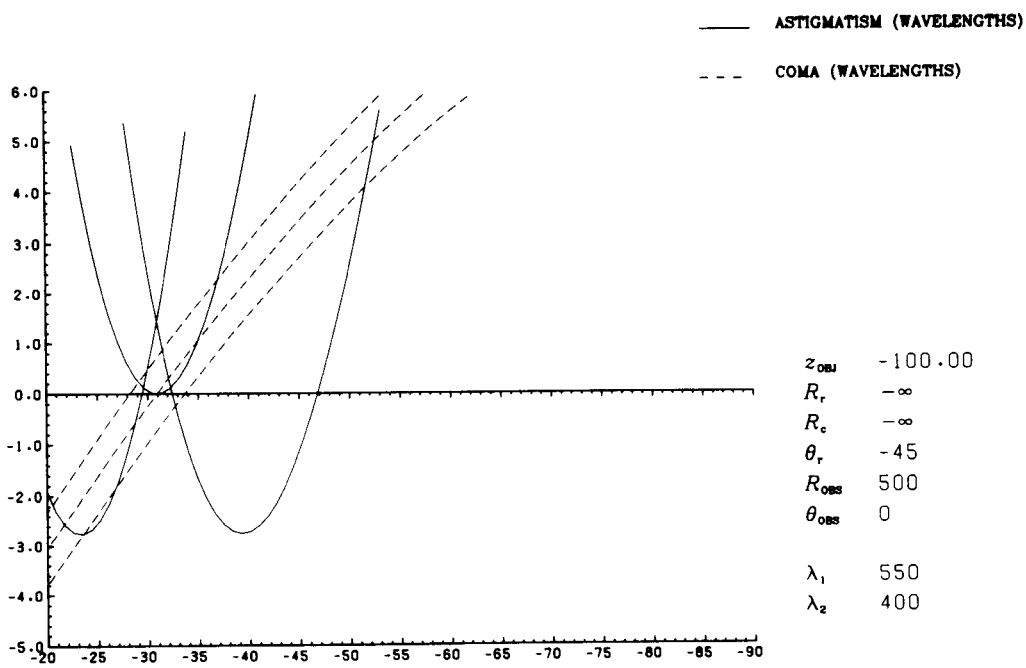

Fig. 7.12 Variation of Coma and Astigmatism in the reconstructed images of an on-axis and two off-axis points (λ_c =400nm).

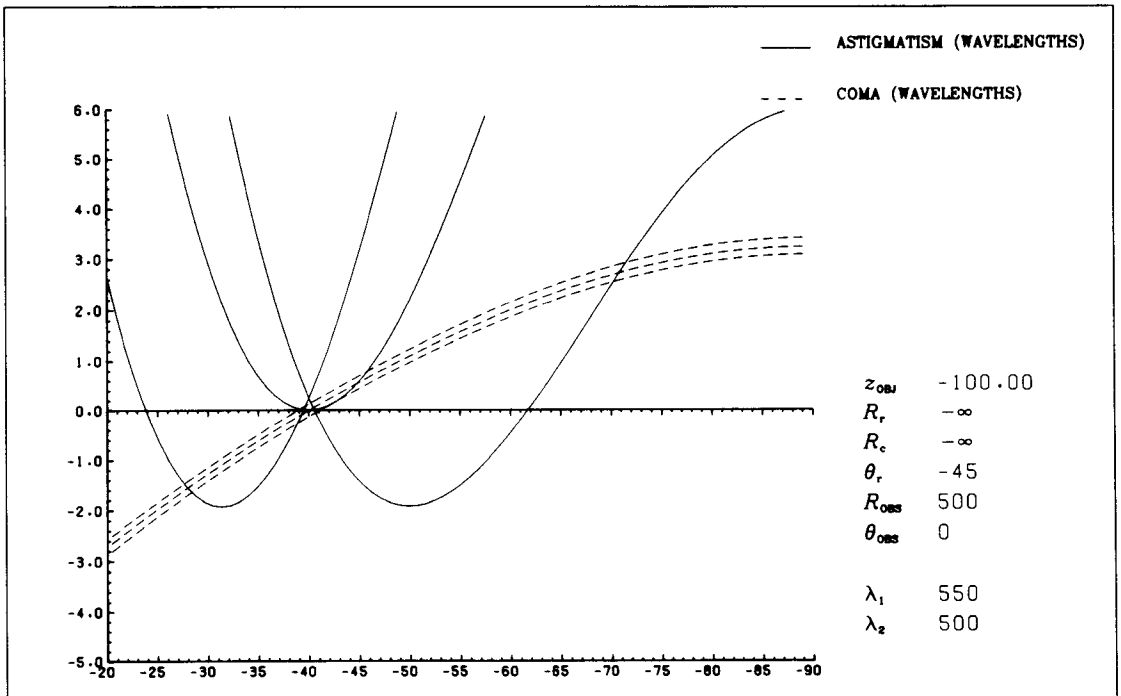

Fig. 7.13 Variation of Coma and Astigmatism in the reconstructed images of an on-axis and two off-axis points (λ_c =500nm).

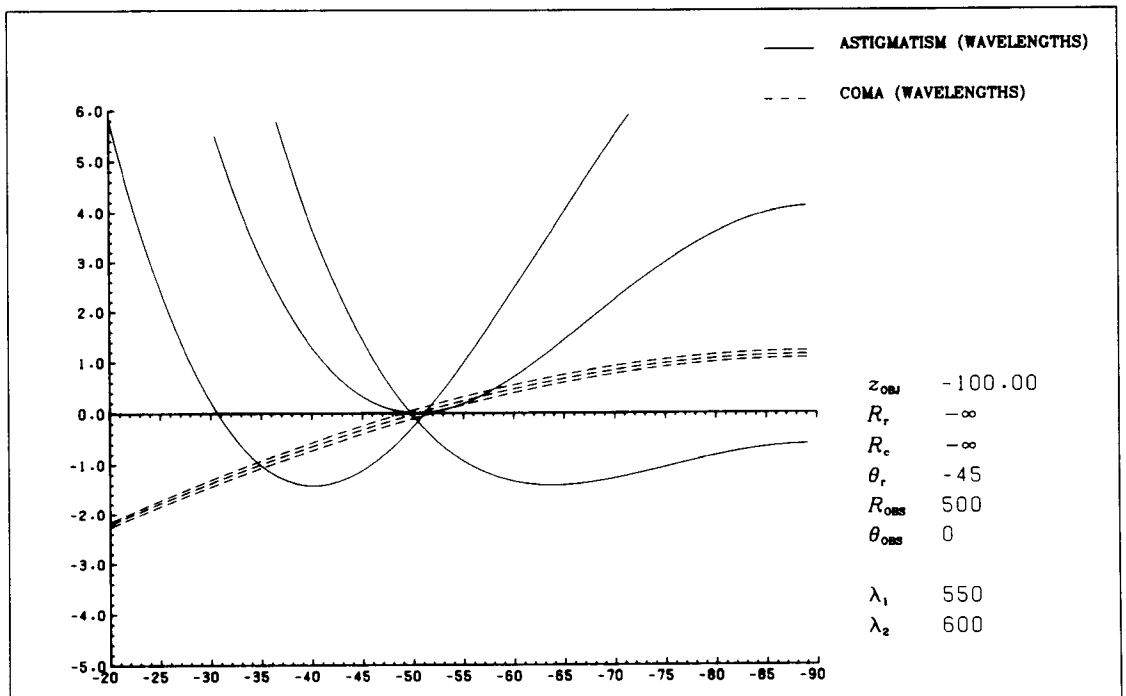

Fig. 7.14 Variation of Coma and Astigmatism in the reconstructed images of an on-axis and two off-axis points (λ_c =600nm).

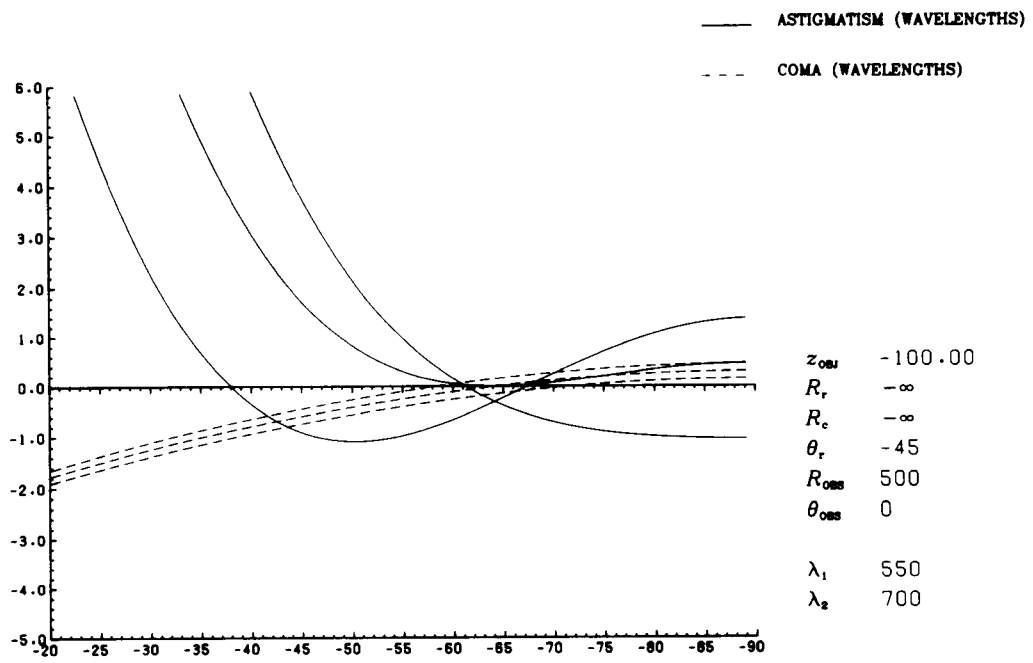

Fig. 7.15 Variation of Coma and Astigmatism in the reconstructed images of an on-axis and two off-axis points ($\lambda_c = 700$nm).

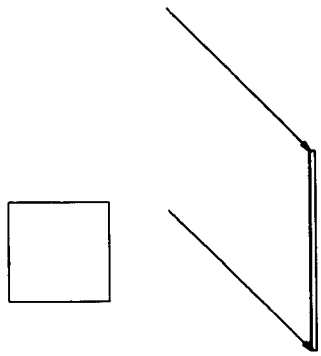

Fig. 7.16a Recording geometry for investigating geometrical distortions in a holographic image. The recording wavelength is 550nm.

7.6.2 Distortion

In the previous section we examined the position and the third order aberrations of a point image when dispersion compensation is employed. In this section we examine the relative geometrical displacements of a set of points, ie. the distortions, produced in dispersion compensation.

Let us consider the geometry in Fig. 7.16*a*. The object consists of a set of points joined in the form of a square. The centre of the object is 100mm from the plate and the observer is 500mm in front of the plate. All points are, as before, in the x–z plane, and the recording arrangement is

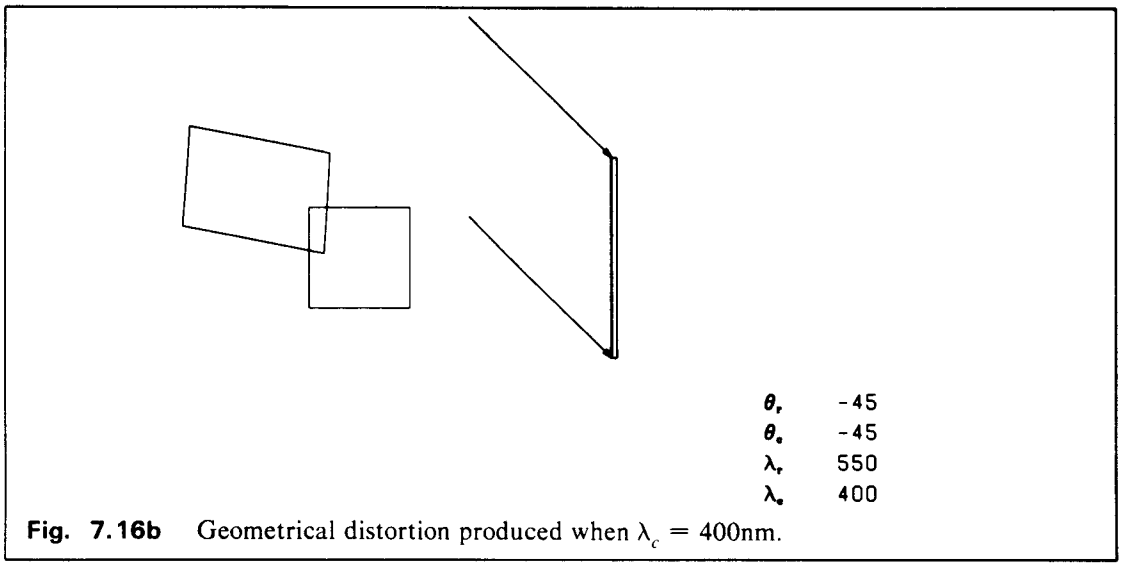

Fig. 7.16b Geometrical distortion produced when $\lambda_c = 400$nm.

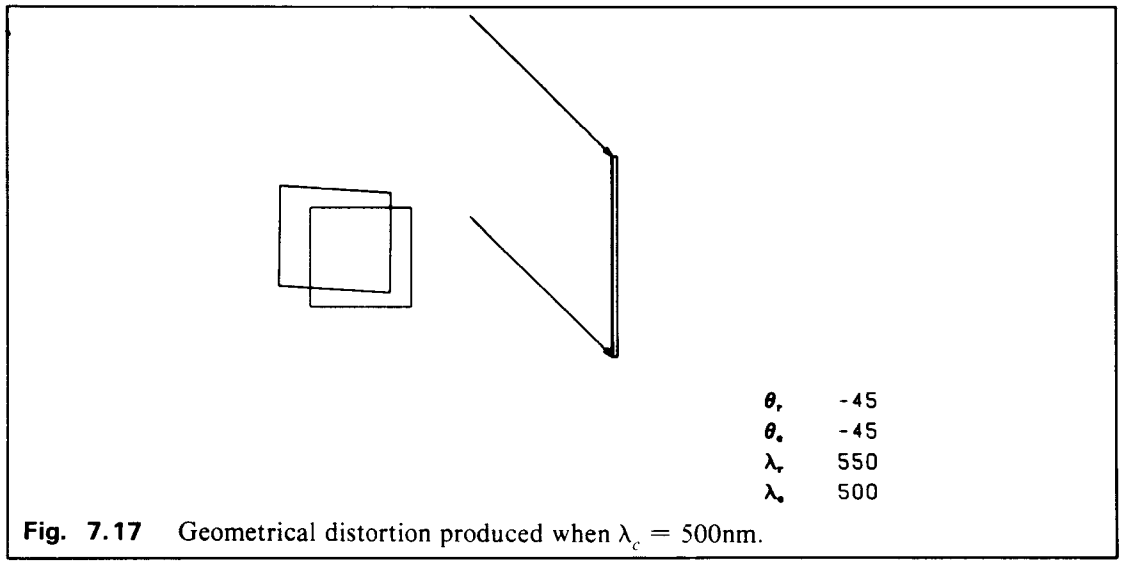

Fig. 7.17 Geometrical distortion produced when $\lambda_c = 500$nm.

as in §7.6.1. Fig. 7.16*b* shows the distortions produced when the reconstruction geometry is identical to the recording geometry, but the wavelength is reduced to 400nm. The resultant image is displaced and distorted. (The shape of the resultant image in Fig. 7.16*b* is determined by ascer-

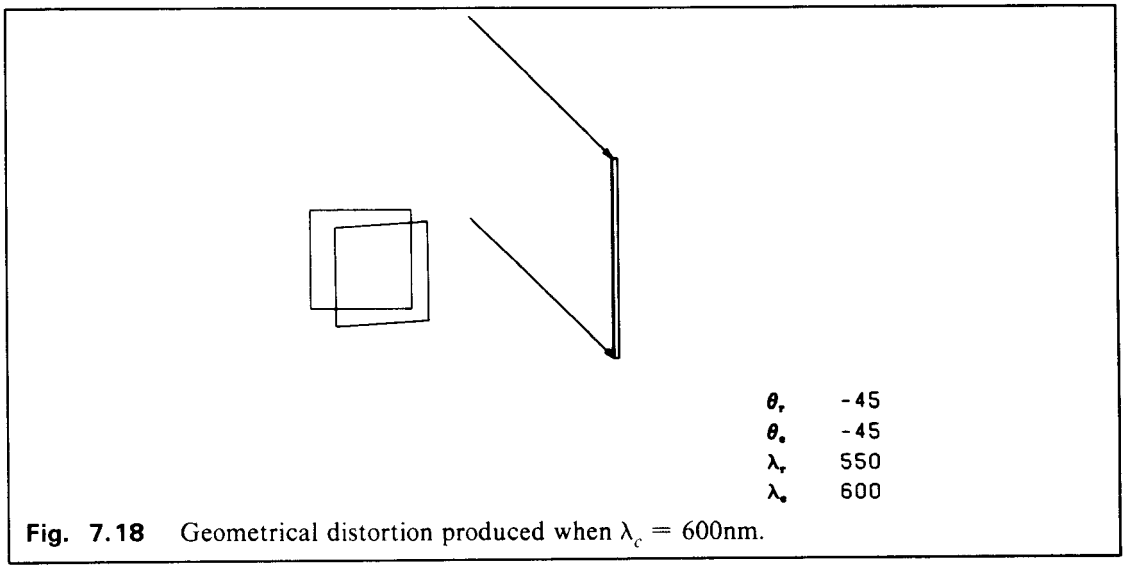

Fig. 7.18 Geometrical distortion produced when $\lambda_c = 600$nm.

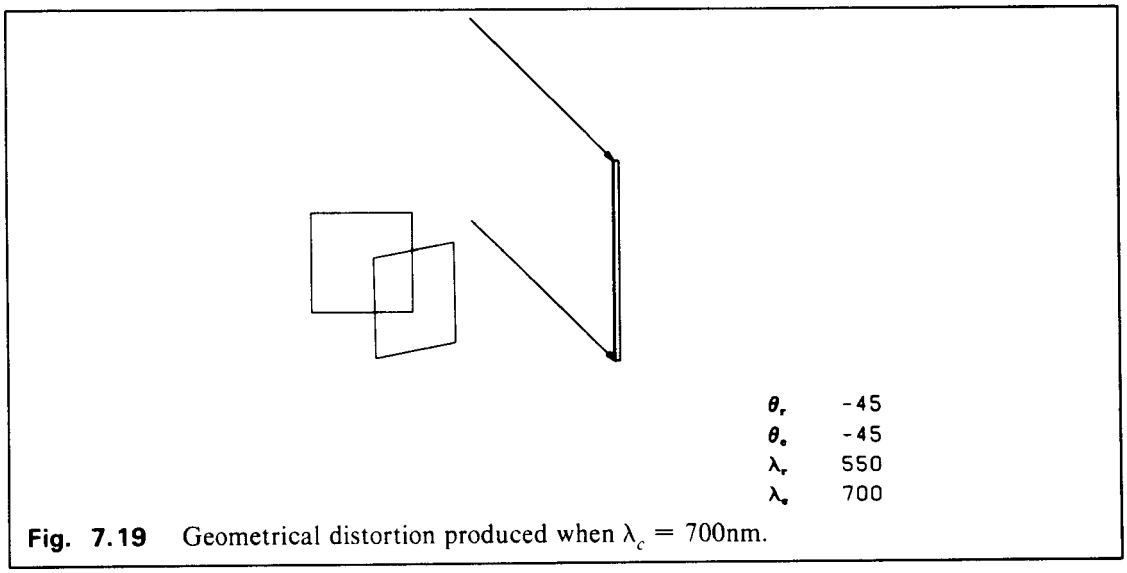

Fig. 7.19 Geometrical distortion produced when $\lambda_c = 700$nm.

taining the positions of the images of eight points, one on each corner of the square and one at the centre of each side, and drawing four cubic spline curves to form the final image.) Figs. 7.17–7.19 show the distortions produced for other wavelengths. When the angle in each case is adjusted to the dispersion-compensated angle, eg. 30.9° for 400nm, the images are near their original positions and the distortion is confined to longitudinal magnification or diminution. Fig. 7.20 shows the distortions for several wavelengths, before and after compensation.

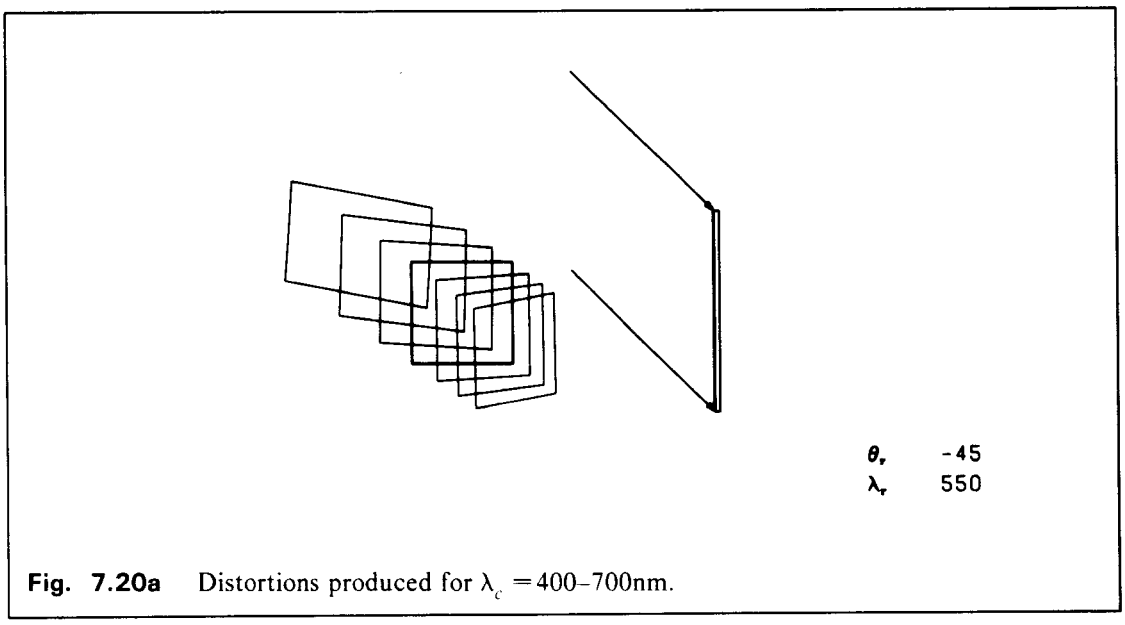

Fig. 7.20a Distortions produced for λ_c = 400–700nm.

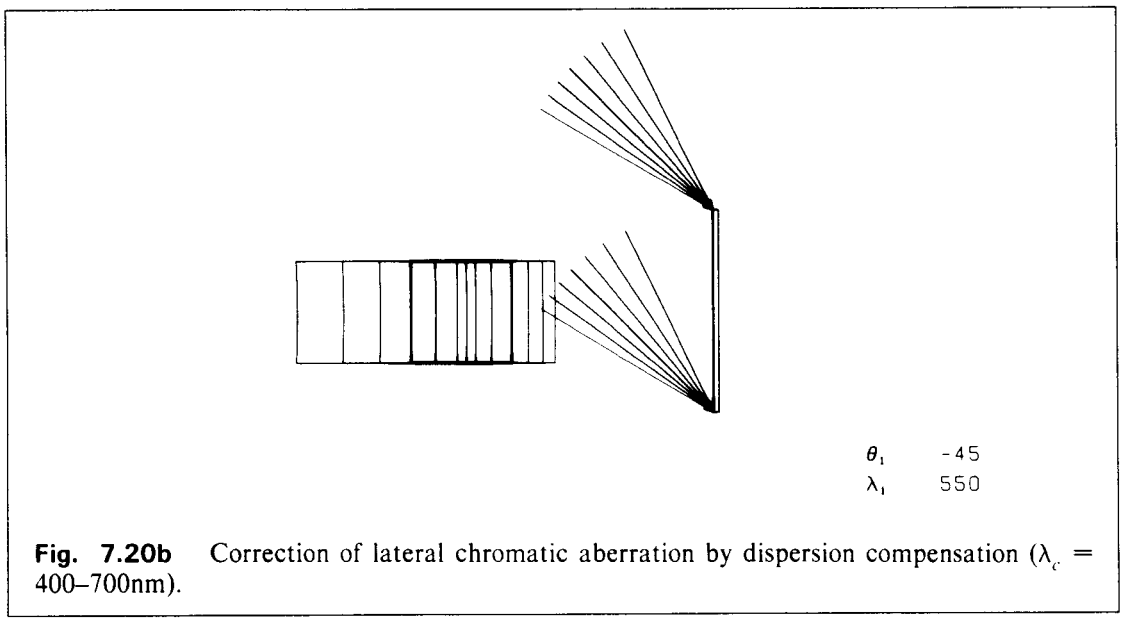

Fig. 7.20b Correction of lateral chromatic aberration by dispersion compensation (λ_c = 400–700nm).

7.7 AN INTERESTING PROPERTY OF A DISPERSION-COMPENSATED SYSTEM

Consider the composite dispersion-compensated system in Fig. 7.21. When collimated white light is incident normally on the diffraction grating, the observer E views a sharp, achromatic, orthoscopic image. What is observed if the system is viewed as in Fig. 7.22, with the hologram towards the light source? Experience with other types of holograms may suggest that the image is pseudoscopic. Surprisingly, however, the image is orthoscopic and undistorted, although mirror-reversed. Let us examine the light path:

Suppose that the hologram and the diffraction grating are made according to the geometries in Fig. 7.4. The recording material may be thick or thin. In the usual reconstruction geometry for dispersion compensation shown in Fig. 7.23 two representative rays are traced, intersecting the hologram at A and B. Note that the hologram has a higher spatial frequency at A. The observer

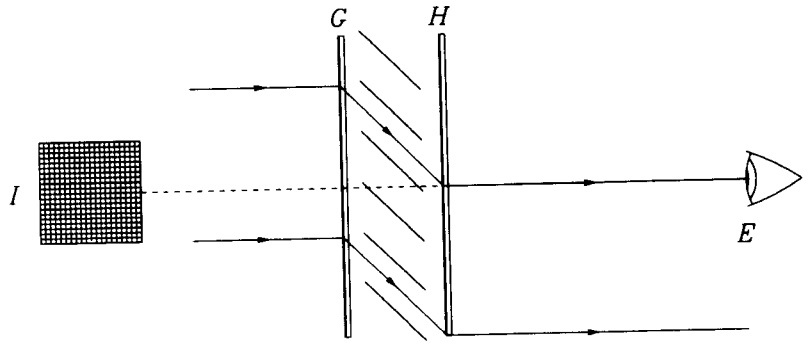

Fig. 7.21 Observation of a dispersion-compensated image.

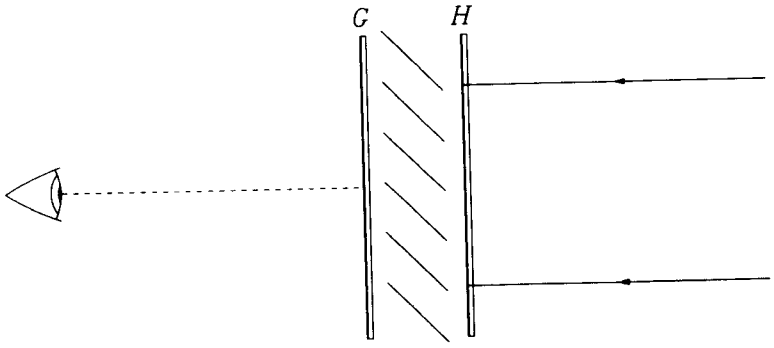

Fig. 7.22 Observation of the system in Fig. 7.21 from the grating side.

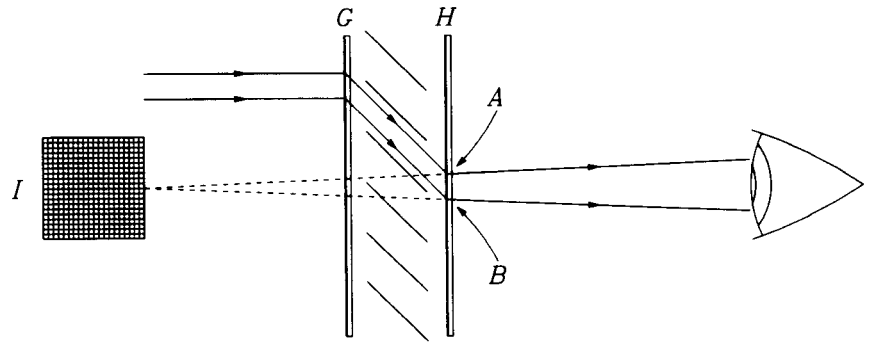

Fig. 7.23 Tracing two representative rays which form a point on the image. The hologram has a higher spatial frequency at A than at B.

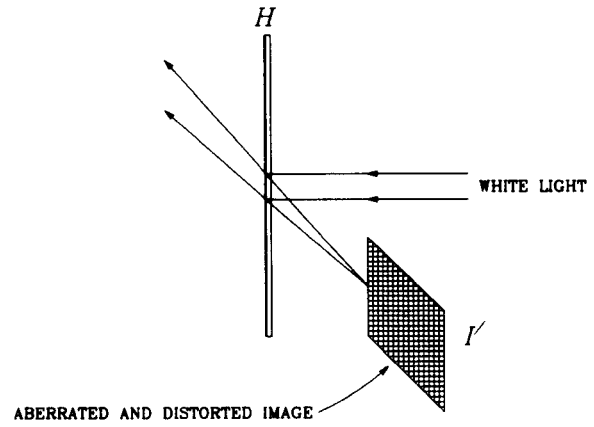

Fig. 7.24 Production of an aberrated and distorted image I' with a reversed reconstruction beam.

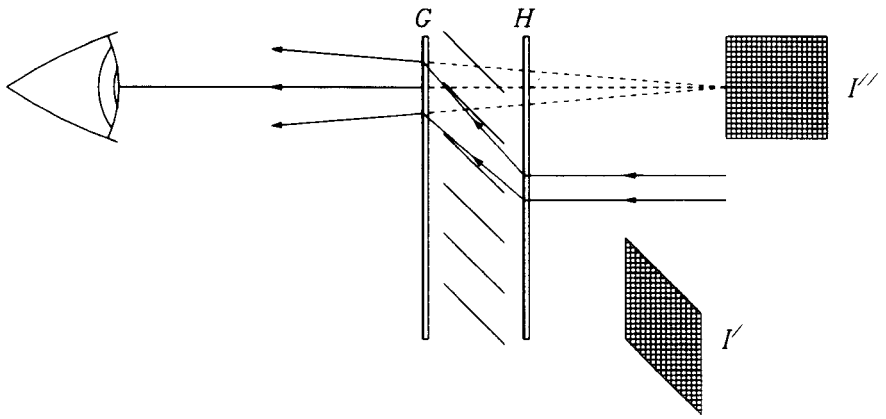

Fig. 7.25 Production of an undistorted but mirror-reversed image I'' by the composite grating–hologram structure.

views a virtual image at I. When the light path is reversed (Fig. 7.24), The Bragg condition is, in the first approximation, satisfied, and a distorted image I' is produced by the hologram. The relative spatial frequencies at A and B in this simple case dictate that the image be virtual. When the rays are traced through the grating (Fig. 7.25), the Bragg condition is again satisfied in the first approximation, and the light is diffracted into the original direction. An image I'' is observed which is virtual and orthoscopic, but mirror-reversed.

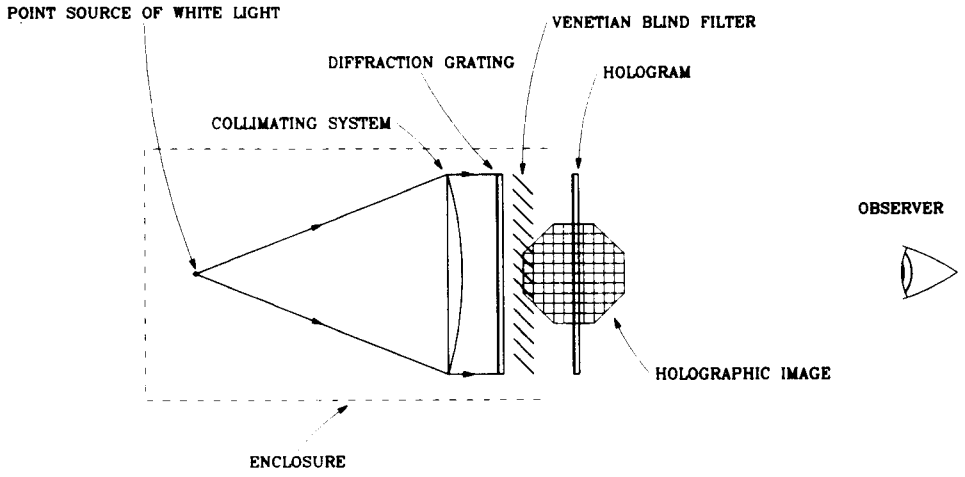

Fig. 7.26 A compact hologram viewing device based on dispersion compensation.

7.8 A COMPACT HOLOGRAM VIEWING DEVICE

The technique of dispersion compensation can be used to produce a compact hologram viewing device [52]. The proposed device (Fig. 7.26) consists, in its simplest form, of a compact white light source—eg. a tungsten-halogen lamp, a collimating element, a diffraction grating, and a 'Venetian-blind' filter. The device can be used to view transmission holograms made to be compatible with the 'compensating' grating—ie. made to have the same average spacial frequency. The reconstruction parameters are automatically set correctly when the hologram is parallel to the diffraction grating. The reconstruction source is normally invisible.

7.9 DISPERSION COMPENSATION IN VOLUME HOLOGRAMS

So far in this Chapter we have used thin grating formulæ in our treatment of dispersion compensation. We now take a more general approach and use a volume grating analysis, which will produce results for both transmission *and* reflection holograms.

Consider the general system in Fig. 7.27 which shows the cross-section of a volume grating of average refractive index n, lying in a medium of unit refractive index. The fringe planes are perpendicular to the plane of the paper. The grating vector $\mathbf{K}$ is perpendicular to the fringe planes, and is of magnitude

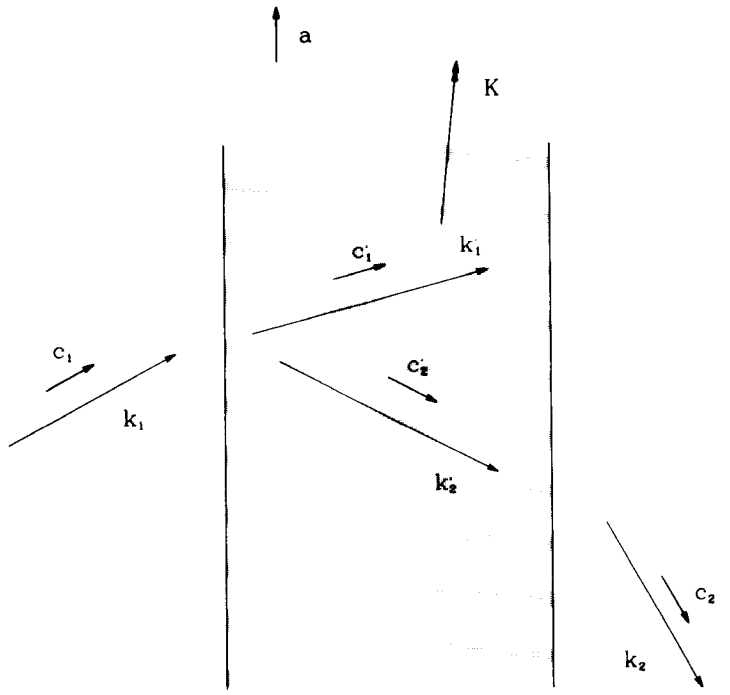

Fig. 7.27 Definition of vectors used in the analysis of dispersion compensation in volume holograms.

$$|\mathbf{K}| = \frac{2\pi}{\Lambda},$$

where Λ is the grating period.

We let a plane wave impinge upon the grating and be diffracted by it. $\mathbf{k}_1$ and $\mathbf{k}_2$ are the propagation vectors of the incident and the diffracted waves respectively, and $\mathbf{k}_1'$ and $\mathbf{k}_2'$ are the corresponding propagation vectors inside the grating. We define $\mathbf{c}_1$, $\mathbf{c}_2$, $\mathbf{c}_1'$ and $\mathbf{c}_2'$ as unit vectors in the respective directions. If the wave number is $k = 2\pi/\lambda$, λ being the wavelength in free space, then

$$\mathbf{k}_1 = k\mathbf{c}_1 \quad \text{and} \quad \mathbf{k}_2 = k\mathbf{c}_2. \tag{7.1}$$

Similarly,

$$\mathbf{k}_1' = k'\mathbf{c}_1' \quad \text{and} \quad \mathbf{k}_2' = k'\mathbf{c}_2' \tag{7.2}$$

where

$$k' = \frac{2\pi n}{\lambda} = nk.$$

If the grating is infinitely thick in all directions, diffraction can only occur when the Bragg condition is completely satisfied, ie. when

$$(\mathbf{k}_1' - \mathbf{k}_2') = \mathbf{K}. \tag{7.3}$$

Practical recording media, however, can usually be regarded as semi-thick. In Fig. 7.27 the extent of the grating is assumed to be infinite in the direction of the unit vector **a**, but finite in the direction perpendicular to it. In this case, let us assume that although the component of the Bragg formula in the direction of **a** must hold, the component perpendicular to it need not hold, because of the finite thickness. In other words, Eqn. 7.3 can be replaced by

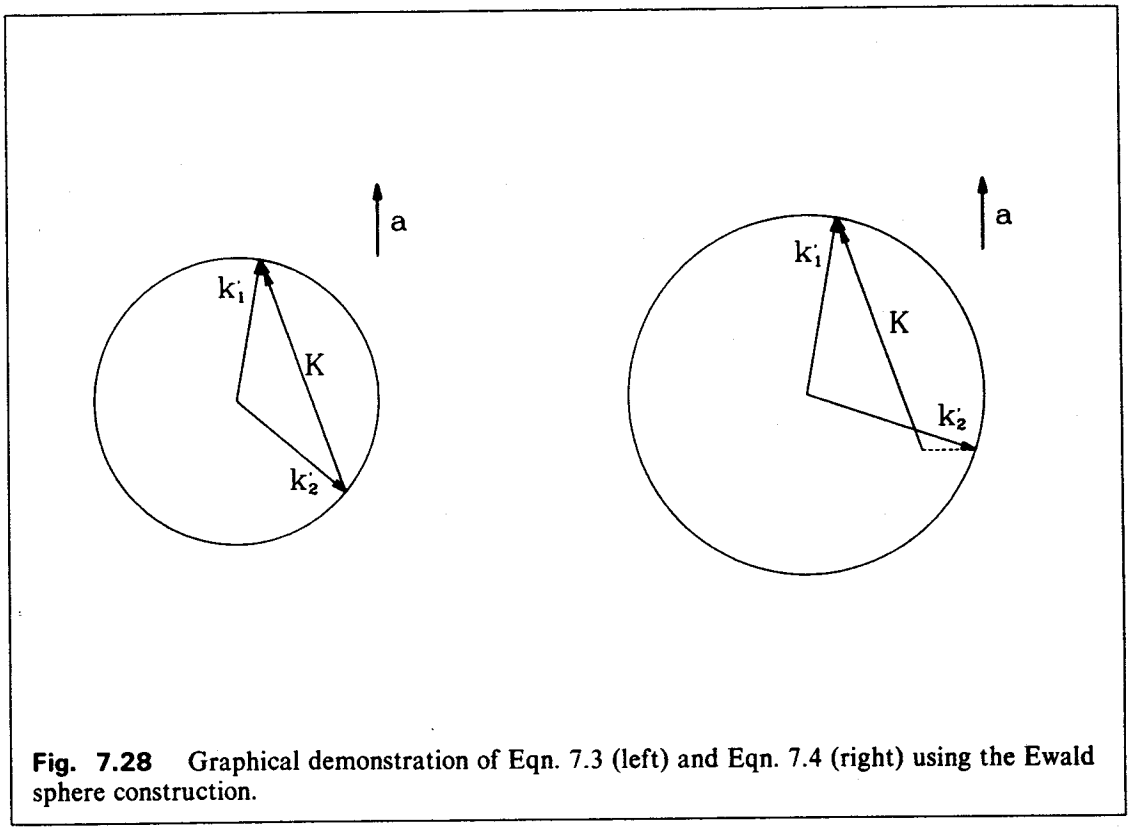

Fig. 7.28 Graphical demonstration of Eqn. 7.3 (left) and Eqn. 7.4 (right) using the Ewald sphere construction.

$$(\mathbf{k}_1' - \mathbf{k}_2') \cdot \mathbf{a} = \mathbf{K} \cdot \mathbf{a}. \tag{7.4}$$

This condition can be graphically demonstrated using the Ewald sphere construction (Fig. 7.28). Now by Snell's law, for surface i,

$$\mathbf{c}_i \cdot \mathbf{a} = n\mathbf{c}_i' \cdot \mathbf{a}.$$

Therefore, using Eqn. 7.2,

$$\mathbf{k}_i' \cdot \mathbf{a} = \mathbf{k}_i \cdot \mathbf{a},$$

and Eqn. 7.4 can be rewritten as

$$(\mathbf{k}_1 - \mathbf{k}_2) \cdot \mathbf{a} = \mathbf{K} \cdot \mathbf{a}. \tag{7.5}$$

The properties of the grating can now be analysed independently of its refractive index. We now consider a system of two parallel volume gratings (Fig. 7.29), the dispersed beam from the first being incident upon the second. We assume that the Bragg condition is completely satisfied for a particular wavelength. Extending the terminology to the wave diffracted from the second grating ($i = 3$), the corresponding equations are:

$$\begin{aligned} (\mathbf{k}_1 - \mathbf{k}_2) \cdot \mathbf{a} &= \mathbf{K}_1 \cdot \mathbf{a}, \\ (\mathbf{k}_2 - \mathbf{k}_3) \cdot \mathbf{a} &= \mathbf{K}_2 \cdot \mathbf{a}. \end{aligned} \tag{7.6}$$

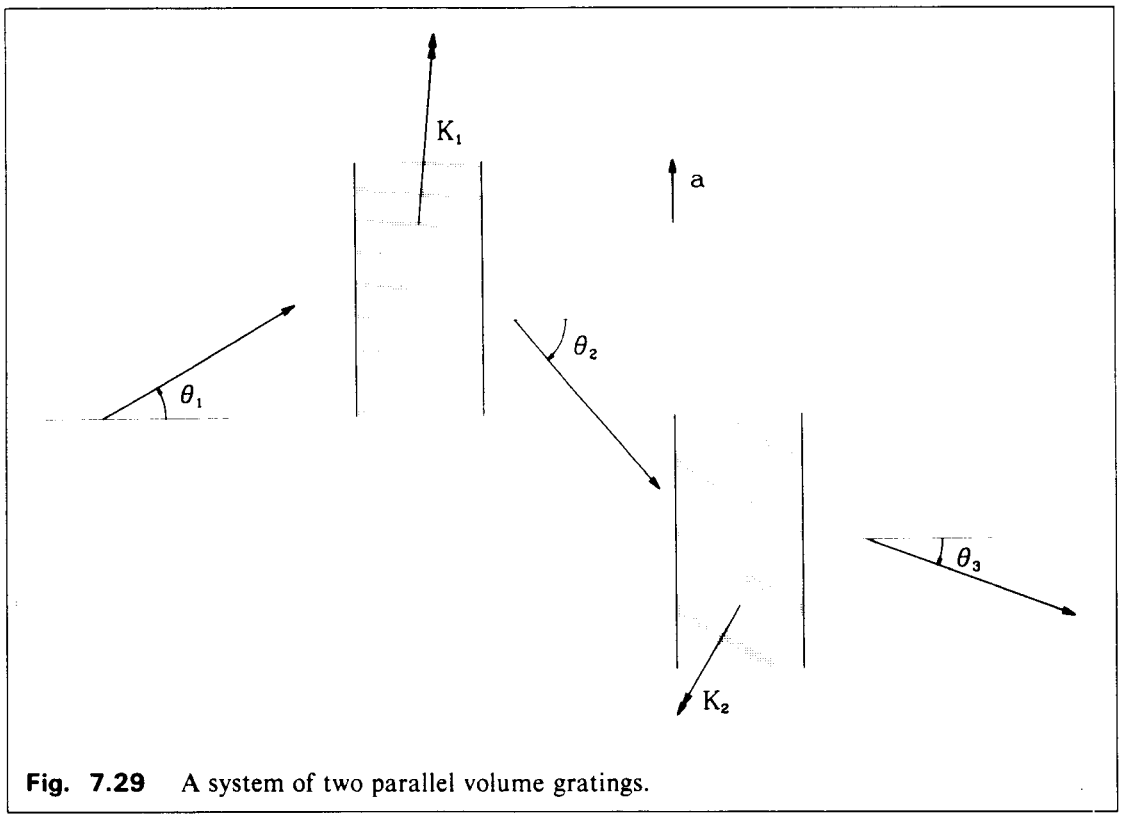

Fig. 7.29 A system of two parallel volume gratings.

If dispersion is compensated so that the beams incident on and emergent from the system are both undispersed, then

$$\frac{d\mathbf{c}_1}{dk} = \dot{\mathbf{c}}_1 = 0 \qquad \text{and} \qquad \frac{d\mathbf{c}_3}{dk} = \dot{\mathbf{c}}_3 = 0.$$

Using this assumption, and differentiating Eqn. 7.6 with respect to k, we obtain

$$\mathbf{c}_1 \cdot \mathbf{a} - k\dot{\mathbf{c}}_2 \cdot \mathbf{a} - \mathbf{c}_2 \cdot \mathbf{a} = 0,$$

and

$$\mathbf{c}_2 \cdot \mathbf{a} + k\dot{\mathbf{c}}_2 \cdot \mathbf{a} - \mathbf{c}_3 \cdot \mathbf{a} = 0,$$

whence

$$\mathbf{c}_1 \cdot \mathbf{a} - \mathbf{c}_3 \cdot \mathbf{a} = 0 \tag{7.7}$$

or

$$\sin\theta_1 = \sin\theta_3, \tag{7.8}$$

where θ_i is the angle of incidence. If we restrict θ_i such that $|\theta_i| < 90^\circ$, Eqn. 7.8 reduces to $\theta_1 = \theta_3$ and is the condition for transmission gratings. Lifting this restriction extends the result to volume gratings.

The Ewald construction again allows a graphical demonstration. Fig. 7.30*a* is the graphical construction for the system in Fig. 7.29, the Bragg condition being completely satisfied, at $k = k_a$ say, in both elements. Fig. 7.30*b* represents the same system with a slightly larger wavenumber for the incident beam, k_b. Constructing according to Eq. 7.6, the final emergent wave vector $\mathbf{k}_{3b}$ is not codirectional with $\mathbf{k}_{3a}$, and therefore dispersion is not compensated. Figs. 7.31–3 illustrate some dispersion-compensated systems and the corresponding graphical constructions.

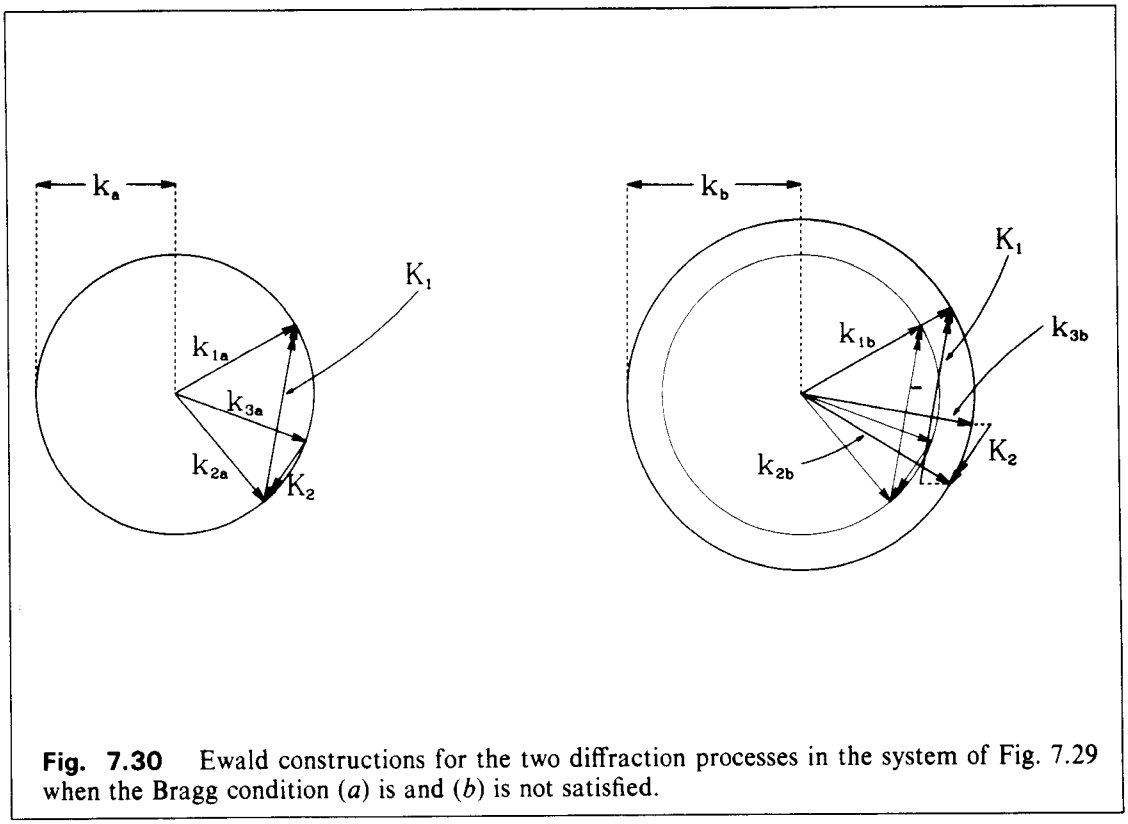

Fig. 7.30 Ewald constructions for the two diffraction processes in the system of Fig. 7.29 when the Bragg condition (*a*) is and (*b*) is not satisfied.

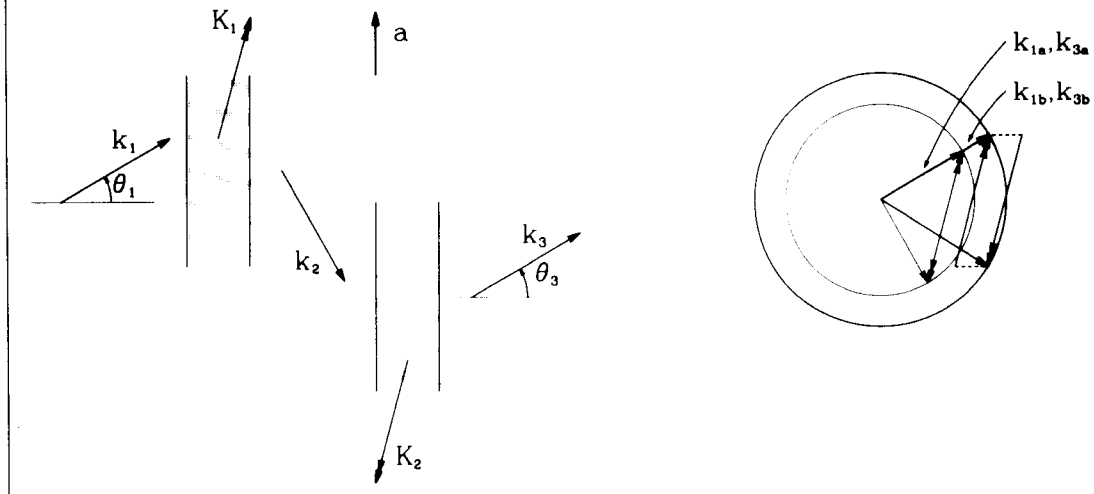

Fig. 7.31 A dispersion-compensated system comprising two volume transmission gratings and the corresponding graphical construction.

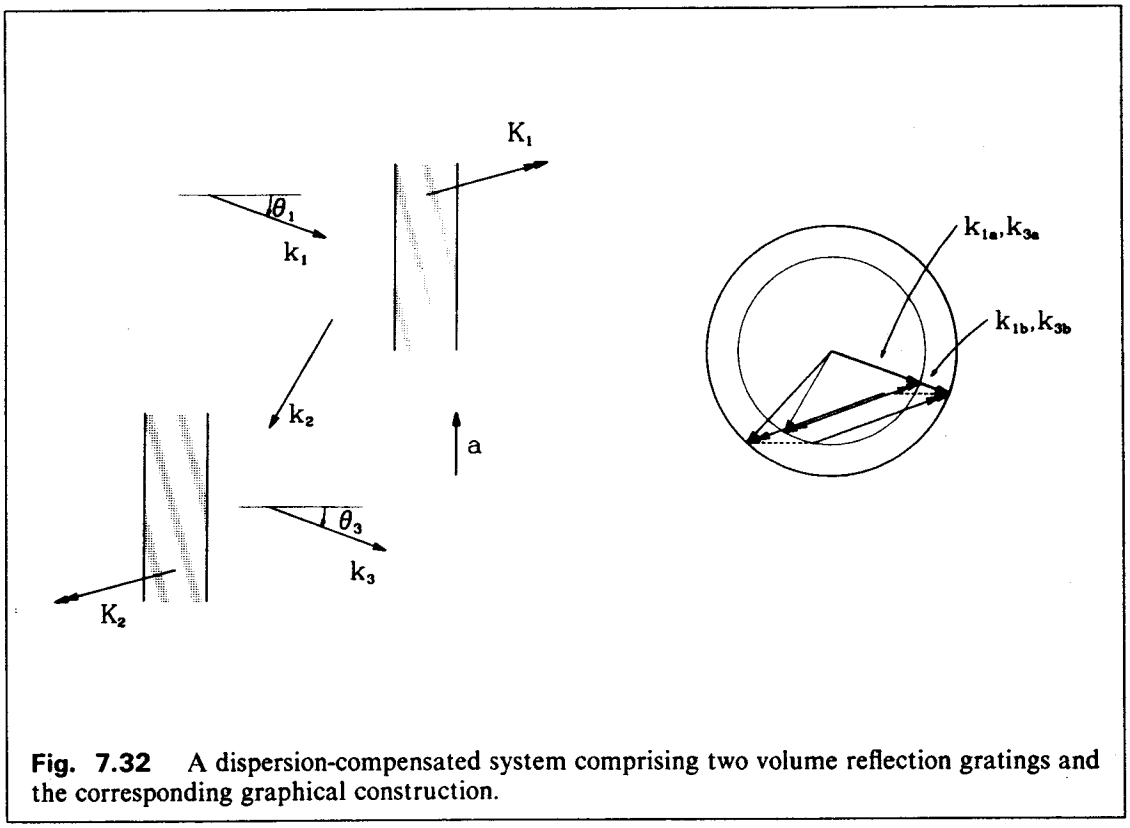

Fig. 7.32 A dispersion-compensated system comprising two volume reflection gratings and the corresponding graphical construction.

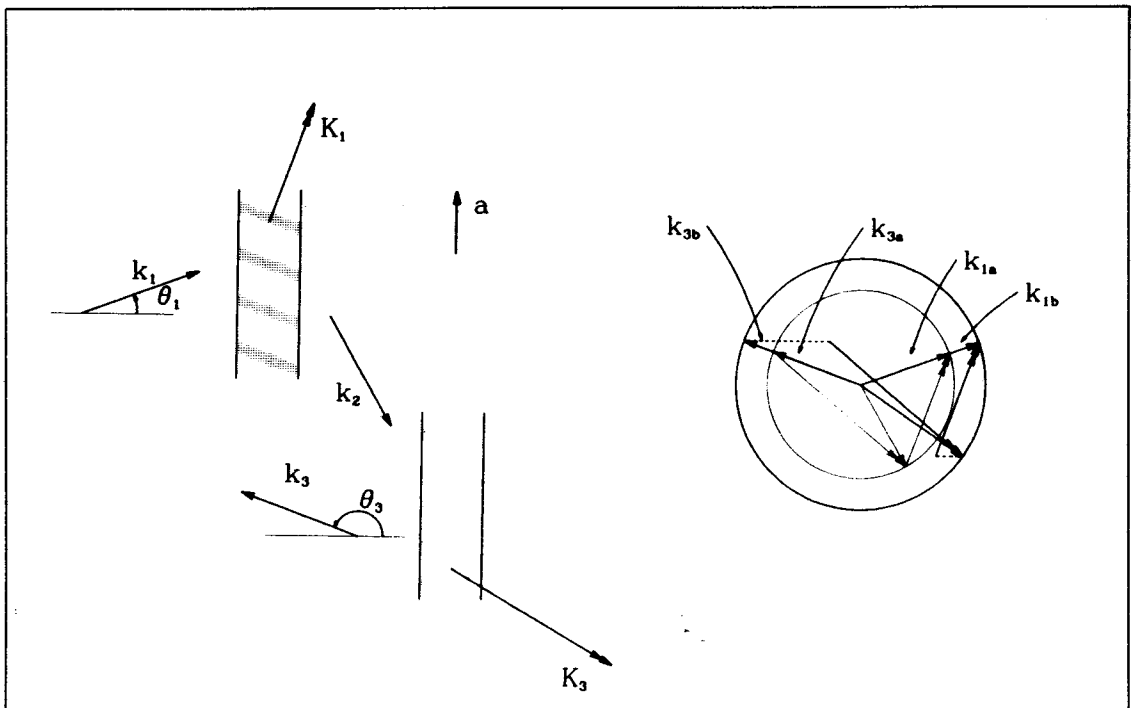

Fig. 7.33 A dispersion-compensated system comprising a volume transmission and a volume reflection grating, and the corresponding graphical construction.

7.10 MULTICOLOUR DISPERSION-COMPENSATED HOLOGRAPHY

We have exploited the wavelength selectivity of volume transmission holograms to produce a new type of multicolour holographic image [8]. Consider the system in Fig. 7.34. An off-axis hologram is made of a diffusely reflecting object using green recording light and a thick emulsion. The image is subsequently reconstructed in a dispersion-compensated system using a thin (non-wavelength-selective) compensating grating—Fig. 7.35. If the thickness and the average refractive index of the emulsion are unchanged, then the hologram will be wavelength-selective towards the green part of the spectrum, and a green image is reconstructed, the colour saturation depending on the wavelength selectivity. A multicolour hologram can be made by superimposing several holograms of the same object recorded using several different wavelengths, the reference angle being adjusted in each recording such that the average spatial frequencies of the holograms are equal, and equal to the spatial frequency of the compensating grating—Fig. 7.36.

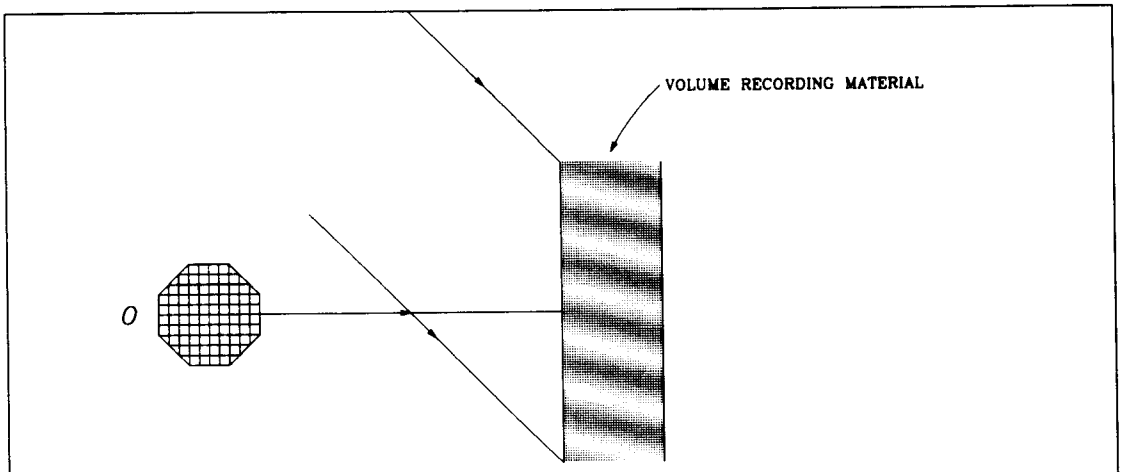

Fig. 7.34 Recording a holographic image in a thick recording medium. The *average* orientation of the fringes is shown.

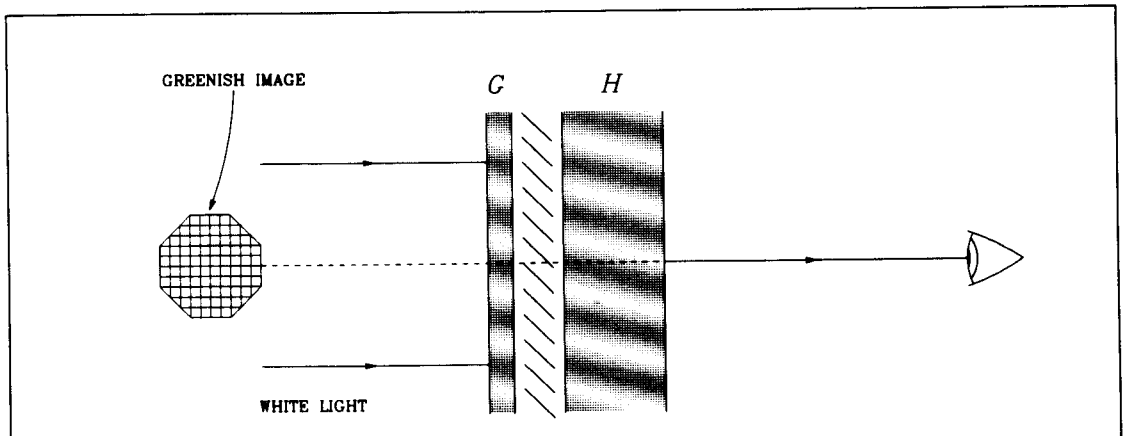

Fig. 7.35 Viewing the image produced in a dispersion-compensated system comprising a thin grating and a thick hologram. A non-achromatic image is observed.

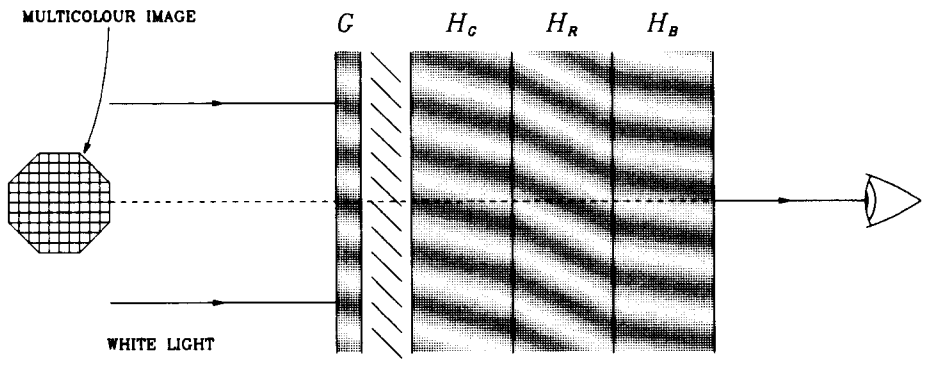

Fig. 7.36 A dispersion-compensated multicolour image produced by superimposing several monochromatic images. The colour saturation in the final image increases with increasing emulsion thickness. The holograms may be recorded in the same panchromatic emulsion.

A property of this type of hologram is that, unlike other multicolour holograms, spurious images are not produced when the wavelength selectivity of the hologram decreases. Light of any wavelength diffracting from any component hologram produces an image superimposed on other images so that the effect of, say, red light diffracting from the 'green' hologram is simply to reduce the colour saturation of the composite image. An example of a dispersion-compensated multicolour hologram is shown in Plate VI. The colour saturation is low partly because present commercially available holographic recording materials lack the required emulsion thickness for this technique.

CHAPTER 8

REFLECTION HOLOGRAPHY

8.1 INTRODUCTION

Reflection holograms are made by introducing reference and object beams from opposite sides of a thick recording material (Fig. 2.11). The interference fringes are approximately parallel to the emulsion surface, and can therefore behave as an interference filter, diffracting only a narrow band of wavelengths. For this reason reflection holograms can be viewed in white light.

8.2 ONE-STEP RECORDING

8.2.1 Projecting a Real Image

Analogously to one-step image-plane holography, an aerial image of an object can be recorded in a reflection hologram by placing a recording material within the aerial image and introducing a reference beam from the opposite side of the emulsion (Fig. 8.1). As before, the imaging system may be a lens or mirror system, or a mirror-beamsplitter combination (§5.2). The problem of vignetting again arises. In reflection holography this can conveniently be tackled by placing a field lens adjacent to the recording plate, on the image side (Fig. 8.2). As the reference beam enters the emulsion from the opposite side, the lens does not interfere with it as it would in transmission holography (cf. §5.2.1).

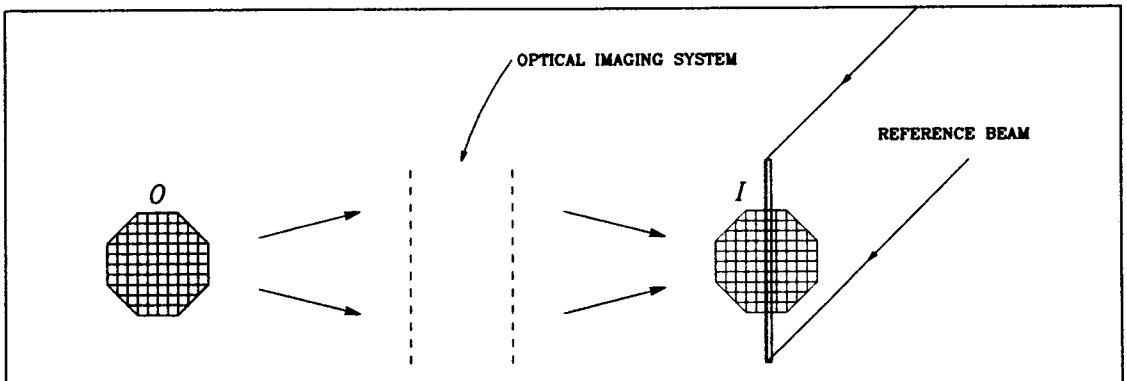

Fig. 8.1 Recording a one-step reflection hologram of a projected image.

8.2.2 Denisyuk Holography

A particularly simple and effective method of recording a reflection hologram in one step is to use one beam to act as the reference *and* the object illuminating beam [57]—Fig. 8.3. The portion of the light passing through the emulsion illuminates the object lying immediately behind the plate. The back-scattered light from the object forms the object beam. An advantage of the method is that if the recording plate and the object are in contact sensitivity to vibration is reduced. Disadvantages of the method are that control of lighting and of beam ratios are very limited.

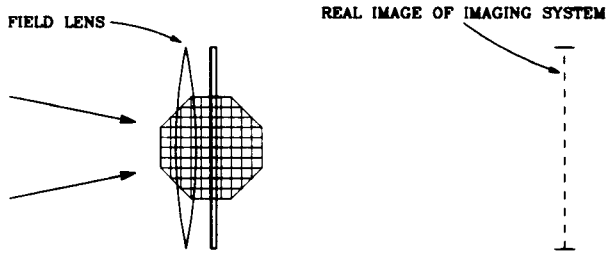

Fig. 8.2 Using a field lens to increase the field of view.

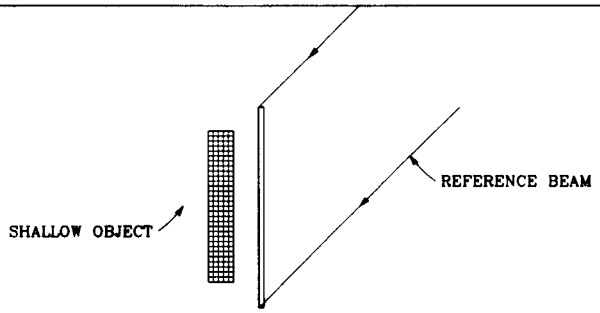

Fig. 8.3 Recording a Denisyuk hologram.

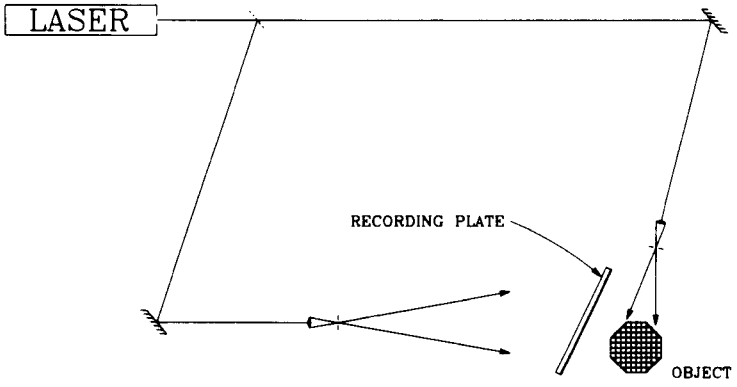

Fig. 8.4 Recording a simple split-beam reflection hologram.

8.2.3 One-Step Split-Beam Recording

A simple reflection hologram can be recorded using an arrangement similar to that used for a simple laser-transmission hologram. Fig. 8.4 shows such an arrangement. The technique requires that the object be placed some distance from the recording plate and the sharpness of the final image is therefore limited.

8.3 TWO-STEP RECORDING

8.3.1 Transmission Master

The usual method of recording a two-step reflection hologram is analogous to two-step image-plane holography (see §5.3). Fig. 8.5 shows the basic arrangement for recording and reconstructing.

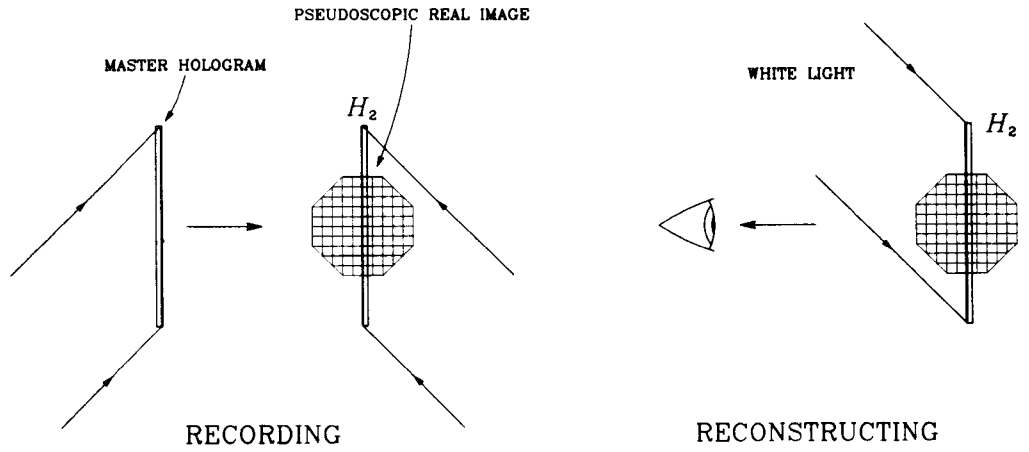

Fig. 8.5 Recording and reconstruction stages in a two-step reflection hologram.

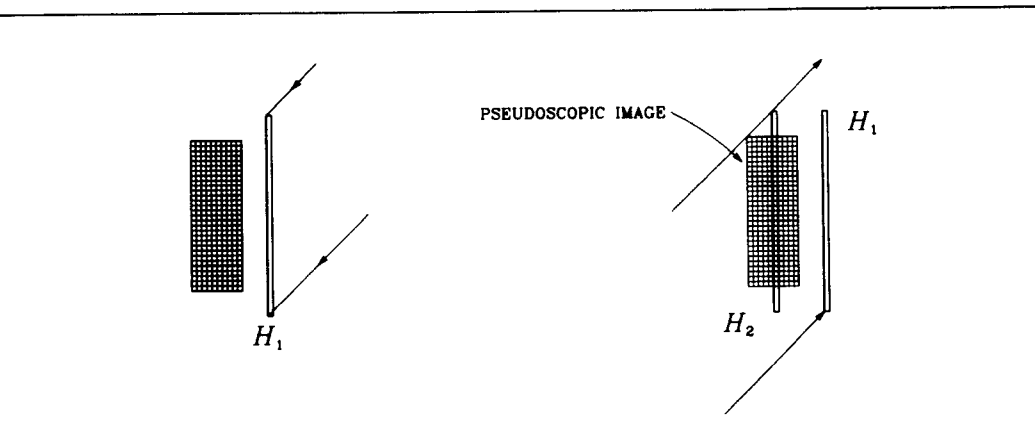

Fig. 8.6 Recording a two-step reflection hologram using a 'Denisyuk' master.

8.3.2 Reflection Master

An interesting two-step method of recording reflection holograms involves using a Denisyuk hologram (§8.2.2) as the 'master' (Fig. 8.6). The method is simple and resistant to vibrations, but suffers from lack of versatility in the lighting arrangement. The master hologram must be processed so as to replay the image in the original wavelength.

8.4 BEAM RATIO

Unlike in transmission holography, intermodulation effects are not normally present in reflection holography. Self-interference of the object beam results in transmission components which are not present when the reflection image is viewed. The beam ratio can therefore be optimized to give maximum fringe modulation. We have found that a beam ratio of 1:1 works well. When the object beam is non-uniform—eg. in one step techniques—then a beam ratio of unity is chosen for the brightest parts of the object beam.

8.5 RECORDING MATERIALS

8.5.1 Spatial Resolution

The spatial resolution required of the recording material in reflection holography is generally greater than in transmission holography. This is because the refractive index of the emulsion increases the spatial frequency , whereas in transmission holography it has no effect. Consider two plane waves incident normally from opposite sides of a volume recording material. From §2.4.2.3, the fringe spatial frequency is

$$\nu = \frac{1}{\Lambda} = \frac{2n}{\lambda}.$$

For $n = 1.5$ and $\lambda = 550\text{nm}$, $\nu = 5455$ lines/mm. This is some four times the spatial frequency in transmission holography (§4.7).

8.5.2 Silver Halide Materials

The most popular commercially available silver halide materials are Agfa–Gevært 8E75HD and 8E56HD emulsions which can produce excellent reflection holograms.

As the wavelength replayed in reflection holograms is directly related to the fringe spacing, control of thickness and refractive index during processing is important. Conventional processing reduces the thickness and the refractive index of the emulsion. Although in transmission holography the two effects tend to compensate Bragg deviations, in reflection holography they have an additive effect [58]. The simplest way of correcting shrinkage is to re-swell the emulsion using a swelling agent [59–61]. Recent chemical processes designed for holography produce only small changes in emulsion parameters [62–65].

8.5.3 Dichromated Gelatin

Dichromated gelatin is a recording material capable of producing very efficient reflection holograms with diffraction efficiencies close to the theoretical limits. The disadvantages of dichromated gelatin are its low sensitivity and its short shelf life. We have produced some very efficient reflection holograms by manufacturing, exposing and processing the recording plates according to the following procedures:

Preparation of gelatin coating:

1. Produce a 4% solution (by weight) of 150 bloom gelatin (produced by BDH chemicals, UK) in distilled water, by adding the gelatin to cold water and slowly heating and stirring until dissolved. Keep solution warm.

2. Thoroughly clean a piece of float glass 30 cm^2 and 3mm thick.

3. Place the glass substrate in a dust-free environment—eg. a laminar flow cabinet—resting on three levelling screws, and adjust screws until substrate is horizontal.

4. Pour 30 ml of gelatin solution onto the substrate, starting at the centre and moving out towards the edges. Using a clean glass rod spread the solution so as to cover the entire substrate surface. (The gelatin solution will be prevented from spilling over the edge by surface tension.)

5. Leave to dry overnight.

Sensitization:

1. Soak plate in Ilford Hypam fixer (diluted 1+4) + hardener [5 min].

2. Wash in running water [5 min]

3. Rinse in distilled water [1 min].

4. Soak in 5% aqueous solution of Ammonium Dichromate + 1 drop Kodak Photo-Flo per 500ml. [5 min]. (Under red safelight.)

5. Carefully wipe glass side of plate using wet tissue.

6. Rest plate at some 30° to horizontal (emulsion upwards), with the lower edge resting on absorbent tissue or blotting paper. Leave to dry for at least 6hrs. Cut into smaller pieces as required.

Exposure:

1. Place shallow object directly onto table surface and rest recording plate on the object. Check for stability of plate relative to object.

2. Expose with 514.5nm laser light (Ar^+) with 45° reference angle. Exposure required is of the order of 0.1 J/cm^2, with good latitude.

Processing:

All steps at 20°C.

1. Soak plate in 0.5% solution of Ammonium Dichromate [5 min].

2. Soak in Ilford Hypam fixer (1+4) + Hardener [5 min].

3. Wash in running water [10 min].

4. Soak in solution of 'Photo-Flo' (1 drop/litre) [30 sec.]

5. Soak in distilled water [2 min].

6. Soak in 50% aqueous solution of Isopropanol (Propan-2-ol) [3 min].

7. Soak in 100% Isopropanol [3 min].

8. Place in tall container of Isopropanol. Gently draw plate out of container and rapidly dry emulsion surface at its interface with liquid, using a hot-air gun (eg. hair dryer).

The above procedures have been applied without the usual strict control over external conditions such as temperature and humidity, and therefore accurate reproducibility is not ensured, but we have found that acceptable display holograms of shallow depth can be obtained by empirical variation of the exposure, to compensate for variations in external parameters. We have also found that if accurate reproducibility is not required, sensitized plates can be used after several months' storage.

8.6 DISPERSION IN REFLECTION HOLOGRAMS

Consider the two recording systems in Fig. 8.7, the terminology following that of §7.9. The transmission grating is recorded using incidence angles θ_1 and θ_2. In the reflection case the corresponding angles are θ_1 and $\theta_3 = (180^\circ - \theta_2)$. In both cases Eqn. 7.5 must be satisfied, ie.

$$(\mathbf{k}_1 - \mathbf{k}_2) \cdot \mathbf{a} = \mathbf{K} \cdot \mathbf{a},$$

which can be rewritten as

$$\frac{2\pi}{\lambda} \sin\theta_1 - \frac{2\pi}{\lambda} \sin\theta_2 = \frac{2\pi}{\Lambda} \cos\phi$$

or

$$d(\sin\theta_1 - \sin\theta_2) = \lambda.$$

This implies that the surface fringe spacing d is identical in the two cases. The dispersion for $\theta_2 =$ constant in the transmission case is given by

$$\frac{d\theta_1}{d\lambda} = \frac{1}{d\cos\theta_1}$$

$$= \frac{\sin\theta_1 - \sin\theta_2}{\lambda\cos\theta_1}. \tag{8.1}$$

For the reflection case, if $\theta_3 =$ constant,

$$\frac{d\theta_1}{d\lambda} = \frac{\sin\theta_1 - \sin\theta_3}{\lambda\cos\theta_1} \tag{8.2}$$

$$= \frac{\sin\theta_1 - \sin\theta_2}{\lambda\cos\theta_1}.$$

The two systems therefore have identical dispersion properties. If $\theta_3 = 180^\circ$, the resultant dispersion is zero if $\theta_1 = 0^\circ$. (This is equivalent to the Gabor in-line hologram in the transmission case.) This arrangement is impractical, as the observer is necessarily in the path of the illuminat-

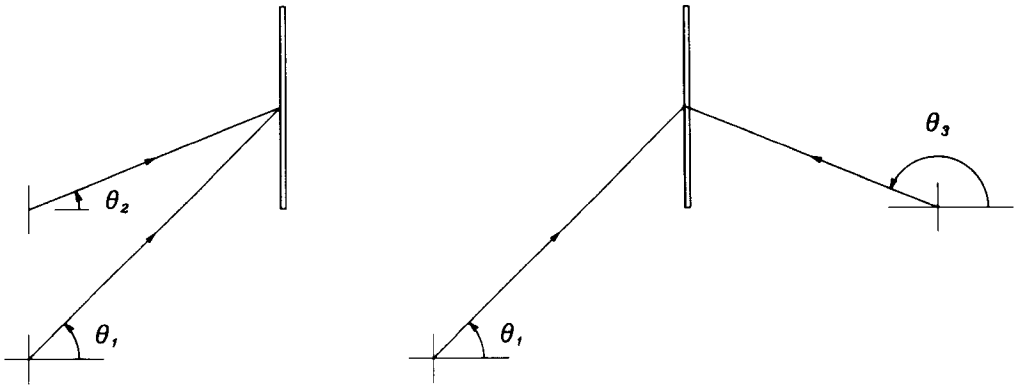

Fig. 8.7 A transmission (left) and a reflection (right) grating with identical dispersive properties.

ing beam during image reconstruction. Examination of Eqn. 8.2 shows that the dispersion is zero whenever $\theta_3 = 180^\circ - \theta_1$. The observer is now angularly separated from the reconstruction beam, but the specular reflection of the beam is superimposed on the image—an arrangement normally unacceptable in display work.

In order to minimize dispersion, if the object beam is on-axis, a small reference angle must be used to record the hologram. It is inconvenient, however, to have inter-beam angles of less than, say, 45°, as the observer may impede the reconstruction beam. We can reduce the dispersion by tilting the recording plate such that the interbeam angle remains at say 45°, and the specular reflection of the reconstruction beam just misses the line of sight of the observer. One practical configuration is one in which $\theta_1 = 15^\circ$ and $\theta_3 = 150^\circ$, the interbeam angle being 45°. Substituting the values into Eqn. 8.2 we obtain

$$\frac{d\theta_1}{d\lambda} = -4.5 \times 10^{-4} \quad \text{deg/nm.}$$

This value is equivalent to $\theta_3 = 165.5^\circ$ if $\theta_1 = 0$, ie. a reference angle of 14.5°.

8.6.1 Chromatic Blur

The chromatic blur in a reflection hologram is given by Eqn. 5.2, ie.

$$\Delta x = D \sin\theta_1 \left(\frac{\Delta\lambda}{\lambda_G}\right).$$

In reflection holography $\Delta\lambda$ is typically 20nm, compared to say 300nm in transmission holography.

8.7 MULTICOLOUR REFLECTION HOLOGRAPHY

Multicolour reflection holograms can be made using any of the recording techniques described, by superimposing two or more reflection holograms made with different wavelengths, but with identical recording geometries. The holograms may be recorded in the same emulsion or in several adjacent emulsions.

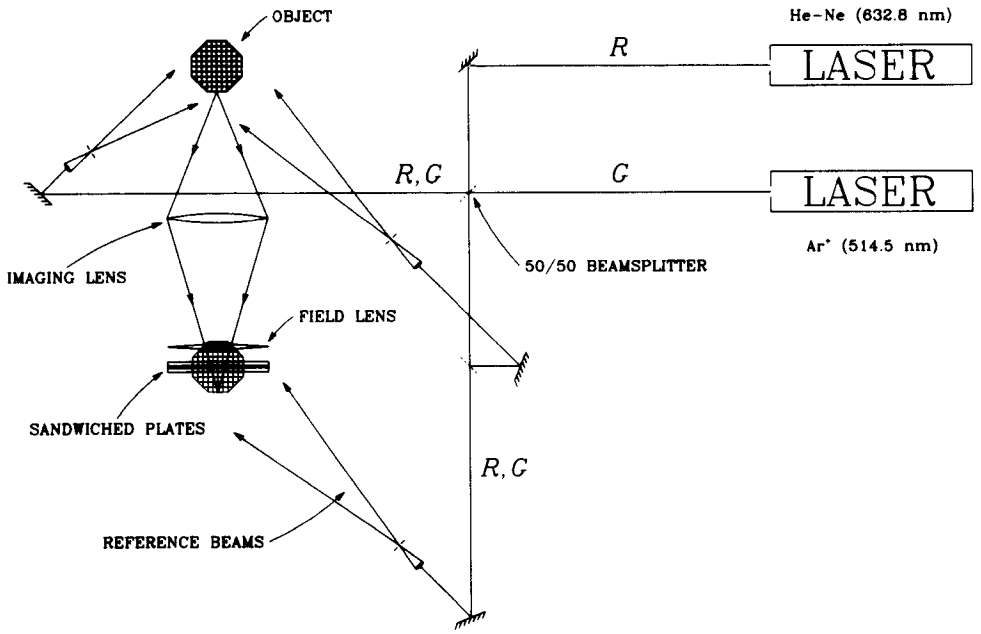

Fig. 8.8 One-step recording of a multicolour reflection hologram.

8.7.1 Using a Reflection Master

We believe that the two-step recording procedure described in §8.3.2 will be of special interest in multicolour reflection holography as the final multicolour image is formed in two simple steps. The main problems presently associated with the technique are the unavailability of panchromatic holographic recording materials and the limitations of the processing techniques.

8.7.2 Experimental Results

We have successfully made multicolour reflection holograms using a one-step technique with a field lens (§8.2.1). Fig. 8.8 shows the recording arrangement. An aerial image of the object is produced by the achromatic lens system. A field lens is placed within the aerial image to reduce the longitudinal distortion and to produce a projection of the imaging lens at some 60cm in front of the recording plate. In our experiments two recording plates were used in contact, namely 8E56HD (blue–green sensitive) and 8E75HD (red sensitive), both manufactured by Agfa–Gevært, the emulsions being in contact. Two wavelengths were used—632.8nm (He–Ne) and 514.5nm (Ar^+). Note that the beamsplitting arrangement conserves light. The two beams were accurately aligned so that both beams simultaneously passed through the same pinhole spatial filter. The plates were exposed simultaneously, separately processed, and placed back in register. As the plates had different chemical characteristics, each plate was processed with a different chemistry in order that both recorded images were reconstructed in the original laser colours. Plate VII shows a photograph of a holographic image thus recorded.

CHAPTER 9

CONCLUDING REMARKS

9.1 INTRODUCTION

In this thesis we have surveyed the field of display holography and investigated specific areas in detail. In particular, we have addressed three important areas in which we have made some original contributions. These areas are (i) image recording, (ii) image display, and (iii) multicolour holography:

9.2 IMAGE RECORDING

Mechanical stability of optical components is one of the fundamental requirements in holography. Based on our investigations, we have designed and built a versatile system specifically for display holography (§3.10). The system has been in use for several years and has proven to be reliable, and could, with modifications, be scaled up to produce larger holograms.

One factor which affects the stability of interference fringes in a holographic set-up is the recording geometry used. We have successfully used the 'parallelogram' arrangement (§4.2), and for the reasons outlined in Chapter 4 we believe it is the best arrangement to use for simple display holography.

When producing a pseudoscopic image from a 'master' hologram, the reconstruction beam must be conjugate to the original reference beam in order to prevent aberrations and distortions in the projected image. We have discovered [41] that by varying the divergence of the reconstruction beam, the apparent position of the image can be shifted (§5.7). The effect can be used in image-plane holography to separate the plane of least dispersion from the hologram plane. The technique lends flexibility to image-plane holography. Our technique has been taken up and studied in more detail by Xu et al [42].

9.3 IMAGE DISPLAY

However good the quality of a display hologram, image display remains a problem. In general, white light reconstruction techniques are adopted so that expensive coherent reconstruction sources are not required. We have investigated the techniques normally employed for white light reconstruction, namely reflection and rainbow holography. We have also investigated another technique, dispersion compensation, which was first proposed in the 1960's. We believe that the application of dispersion compensation to display holography has not been given the attention it deserves.

We have incorporated a dispersion-compensating grating in a compact hologram viewing device (§7.8), which could be mass-produced. When a hologram, recorded at the correct reference angle, is placed adjacent to the front screen of the viewer, the reconstruction geometry is correctly set automatically. The image then produced is "black and white", and as we have shown in §7.6, has low aberrations and distortions. We believe that the proposed device has two important advantages over other white light reconstruction techniques—firstly, as the reconstruction parameters are automatically set when the hologram is placed in position, the observer is relieved of the requirement to align the system; secondly, the compact nature of the device makes for portability and ease of use.

We have observed an interesting property of a ccomposite dispersion-compensated hologram system comprising a diffraction grating, a hologram, and a miniature Venetian blind filter (§7.7) sandwiched together. An achromatic image is seen when the structure is held directly between a light source and an observer (Fig. 7.21). When the structure is rotated through 180°, so that the diffraction grating is closest to the observer, an identical but mirror-reversed image is observed. This structure could be manufactured by embossing the diffraction grating and hologram onto the two sides of the venetian blind filter.

It is sometimes not appreciated that volume reflection holograms suffer from chromatic dispersion, although the magnitude of the dispersion is generally small because of the narrow reflection bandwidth. We have investigated the possibility of using reflection holograms or gratings in a dispersion-compensated system (§7.9). Our analysis shows that it is possible to compensate for the residual dispersion in a reflection hologram by using a transmission or a reflection compensating grating.

9.4 MULTICOLOUR HOLOGRAPHY

A major objective in display holography is the production of images in natural colour. It has been shown that images with high colour fidelity can be obtained using just three recording wavelengths if these are near 450, 540, and 610nm (§2.5). We have successfully produced multicolour holograms using laser transmission and reflection techniques. The method used to make the reflection holograms (§8.7.2) can be used to produce high quality images in a single exposure and is therefore commercially attractive. A potentially simple method of making image-plane multicolour reflection holograms is to use the Denisyuk [57] technique to make the master *and* the transfer holograms (§8.7.1), although precise control of the emulsion parameters is then required.

Using dispersion compensation (§7.10) we have proposed and demonstrated a new technique of multicolour holography. The holograms produced are compatible with the proposed hologram viewing device.

REFERENCES

1. W. T. Welford, "A Vector Raytracing Equation for Hologram Lenses of Arbitrary Shape", *Opt. Commun.* **14**, 322–3 (1975).

2. Edwin B. Champagne, "Nonparaxial Imaging, Magnification, and Aberration Properties in Holography", *JOSA* **57**, 51–5 (1967).

3. M. Born and E. Wolf, *Principles of Optics*, Pergamon Press Ltd., Oxford, 1975.

4. M. G. Moharam and T. K. Gaylord, "Diffraction Analysis of Dielectric Surface-Relief Gratings", *JOSA* **72**, 1385–92 (1982).

5. Kiyoshi Yokomori, "Dielectric Surface-Relief Gratings with High Diffraction Efficiency", *Appl. Opt.* **23**, 2303–10 (1984).

6. Herwig Kogelnik, "Coupled Wave Theory for Thick Hologram Gratings", *Bell Sys. Tech. J.* **48**, 2909–47 (1969).

7. Emmett N. Leith and Juris Upatnieks, "Wavefront Reconstruction with Diffuse Illumination and Three-dimensional Objects", *JOSA* **54**, 1295–1301 (1964).

8. Kaveh Bazargan, "Review of Colour Holography", *Proc. SPIE* **391**, 11–18 (1983).

9. Commission Internationale de l'Éclairage, *Proceedings of the Eighth Session*, Cambridge, England, 1931.

10. W. D. Wright, *The measurement of Colour*, 4th Ed., Adam Hilger, London, 1969.

11. W. A. Thornton, "Luminosity and Color-Rendering Capability of White Light", *JOSA* **61**, 1155–63 (1971).

12. Wolfgang Walter, "Optimum Lamp Spectra", *J. IES* **7**, 66–73 (1978).

13. V. G. Komar and Yu. N. Ovechkis, "Colour Rendering of Holographic Images", *Tekh. Kino & Telev. (USSR)*, No.9, 18–22 (1976)—In Russian.

14. G. Ya. Buimistryuk and A. Ya. Dmitriev, "Selection of Laser Emission Wavelengths to Obtain Colour Holographic Images", *Izv. VUZ Priborostr. (USSR)* **25**, 79–82 (1982)—In Russian.

15. A. A. Friesem and R. J. Fedorowicz, "Recent Advances in Multicolor Wavefront Reconstruction", *Appl. Opt.* **5**, 1085–6 (1966).

16. A. A. Friesem and R. J. Fedorowicz, "Multicolor Wavefront Reconstruction", *Appl. Opt.* **6**, 529–36 (1967).

17. Jiří Růzek and Josef Muzık, "Some Problems of Colour Holography", *Tesla Electron.* **9**, 60–61 (1976).

18. Nils Abramson, *The Making and Evaluation of Holograms*, Academic Press, London, 77 (1981).

19. R. J. Collier, C. B. Burckhardt &L. H. Lin, *Optical Holography*, Academic Press, New York, 1971, p. 168.

20. E. Hecht and A. Zajac, *Optics*, Addison–Wesley Publishing Company, 1974, p. 235.

21. R. N. Smartt, "A Variable Transmittance Beam Splitter", *Appl. Opt.* **9**, 970–71 (1970).

22. D. Bertani, M. Cetica, and R. Polloni, "A Simple Variable-Ratio Beam Splitter for Holography", *J. Phys. E: Sci. Instrum.* **16**, 602–3 (1983).

23. Ref. 20, p. 168.

24. Ref. 19, p. 175.

25. Howard M. Smith, *Principles of Holography*, John Wiley & Sons, 2nd Ed., 1975, p. 132.

26. Richard Foley and Frank Wendt, "Making a High Efficiency Antihalation Backing for Photographic Plates which Eliminates Interference Bands Produced by Coherent Light", *Appl. Opt.* **6**, 977–8 (1967).

27. O. D. D. Soares, "Elimination of Rear Reflections in Holographic Plates", *Am. J. Phys.* **48**, 409–10 (1980).

28. Ref. 20, p. 245.

29. Technical Information, NDT/Holography Division, Agfa Gevaert.

30. N. J. Phillips and D. Porter, "An Advance in the Processing of Holograms", *J. Phys. E: Sci. Instrum.* **9**, 631–4 (1976).

31. G. W. Stroke, "White-Light Reconstruction of Holographic Images Using Transmission Holograms Recorded with Conventionally-Focused Images and 'In-Line' Background", *Phys. Letts* **23**, 325–7 (1966).

32. Lowell Rosen, "Holograms of the Aerial Image of a Lens", *Proc. IEEE* **55**, 79–80 (1966).

33. W. E. Kock, L. Rosen and G. W. Stroke, "Focused-Image Holography—A Method for Restoring the Third Dimension in the Recording of Conventionally-Focused Photographs", *Proc. IEEE* **55**, 80–81 (1966).

34. F. B. Rotz and A. A. Friesem, "Holograms with Nonpseudoscopic Real Images", *Appl. Phys. Letts.* **8**, 146–8 (1966).

35. Gerald B. Brandt, "Image Plane Holography", *Appl. Opt.* **8**, 1421–9 (1969).

36. I. S. Klimenko and G. V. Skrotskiĭ, "Focused-Image Holography", *Sov. Phys.-Usp.* **16**, 88–98 (1973).

37. Poohsan N. Tamura "One-Step Rainbow Holography with a Field Lens", *Appl. Opt.* **17**, 3343 (1978).

38. Stephen A. Benton, Herbert S. Mingace, Jr., and William R. Walter, "One-Step White-Light Transmission Holography", *Proc SPIE* **215**, 156–61 (1980).

39. Sh. D. Kakichashvili and V. I. Kakichashvili, "Reconstruction of Focused Holograms with Normal Perspective", *Sov Phys -Tech Phys* **16**, 1184–5 (1972).

40. P. Hariharan, Z. S. Hegedus and W. H. Steel, "One-Step Multicolour Rainbow Holograms with Wide Angle of View", *Opt Act* **26**, 289–91 (1979).

41. K. Bazargan and M. R. B. Forshaw, "An Image-Plane Hologram with Non-Image-Plane Motion Parallax", *Opt Commun* **32**, 45–7 (1980).

42. Xu Shenchu and Liu Shou, "White-Light Reconstruction Holography Improved with Astigmatism", *Laser J (China)* **8**, 8–12—refs. on p. 7 (1981)—In Chinese.

43. I. S. Klimenko, E. G. Matinyan and G. V. Strotskii, "Properties of Nonlinear Recording of Focused-Image Holograms", *Opt Spectrosc* **34**, 474–5 (1973).

44. James C. Wyant, "Image Blur for Rainbow Holograms", *Opt Lett* **1**, 130–32 (1977).

45. S. A. Benton, "Hologram Reconstructions with Extended Incoherent Sources", *JOSA* **59**, 1545 (1969)—Abstract only.

46. Hsuan chen and F. T. S. Yu, "One-Step Rainbow Hologram", *Opt Lett* **2**, 85–7 (1978).

47. S. A. Benton, "Method of Making Reduced Bandwidth Holograms", U.S. Patent 3,633,989 (1972).

48. Emmett N. Leith, Hsuan Chen, and James Roth, "White Light Hologram Technique", *Appl Opt* **17**, 3187–8 (1978).

49. S. A. Benton, "Photographic Holography", *Proc SPIE* **391**, 2–9 (1983).

50. H. Chen, A. Tai and F. T. S. Yu, "Generation of Color Images with One-Step Rainbow Holograms", *Appl Opt* **17**, 1490–91 (1978).

51. P. Hariharan, W. H. Steel and Z. S. Hegedus, "Multicolor Holographic Imaging with a White-Light Source", *Opt Lett* **1**, 8–9 (1977).

52. K. Bazargan, "A Hologram Viewing Device", British Patent 8303465, US Patent 465620 (Filed 1982).

53. Henri Paques, "Achromatization of Holograms", *Proc IEEE* **54**, 1195–6 (1966).

54. C. B. Burckhardt, "Display of Holograms in White Light", *Bell Sys Tech J* **45**, 1841–4 (1966).

55. D. J. De Bitetto, "White-Light Viewing of Surface Holograms by Simple Dispersion Compensation", *Appl Phys Letts* **9**, 417–8 (1966).

56. "Light Control Film", Industrial Optics Division, 3M Center, St. Paul, Minnesota 55144, USA

57. Yu. N. Denisyuk, "Photographic Reconstruction of the Optical Properties of an Object in its Own Scattered Radiation Field", *Sov. Phys.-Doklady* **7**, 543–5 (1962).

58. C. Durou, J.–P. Hot and R. Lefèvre, "Simultaneous Effects of Shrinkage and Refractive Index Fall of the Photographic Emulsion in Holography", *Nouv. Rev. Optique* **7**, 87–94 (1976)—In French.

59. L. H. Lin and C. V. LoBianco, "Experimental Techniques in Making Multicolor White Light Reconstructed Holograms", *Appl. Opt.* **6**, 1255–8 (1967).

60. M. I. Dzyubenko, V. A. Krishtal, A. P. Pyatikop and V. V. Shevchenko, "Parameters of Three-Dimensional Holograms on High-Resolution Emulsions", *Opt. Spectrosc.* **38**, 429–31 (1975).

61. N. Nishida, "Correction of the Shrinkage of a Photographic Emulsion with Triethanolamine", *Appl. Opt.* **9**, 238–40 (1970).

62. Stephen A. Benton, "Intra-Emulsion Diffusion-Transfer Processing of Volume Dielectric Holograms", *JOSA* **64**, 1393–4 (1974)—Abstract only.

63. N. J. Phillips, A. A. Ward, R. Cullen, and D. Porter, "Advances in Holographic Bleaches", *Phot. Sci. & Eng.* **24**, 120–4 (1980).

64. D. J. Cooke and A. A. Ward, "Reflection-Hologram Processing for High Efficiency in Silver-Halide Emulsions", *Appl. Opt.* **23**, 934–41 (1984).

65. W. Spierings, "'Pyrochrome' Processing Yields Color-Controlled Results with Silver-Halide Materials", *Holosphere* **10** (nos. 7,8), 1–7 (1981).

APPENDIX:

COLOUR PLATES AND PUBLICATIONS

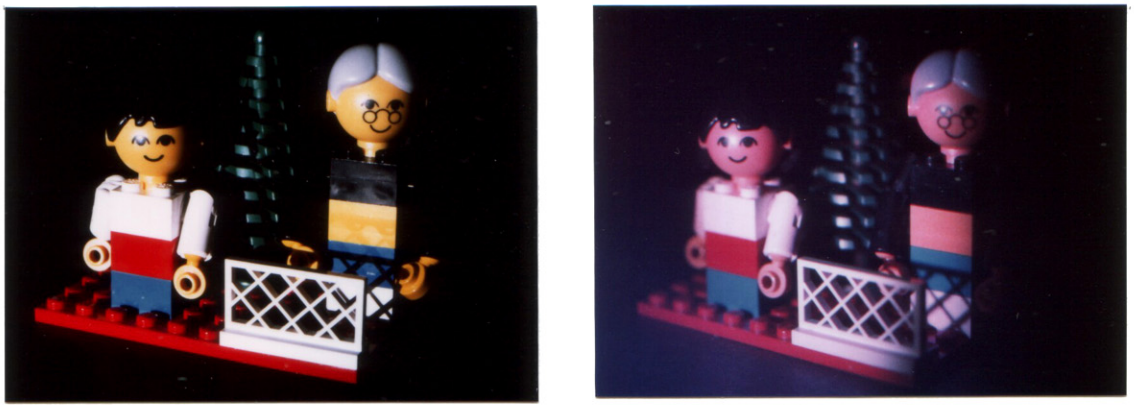

Plate I Colour distortion in a multicolour holographic image caused by non-optimal choice of recording wavelengths. *Left*: Object, *Right*: Image. The hologram was recorded using the arrangement shown in Fig. 4.10.

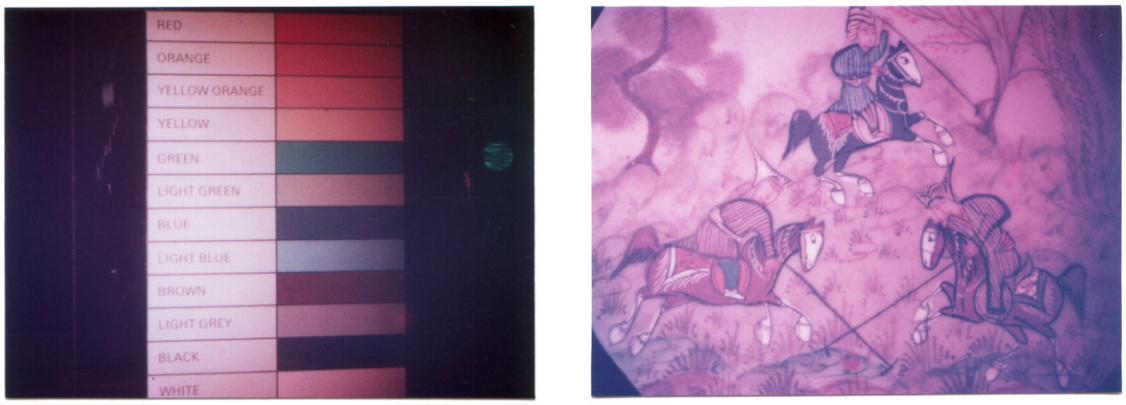

Plate II Multicolour holographic images recorded using the arrangement shown in Fig. 4.10.

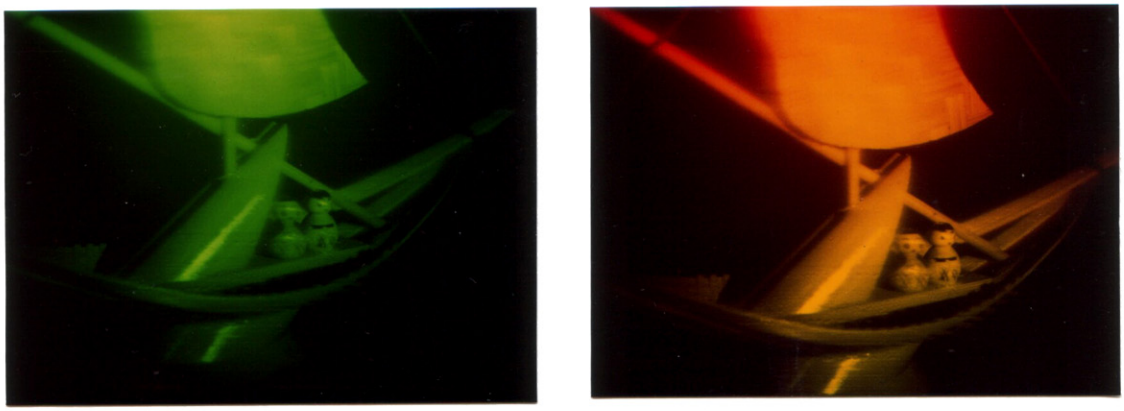

Plate III Images from a rainbow hologram, viewed from different slit image positions. The perspective is identical in both cases.

Plate IV Image from a rainbow hologram, viewed from a position not coincident with a slit image. Each part of the image is seen in a different spectral colour.

Plate V Correction of lateral chromatic aberration using dispersion compensation. *Left*: Uncorrected image, *Right*: Corrected image.

Plate VI Multicolour dispersion-compensated image recorded using two wavelengths, 514.5nm and 632.8nm and viewed using white light (§7.10).

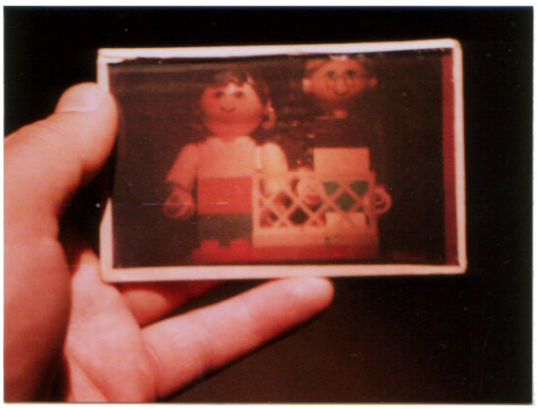

Plate VII Multicolour reflection holographic image viewed using white light (§8.7.2).

AN IMAGE-PLANE HOLOGRAM WITH NON-IMAGE-PLANE MOTION PARALLAX

K. BAZARGAN and M.R.B. FORSHAW
Blackett Laboratory, Imperial College, London SW7 2BZ, UK

Received 28 September 1979

Image-plane holograms, made using the two-stage process of Rotz and Friesem, provide achromatic or near-achromatic images only when the image straddles the plane of the second hologram. It is shown that in certain circumstances it is possible to generate nearly-achromatic images which appear to lie completely behind the second hologram plane.

1. Introduction

One of the uses of image-plane holography is to allow achromatic or nearly-achromatic images to be obtained with polychromatic sources of finite angular extent. Such holograms are usually made in one of two ways. One can image the scene by means of a lens onto or near the hologram plane [1,2]. Alternatively a conventional Fresnel hologram is made with a collimated or nearly-collimated reference beam and then a second, image-plane hologram is made using the real primary image generated from the first [3]. Nearly-achromatic black-and-white images can then be obtained by illuminating the image-plane hologram with a white-light source. The resulting images are strictly achromatic only for those image points which lie exactly in the hologram plane, but acceptably small chromatic dispersion is obtained for image points which lie within a centimetre or so on either side of the hologram, depending upon the hologram geometry. Image points which are much further away become unacceptably blurred by spectral dispersion. Consequently, good images can only be obtained for small image depths and these images must lie very close to the hologram plane.

We wish to report that it is possible, using a modification of the two-stage process, to produce nearly-achromatic white-light images which appear visually to lie completely behind the hologram plane.

2. Experiment

Fig. 1. shows diagrammatically the different stages involved. The first hologram is made with the reference source R1 at a finite distance (0.5–1.0 m) from

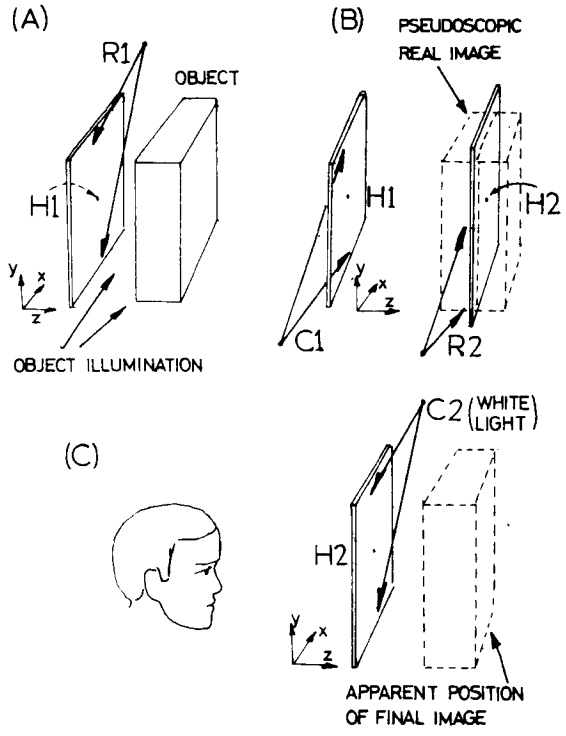

Fig. 1. Recording geometry for first (a) and second (b) holograms; viewing geometry for second hologram (c).

the hologram and the central object plane lying parallel to the hologram. The object depth should be restricted to a few cm and the object-hologram separation should be less than about 15 cm. The hologram is exposed and processed normally, then illuminated by a reconstructing source C1 ($\lambda_c = \lambda_r$) whose y and z coordinates are of opposite sign to those of R1. A pseudoscopic, aberrated, real image is thus produced. A second photographic plate is placed in or near the central plane of this real image and illuminated with a reference source R2 having the same wavelength as C1. The distance R2–H2 should be comparable with or greater than R1–H1. After normal exposure and processing the second hologram is illuminated with a white-light source C2 whose y and z coordinates, relative to the second hologram, have opposite sign to those of R2. A nearly-achromatic, orthoscopic image is produced which can be examined visually.

If this image is viewed with the observer's eyes aligned along the y-axis of the second hologram then the stereoscopic and motion parallax effects are such that the image appears to lie in or near the hologram plane, more or less as in conventional image-plane holograms. However, if the observer's eyes are aligned along the x-axis then the image appears to lie completely or almost completely behind the hologram. Although typical images show signs of non-chromatic distortion and aberrations, these are usually well within the bounds of visual acceptability. The spectral dispersion which is characteristic of ordinary image-plane holograms is still present, but the plane of minimum blurring now appears to lie well behind the hologram.

3. Theory

Champagne's theory for holographic aberrations [4] can be used to compute the image distortions and primary aberration coefficients for the first holographic image. It can be shown that the distortions and non-chromatic aberrations which are produced by the second hologram are much smaller than those of the first stage, because the image distances are much smaller. The second stage can therefore be neglected as a source of non-chromatic aberrations and it may be considered to be simply a means for turning the first-stage, aberrated, pseudoscopic image into a final orthoscopic image.

As an example of the effects involved in the first imaging step, consider an object consisting of two planes P1 and P2 lying parallel to the (x_1, y_1) plane, at distances z_1 = 50 mm and 70 mm. Bearing in mind that the final image will be examined visually, with typical viewing distances of 250 mm or greater, then it can be shown that the only effects of any significance are geometrical image distortion and x- and y-astigmatism. With a reference source R1 located in the plane $x_1 = 0$ at a radial distance R1–H1 = 500 mm and with the central ray R1H1 making an angle of 80 degrees with the hologram normal, the first stage has a y-magnification of 25% for the P1 plane and 40% for P2.

Of more significance for the present discussion is the fact that the astigmatism coefficients A_x and A_y are almost constant over the hologram surface, producing tangential and sagittal focal surfaces lying at different distances from the hologram as shown in fig. 2. The images of P1 and P2 are aberrated so that lines lying parallel to the x_1-axis are imaged closer to the hologram than lines parallel to the y_1-axis. If the exposure of the second hologram is then made with the plate located at a distance of 55–65 mm from the hologram then the x-astigmatic surfaces will be located more or less equally on either side of the plate, as in conventional image-plane holography. The y-astigmatic surfaces will lie mainly behind the hologram when the final image is reconstructed.

When a white-light source is used for reconstruc-

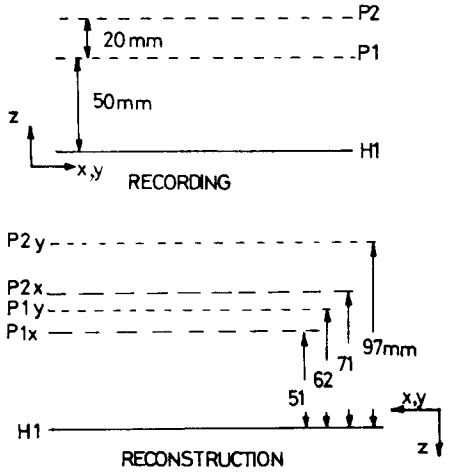

Fig. 2. Location of object and image planes for example in text.

tion then two effects are visually dominant and can be predicted theoretically. The difference in the x- and y-astigmatism does not produce a noticeable visual aberration: because the eye samples only a small portion of the hologram (typically less than 1 mm) the resulting image points are negligibly blurred. However, the tangential and sagittal image surfaces are such that the image appears to lie *in* the hologram plane when viewed parallel to the (y_2, z_2) plane but *behind* the hologram when viewed at right-angles to this plane. Of equal significance is the fact that the chromatic dispersion is the same for both apparent image locations, with the plane of minimum dispersion corresponding to the real image plane whose astigmatic circle of least confusion intersected the second hologram.

Fig. 3. White-light reconstruction using new technique: apparent image location is 15 mm behind hologram plane. Object size = 200 × 100 × 25 mm.

4. Discussion

We have described a modification of the two-stage image-plane hologram process first described by Rotz and Friesem. By introducing controlled amounts of astigmatism during the first recording stage it is possible to produce white-light, nearly-achromatic images which appear to lie behind the hologram plane. Fig. 3 shows that these images can have excellent visual definition: the object from which this white-light holographic image was obtained had dimensions of 200 × 100 × 25 mm.

The technique has both theoretical and practical interest. To the best of the authors' knowledge the effects of astigmatism on the stereoscopic and motion parallax properties of visual images have not been reported before. From the practical standpoint the technique offers an extra degree of flexibility over conventional image-plane holograms, which can provide only a limited range of image locations unless vertical parallax and visual accommodation is dispensed with [5]. Even with a limited image depth, the fact that parts of the image lie in front of the hologram can cause visual confusion when ordinary image-plane holograms are examined: this visual confusion has long been known in stereoscopic imaging [6]. By permitting the visual image to lie entirely behind the hologram plane, the present technique eliminates this source of visual confusion.

Acknowledgement

The authors are grateful to Professor W.T. Welford for his courtesy in extending to them the hospitality of the Optics Department at Imperial College.

References

[1] L. Rosen, Appl. Phys. Lett. 9 (1966) 337.
[2] G.W. Stroke, Phys. Lett. 23 (1966) 325.
[3] F.B. Rotz and A.A. Friesem, Appl. Phys. Lett. 8 (1966) 146.
[4] E.B. Champagne, J. Opt. Soc. Amer. 57 (1967) 51.
[5] T. Kubota and T. Ose, Opt. Commun. 28 (1979) 159.
[6] J.T. Rule, J. Opt. Soc. Amer. 31 (1941) 325.

A Reprint from the

PROCEEDINGS

Of SPIE-The International Society for Optical Engineering

Volume 391

Optics in Entertainment

January 20-21, 1983
Los Angeles, California

Review of Colour Holography

Kaveh Bazargan
Imperial College of Science and Technology, London SW7 2BZ and
New Holographic Design Ltd., 1A Farm Place, London W8 7SX

Invited Paper

© 1983 by the Society of Photo-Optical Instrumentation Engineers
Box 10, Bellingham, Washington 98227-0010 USA. Telephone 206/676-3290

Review of Colour Holography

Kaveh Bazargan

Imperial College of Science and Technology, London SW7 2BZ
and
New Holographic Design Ltd, 1A Farm Place, London W8 7SX

Abstract

The aim of this report is firstly to review colour display holography and secondly to present some of the work carried out in our laboratories in this field. An historical introduction is presented, setting out key events in the development of colour holography, and several historical parallels are drawn with colour photography. Laser illuminated colour holography and its problems, in particular that of spurious images is discussed. White-light-viewable colour holograms are divided into reflection, rainbow and dispersion-compensated types. The latter is a description of recent experiments by us. Colour rendition in holographic images is discussed. It is concluded that improvements in panchromatic photographic emulsions, and development of inexpensive lasers operating at or near 450, 540 and 610 nm may be the most important future developments for colour holography.

Historical Introduction

In 1964, Leith and Upatnieks[1] reported the successful off-axis holographic recording of diffusely reflecting objects. In the same communication they indicated that multicolour holographic images could be obtained by the simple superposition of three holograms formed using three additive primary colours. Predicting the six spurious images that would be formed by each reconstruction beam undergoing two unwanted diffraction processes, they suggested that the reference beams be introduced at different angles to the photosensitive plate, thus angularly separating the desired and the undesired images. Results from the first multicolour holograms made[2], however, showed that Bragg-diffraction effects from relatively thick photographic emulsions (Kodak 649F) could suppress unwanted diffraction even when identical reference beam angles were used. Pennington et al[2] used the argon 488 nm and the He-Ne 633 nm wavelengths, and an inter-beam angle of 90^{o}, and found no spurious images. Later work[3,4], however, was to show that this method is not entirely satisfactory when spectrally close wavelengths, e.g. green and blue, are present.

Mandel[5] investigated the problem of spurious images, neglecting emulsion thickness effects, and found that if a restricted viewing angle is acceptable, the unwanted images need not overlap with the wanted image, and can be angularly separated from the latter. Marom[6] produced a more accurate formulation.

Reflection holography was invented by Denisyuk[7] in 1962, and the general theory was developed by van Heerden[8]. Reflection holograms have an advantage over the transmission type for multicolour imaging, in that they do not normally produce spurious images. The photographic analogue of reflection holography is the interference photography of Gabriel Lippmann[9].

The first multicolour reflection holograms were reported by Lin et al[10], using two wavelengths and a 2-dimensional object, closely followed by Upatnieks et al[11] using three wavelengths and a 3-dimensional object. Subsequent work by Lin et al[12] discussed some of the practical problems of multicolour reflection holography, including emulsion shrinkage and choice of reconstructing light.

Two novel solutions to the problem of spurious images - coding the reference beam, and non-overlapping spatial multiplexing - were put forward by Collier et al[13] in 1967. The latter technique, which involves the spatial division of the hologram into many small monochromatic holograms, is analogous to the screen-plate techniques in early photography[14,15]. The former technique usually requires critical alignment in the reconstruction stage, and is therefore limited to laboratory use.

In 1973 Noguchi[16] attempted the first quantitative study of colour fidelity in multicolour holograms, using specular object beams. He used four wavelengths and obtained excellent colour rendition in two out of four test objects and acceptable rendition in the other two. Although several assumptions have been made which must be examined more closely, the results are promising, as are those from 'NIKFI'[17] in the USSR, which suggest that using four recording wavelengths colour fidelity comparable to the best photographic reproduction techniques is attainable.

The Rainbow hologram was invented by Benton[18] in 1969. It is made by transferring an image from a narrow strip hologram, containing little vertical parallex, onto a secondary plate, and illuminating the latter with white light. In 1977 Hariharan[19] extended the process to yield multicolour images, by simply transferring three images from three separate master holograms, using identical recording geometries for each. The final hologram exhibited a good multicolour image when viewed at the correct height and distance from the hologram. (An exact analogy is again found in early photography; the method bears a close resemblance to the diffraction photography process of R.W. Wood[20,21].) This method was laborious and therefore not completely satisfactory, and was simplified by the use of the one-step rainbow process[22,23]. The latter method, in its original form, can produce a multicolour image in a single step, but with a serious drawback: the process yields either an orthoscopic image with vignetting due to the imaging lens, or an unvignetted but pseudoscopic image. Tamura[24] solved the problem by using a field lens in the image plane to project the viewing slit into the viewing zone. A simpler solution was suggested by Benton[25] who used the method of varying the reconstruction beam distance to form a real viewing aperture. He also suggested viewing the conjugate diffraction order which formed an unvignetted image.

The successful recording of volume holograms in Dichromated Gelatin (DCG)[26], and its sensitisation to red light[27] enabled Kubota et al[28] to record the first colour reflection hologram in DCG in 1979.

Recent theoretical work in the USSR[29,30] has shown that excellent colour rendition can be obtained with only three laser emission lines if these are near 450, 540 and 610 nm.

Laser transmission holograms

The simplest multicolour hologram is that made by superposing several transmission holograms, using different wavelengths, but identical recording geometries. Upon reconstruction with the superposed reference beams a geometrically undistorted multicolour image is formed at the original position of the object. However, each reconstruction beam is also diffracted from holograms formed by the other wavelengths, thus forming a number of aberrated spurious images near the required image[1]. If the reference beam angle of incidence is large enough, if the recording wavelengths have large spectral separations, and if the object subtends a small angle at the hologram, then the spurious images do not overlap with the required image, but are scattered around it[5,6]. It is, however, desirable to eliminate the spurious images altogether, and several solutions have been proposed. One consequence of multicolour laser illumination is the incoherently superposed speckle patterns. Although the resultant subjective speckle is reduced[31], the differing speckle sizes and localisations have been found to lead to observer fatigue[32].

Suppression of spurious images

(a) Thin holograms. If the plate has negligible thickness compared to the fringe separation, then the hologram does not exhibit volume or 'Bragg' effects, and can be treated as a 2-dimensional or surface grating. Two methods have been proposed for the inhibition of spurious images or 'cross-talk' in 2-dimensional colour holograms:

(i) Spatial multiplexing. One way of inhibiting cross-talk between different wavelengths is to divide the hologram into a large number of small monochromatic holograms of alternating colours, and reconstructing with an appropriately composed reconstruction beam[13]. A variation is to 'code' only the object beam with a mask of alternating colours[33,34].

(ii) Coded reference beams. Another solution for suppresing spurious images involves passing the superposed reference beams through a diffusing medium prior to illuminating the plate, and using the identical beam for reconstruction[13]. As the shape of the diffused wavefront is strongly wavelength-dependent, each beam records its own 'coded' hologram, reconstructing only in an identically coded beam. Although no spurious images are formed, unwanted diffraction produces a background noise in the vicinity of the image, thus reducing contrast. The noise is delocalised, and therefore less objectionable, if the reference beams are expanded prior to diffusion. Apart from the noise, one disadvantage of this method is the need for accurate replacement of the hologram for image retrieval.

(b) Volume holograms. The preceding techniques assume negligible thickness for the recording medium. In practice, most suitable recording methods have thicknesses several times the optical wavelengths - a feature that can be beneficially applied to the present problem. It is a property of the thick or volume hologram that, in general, reconstruction only occurs if the wavelength and the angle of incidence of the reconstruction beam are close to those used for recording.

(a) (b)

Figure 1: Examples of three-colour laser transmission holograms made using the wavelength and angle selectivity of thick emulsions to suppress spurious images. The wavelengths used were 476 nm (Ar), 514 nm (Ar), and 633 nm (He-Ne). The first two were recorded on Agfa-Gevaert 8E56HD plates, and the last on 8E75HD plates. The two plates were sandwiched, emulsion to emulsion, and exposed to the three wavelengths simultaneously. After processing, the plates were replaced in register. The blue and the red reference beams fell on the plates at incidence angles of 70^{o} and 30^{o} respectively, from the same side of the object, and the green reference beam at 45^{o} from the opposite side. No spurious images were observed. (a) Photograph of a test-object in white light (Tungsten). (b) Photograph of the reconstruction of a three-colour hologram of (a). (c) Photographs of the holographic reconstructions of a three-dimensional object, reconstructed in single wavelengths, two wavelengths, and in all three wavelengths (bottom photograph). The colour distortion in the originally yellow faces of the figures has been observed before[3,4,31] and is, we believe, due to the non-optimal choice of the three wavelengths.

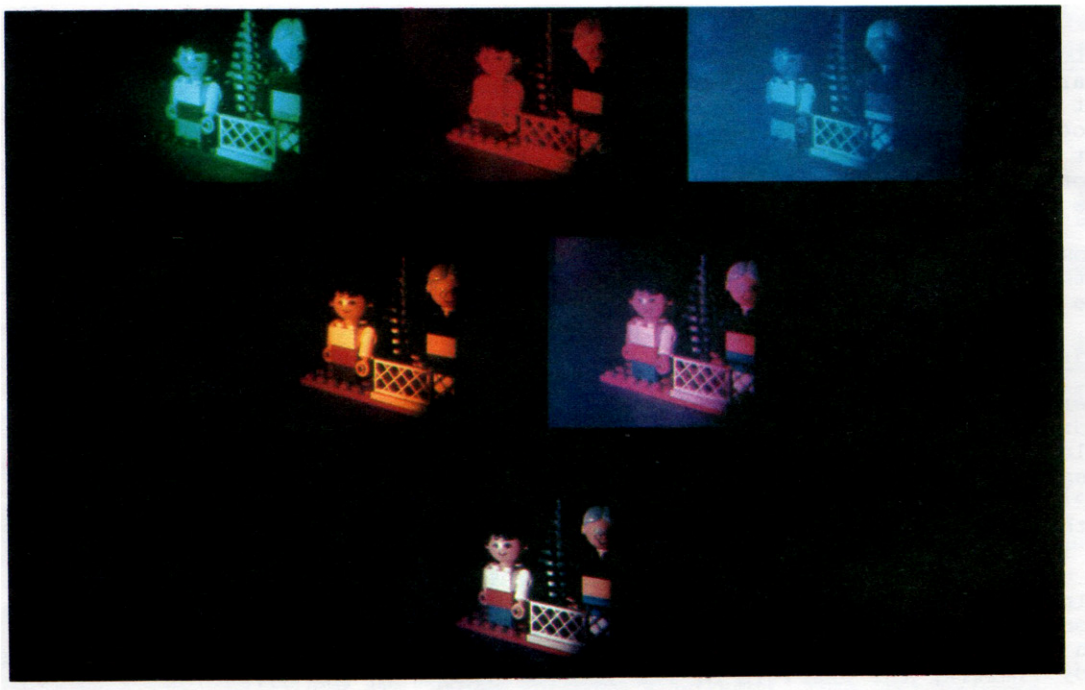

(c)

If the recording material is sufficiently thick and the recording wavelengths are spectrally well separated, an arrangement with identical reference beam angles may be used, each component hologram reconstructing only the required images (if the recording material is very thick - e.g. 100μ - then white light illumination may be used[35]). It has been found[3,4] that using an inter-beam angle of 100°, Kodak 649F spectroscopic plates (thickness = 12μ) exhibit sufficient selectivity to suppress cross-talk between red and blue or red and green images, but not between blue and green ones. Using the more sensitive Agfa-Cevaert emulsions (thickness = 6μ) and more convenient inter-beam angles (e.g. 45°) the latter method is not effective. Total suppression of cross-talk for three primary colours can be achieved by further use of the Bragg effect. If the reference beams impinge upon the plate at judiciously chosen, differing angles of incidence, wavelength and angle deviations from the Bragg condition reinforce each other and eliminate spurious images (Fig. 1). Although high quality images can be obtained with this method, the cumbersome recording and reconstructing arrangements render it unsuitable for routine applications.

Image plane holograms

By recording a transmission hologram in the plane of the real image formed by a lens an image-plane hologram is formed. In this case a virtual, finite aperture is present in the reconstruction. By angularly separating the recording beams, and using a field lens in the reconstruction, Tatuoka[36] obtained a 3-colour hologram which was free of spurious images when viewed within a small viewing aperture. The separation of the reconstruction beams is, however, inconvenient. If the image depth is small, spectrally filtered white-light illumination may be used.

White-light-viewable holograms

(a) Reflection holography

A multicolour reflection hologram is made by the incoherent superposition of several reflection holograms in the same emulsion[10-12,37], or in several adjacent emulsions[38-40]. The two main problems are shrinkage of the emulsion due to chemical processing, and decrease in diffraction efficiency due to high information density.

(i) Emulsion shrinkage. In normal photographic processing the latent image is chemically developed and subsequently fixed. During fixation unexposed silver halide is removed to avoid printout and consequent image degradation. This causes a reduction of the emulsion thickness by some 10-20% and the colours of the reconstructed image are consequently distorted. The simplest way of avoiding shrinkage is to remove the fixing stage[10] but the life of the hologram is then limited. Although shrinkage can be corrected be reswelling using e.g. triethanolamine[12,41,42] or sorbitol[38], the process is not entirely satisfactory. Recent advances[43-46] obviate the need for photographic fixation, and maintain the original thickness and refractive index of the emulsion.

(ii) Loss of diffraction efficiency. When several sets of holographic interference fringes are superimposed on a single emulsion, the total diffracted light flux is less than that in a monochromatic hologram, partly due to the increase in information density[47]. One method of preventing this degradation is to have two or more emulsions to record the component holograms and to sandwich these after exposure[38-40] although the registration of the component holograms can be tedious. This method allows the best choice of recording materials for each wavelength.

Dichromated gelatin has a higher information storage capacity than photographic emulsions due to its higher spatial resolution and higher refractive index modulation capacity[48], and therefore has a great potential in colour reflection holography.

(b) 'Rainbow' or 'Benton' holograms

Another method of producing white-light-viewable multicolour images is to use the Rainbow or 'Benton' technique[18]. This is a derivative of the normal transmission image-plane holography, whereby a transmission hologram is made of a real image close to or straddling the plate, using either an imaging lens[49,50] (one-step technique) or a 'master' hologram[51] (two-step technique). Upon reconstruction by a point source of white light each wavelength produces its own image within a finite viewing aperture corresponding to the original imaging aperture. If the image lies in the plane of the final hologram, all spectral components are superimposed, resulting in a sharp, achromatic image. However, image points not in this plane suffer blurring, mainly due to transverse chromatic aberration, which, in the first order approximation, is proportional to the spectral bandwidth of the light reaching the observer. In the Benton modification this blurring is reduced by limiting the aperture of the imaging system in the direction of dispersion. This involves introducing a slit aperture in the one-step method, or using a strip hologram in the original two-step method. If this aperture is narrow enough (typically 1 cm) the

reconstructed viewing apertures are spatially separated according to wavelength. The image is no longer achromatic, but the blurring is reduced, thereby greatly increasing the useful image depth. (By introducing a cylindrical lens in the recording system image depth is further extended). The observer sees a continuum of spectrally coloured images as he moves his head vertically (the viewing aperture is normally aligned horizontally). At the position corresponding to the original aperture, an aberration-free image is seen in the colour of the original laser beam.

The Benton technique is readily extended to multicolour imaging by incoherent superposition of several holograms, using identical geometries. With the two-step technique, separate 'masters' and exposures are necessary for each wavelength[19], but by using an imaging lens the component holograms can be formed simultaneously[23]. A faithfull multicolour image is observed at the position corresponding to the original slit aperture, but departure from this position results in the appearance of false colours.

The orthoscopic image obtained from a simple one-step rainbow hologram produces severe vignetting unless large aperture imaging optics are employed[52]. One solution is to place a field lens in the plane of the focused image, thus forming a real image of the slit-aperture[24] (c.f. ref. 36). The same effect is more conveniently achieved by using a short reference and a long reconstruction beam[25,53]. Both methods can also serve to reduce distortions caused by the imaging system[53]. A third solution[25] is to view the conjugate diffraction order, which has opposite depth parallax to the primary image. This method, however, produces a mirror reversal of the image, and requires the interfering beams to fall onto the plate symmetrically, to avoid detrimental volume effects.

(c) Dispersion-compensated holograms

In recent experiments in our laboratories we have obtained multicolour holographic images using the technique of dispersion compensation[54-56]. The method of producing achromatic images according to Burckhardt[55] employs a thin compensating diffraction grating, a thin hologram, and a miniature Venetian-Blind structure. The thin hologram has no colour selectivity. By using a semi-thick recording material, such as a photographic emulsion, the hologram can show diffraction selectivity towards the wavelength used to record it. In our method we superimpose several holograms of the same object, made with different wavelengths, and with the reference beam angles such that the average fringe spatial frequencies of all component holograms are equal, and equal to that of the compensating grating. Upon reconstruction the wavelength biases of each hologram combine to form a multicolour image, the colour saturation of which increases with increased thickness.

Pseudocolour holograms

It is possible to produce multicolour white-light-viewable holograms using a single wavelength in recording. The reconstructed colours are artificial, however, and do not, in general, correspond to the colours of the object. Pseudocolour holograms can be produced by either rainbow[57-59] or reflection techniques[60].

(i) Rainbow method

If several rainbow holograms are superimposed on the same plate, each having been formed using a different interbeam angle, and the composite hologram is then illuminated by a single point-source of white light, the position of, say, the green viewing slit is different for each hologram. At any particular viewing position, therefore, each image is seen in a different spectral colour.

Although both coherent[59] and incoherent[57-58] superposition can be used, the former is preferred, as it requires fewer steps and leads to brighter images. The component hologram can be either of different objects, or of the same object illuminated in different ways, in which case nonspectral colours can be synthesized.

(ii) Reflection method

Pseudocolour images in reflection holograms can be produced either by swelling the emulsion by different amounts between sequential exposures, or by changing the reference beam angle, or by a combination of both[60].

Colour fidelity

If several spectral colours are plotted on a Maxwell colour triangle (e.g. the 1931 CIE chromaticity diagram) and the points are joined to form a polygon, then all colours represented by points lying within the polygon can be visually matched by an appropriate mixture of those spectral colours. It is often incorrectly assumed that if spectral colours

are used to record a multicolour hologram, all object colours within the polygon will be faithfully reproduced. In fact the colour reproduced depends only upon the spectral reflectivity of the object at those discrete wavelengths, whereas the natural colour observed in ordinary white light is a function of its reflectivity over the entire visible spectrum[61].

The ideal set of wavelengths for holography is one in which all objects, when illuminated by the set, and when illuminated by a standard white light source, appear to be in the same colour, i.e. that the two colours are metameric. The key paper in this field is that of W.A. Thornton[62]. He shows that the best colour-rendering index of any white light is of that composed of three narrow spectral bands around 450, 540 and 610 nm, and that the presence of wavelengths near 500 and 580 nm reduce the colour rendering capability. So the colour rendition obtained by three laser emission lines near the first three wavelengths can hardly be improved upon. These results have been confirmed by extensive theoretical work in the USSR[29,30]. Komar et al[29] recommend using the commonly available 458 nm (Ar), 568 nm (Kr), and 633 nm (He-Ne) lines for colour holography, in view of the above results.

Conclusions

The prospects for significant advances in the production of colour display holograms are good. Improvements in panchromatic photographic emulsions , obviating the need for sandwiching several emulsions, will be welcomed, particularly in reflection holography. Colour dispersion-compensated holography is currently being investigated in our laboratories. It is clear from theoretical work that using laser lines near 450, 540 and 610 nm, colour rendition in holographic images is equal if not superior to that of photographic reproduction systems currently available. The availability of inexpensive lasers emitting these wavelengths with sufficient coherence length and power will facilitate the manufacture of high quality colour holograms.

Acknowledgements

I am indebted to Dr. R. W. Smith and Dr. M. R. B. Forshaw for encouragement and useful discussions, and to Dr. R. W. G. Hunt for bringing to my attention reference 62.

References

1. Leith, E. N. and Upatnieks, J., "Wavefront Reconstruction with Diffuse Illumination and Three-Dimensional Objects," JOSA, Vol. 54, pp. 1295-1301. 1964.
2. Pennington, K. S. and Lin, L. H., "Multi-Color Wavefront Reconstruction," Appl. Phys. Lett., Vol. 7, pp. 56-57. 1965.
3. Friesem, A. A. and Fedorowicz, R. J.,"Recent Advances in Multicolor Wavefront Reconstruction," Appl. Opt., Vol. 5, pp. 1085-1086. 1966.
4. Friesem, A. A. and Fedorowicz, R. J., "Multicolor Wavefront Reconstruction," Appl. Opt, Vol. 6, pp. 529-536. 1967.
5. Mandel, L., "Color Imagery by Wavefront Reconstruction," JOSA, Vol. 55, pp. 1697-8, 1965.
6. Marom, E., "Color Imagery by Wavefront Reconstruction," JOSA, Vol. 57, pp. 101-102. 1967.
7. Denisyuk, Yu. N., "Photographic Reconstruction of the Optical Properties of an Object in its own Scattered Radiation Field," Sov. Phys.-Doklady, Vol. 7, pp. 543-545. 1962.
8. Van Heerden, P. J., "Theory of Optical Information Storage in Solids", Appl. Opt., Vol. 2, pp. 393-400. 1963.
9. Lippmann, G., "La Photographie des Couleurs", C.r.hebd. Séanc. Acad. Sci., Paris. Vol. 112, pp. 274-275. 1891. (In French).
10. Lin, L. H., Pennington, K. S., Stroke, G. W. and Labeyrie, A. E., "Multicolor Holographic Image Reconstruction with White-Light Illumination," Bell Sys. Tech. J., Vol. 45, pp 659-661. 1966.
11. Upatnieks, J., Marks, J. and Fedorowicz, R., "Color Holograms for White Light Reconstruction," Appl. Phys. Lett., Vol. 8, pp. 286-7. 1966.
12. Lin, L. H., Lo Bianco, C. V., "Experimental Techniques in making Multicolor White Light Reconstructed Holograms," Appl. Opt, Vol. 6, pp. 1255-8. 1967.
13. Collier, R. J. and Pennington, K. S., "Multicolor Imaging from Holograms Formed in Two-Dimensional Media," Appl. Opt, Vol. 6., pp. 1091-5. 1967.
14. Hauron, L.Ducos du, French Patent, 83,061. 1868.
15. Wall, E. J., The History of Three-Color Photography, Boston Mass: American Photographic Publishing Company, 1925, pp. 454-538. (Reprinted by Focal Press, London 1970)
16. Noguchi, M., "Color Reproduction by Multicolor Holograms with White-Light Reconstruction," Appl. Opt, Vol. 12, pp. 496-499. 1973.

17. Komar, V. G., "Progress of the Holographic Movie Process in the USSR", Proc.SPIE (Three-Dimensional Imaging), Vol. 120, pp. 127-144, 1977.
18. Benton, S. A., "Hologram Reconstructions with Extended Incoherent Sources," JOSA, Vol. 59, p. 1545. 1969. (Abstract only).
19. Hariharan, P., Steel, W.H. and Hegedus, Z. S., "Multicolor Holographic Imaging with a White-Light Source," Opt. Lett, Vol. 1., pp.8-9, 1977.
20. Wood, R. W., "The Diffraction Process of Colour Photography," Nature, Vol. 60., pp. 199-201. 1899.
21. Biedermann, K., "Image Encoding in Modulated Gratings from 1899 to 1970," Opt. Act, Vol. 17, pp. 631-635. 1970.
22. Chen, H. and Yu, F. T. S., "One-Step Rainbow Hologram," Opt. Lett., Vol. 2, pp. 85-87. 1978. (See also Benton, S.A., "Method for Making Reduced Bandwidth Holograms", U.S. Patent 3,633,989. 1972).
23. Chen, H., Tai, A. and Yu, F. T. S., "Generation of Color Images with One-Step Rainbow Holograms," Appl. Opt., Vol. 17, pp. 1490-1491. 1978.
24. Tamura, P. N., "One-Step Rainbow Holography with a Field Lens," Appl. Opt., Vol. 17, p.3343. 1978.
25. Benton, S. A., Mingace, H. S. and Walter, W. R., "One-Step White-Light Transmission Holography", Proc. SPIE (Recent Advances in Holography), Vol 215, pp. 156-161. 1980.
26. Shankoff, T. A., "Phase Holograms in Dichromated Gelatin," Appl. Opt, Vol. 7, pp. 2101-2105. 1968.
27. Kubota, T., Ose, T., Sasaki, M., and Honda, K., "Hologram Formation with Red Light in Methylene Blue Sensitized Dichromated Gelatin," Appl. Opt., Vol. 15., pp. 556-558. 1976.
28. Kubota, T. and Ose, T., "Lippmann Color Holograms Recorded in Methylene-Blue-Sensitized Dichromated Gelatin," Opt. Lett., Vol. 4, pp. 289-291. 1979.
29. Komar, V. G. and Ovechkis, Yu.N., "Colour Rendering of Holographic Images", Tekh.Kino. and Telev. (USSR), No. 9, pp. 18-22. 1976. (In Russian).
30. Buimistryuk, G. Ya. and Dmitriev, A. Ya., "Selection of Laser Emission Wavelengths to obtain Colour Holographic Images", Izv.VUZ Priborostr (USSR), Vol. 25, pp. 79-82. 1982. (In Russian).
31. Ruzek, J. and Muzik, J., "Some Problems of Colour Holography", Tesla Electron., Vol. 9, pp. 60-61. 1976.
32. Clay, B. R. and Gore, D. A., "Holographic Moving Map Display," Proc. SPIE, Vol. 45, pp. 149-155. 1974.
33. Lessard, R. A., Som, S. C. and Boivin, A., "New Technique of Color Holography," Appl. Opt., Vol. 12., pp. 2009-2011. 1973.
34. Lessard, R. A., Langlois, P., and Boivin, A., "Orthoscopic Color Holography of 3-D Objects," Appl. Opt, Vol. 14, pp. 565-566. 1975.
35. Kurtzner, E. T. and Haines, K. A., "Multicolor Images with Volume Photopolymer Holograms," Appl. Opt., Vol. 10, pp. 2194-2195. 1971.
36. Tatuoka, S., "Color Image Reconstruction by Image Plane Holography," Jap.J. Appl. Phys., Vol. 10, pp. 1742-1743. 1971.
37. Stroke, G. W., Zech, R. G., "White-Light Reconstruction of Color Images from Black-and-White Volume Holograms Recorded on Sheet Film," Appl. Phys. Lett., Vol. 9, pp 215-217. 1966.
38. Hariharan, P., "Improved Techniques for Multicolour Reflection Holograms," J.Opt. (France), Vol. 11, pp. 53-55. 1980.
39. S'inov, V.Kh, Spasov, G. A., and S'inov, S.Kh., "Increasing the Diffraction Efficiency during the Recording of Colour Reflection Holograms", Zh.Nauchnoi and Prikl. Fotogr. and Kinematogr. (USSR), Vol. 26., pp. 413-416. 1981. (In Russian).
40. Sobolev, G. A. and Serov, O. B., "Recording Color Reflection Holograms", Sov. Tech. Phys. Lett., Vol. 6, pp. 314-315. 1980.
41. Dzyubenko, M. I., Krishtal, V. A., Pyatikop, A. P., and Shevchenko, V. V., "Parameters of Three-Dimensional Holograms on High-Resolution Emulsions," Opt. Spectrosc. Vol. 38, pp. 429-431. 1975.
42. Nishida, N., "Correction of the Shrinkage of a Photographic Emulsion with Triethanolamine," Appl. Opt., Vol. 9, pp. 238-240. 1970.
43. Benton, S. A., 'Intra-Emulsion Diffusion-Transfer Processing of Volume Dielectric Holograms," JOSA, Vol. 64, pp. 1393-1394. 1974. (Abstract only).
44. Joly, L. and Vanhorebeek, R., "Development Effects in White-Light Reflection Holography," Phot. Sci.and Eng., Vol. 24, pp. 108-113. 1980.
45. Phillips, N. J., Ward, A. A., Cullen, R., and Porter, D., "Advances in Holographic Bleaches", Phot. Sci. and Eng., Vol, 24, pp. 120-124. 1980.
46. Spierings, W.,"'Pyrochrome' Processing Yields Color-Controlled Results with Silver-Halide Materials", Holosphere, Vol. 10, nos. 7,8, pp. 1-7. 1981.
47. Collier, R. J., Burckhardt, C. B., and Lin, L. H., Optical Holography, Academic Press, 1971, pp. 512-514.
48. Chang, B. J. and Leonard, C. D., "Dichromated Celatin for the Fabrication of Holographic Optical elements," Appl. Opt., Vol. 18, pp. 2407-2417. 1979.

49. Rosen, L., 'Focused-Image Holography with Extended Sources," Appl. Phys. Lett., Vol. 9, pp. 337-339. 1966.
50. Stroke, G. W., "White-Light Reconstruction of Holographic Images using Transmission Holograms Recorded with Conventionally-Focused Images and 'In-Line' Background,' Phys. Lett. Vol. 23, pp 325-327. 1966.
51. Rotz, F. B. and Friesem, A. A., "Holograms with Nonpseudoscopic Real Images," Appl. Phys. Lett., Vol. 8, pp. 146-148. 1966.
52. Hariharan, P., Hegedus, Z. S. and Steel, W. H., "One-Step Multicolour Rainbow Holograms with Wide Angle of View," Opt. Act., Vol. 26, pp. 289-291. 1979.
53. Kakichashvili, Sh.D. and Kakichashvili, V. I., "Reconstruction of Focused Holograms with Normal Perspective," Sov. Phys. - Tech. Phys., Vol. 16, pp. 1184-1185. 1972.
54. Paques, H., "Achromatization of Holograms", Proc. IEEE, Vol 54. pp. 1195-1196. 1966.
55. Burckhardt, C. B., "Display of Holograms in White Light." Bell Sys. Tech. J., Vol. 45, pp. 1841-1844. 1966.
56. De Bitetto, D. J., "White-Light Viewing of Surface Holograms by Simple Dispersion Compensation," Appl. Phys. Lett., Vol. 9, pp. 417-418. 1966.
57. Tamura, P. N., "Multicolor Image from Superposition of Rainbow Holograms," Proc. SPIE (Clever Optics), Vol. 126, pp.59-66. 1977.
58. Tamura, P. N., "Pseudocolor Encoding of Holographic Images using a Single Wavelength," Appl. Opt., Vol. 17, pp. 2532-2536. 1978.
59. Chen, Y-S, Wang, Y-T, and Dong, B-Z, "A New Method of Color Holography," Act. Phys. Sin., Vol. 27., pp. 723-9. 1978. (In Chinese).
60. Hariharan, P., "Pseudocolour Images with Volume Reflection Holograms," Opt. Commun., Vol. 35, pp. 42-44. 1980.
61. See footnote in Reference 1.
62. Thornton, W. A., "Luminosity and Color-Rendering Capability of White Light," JOSA, Vol. 61, pp. 1155-1163. 1971.